Electrophysiological dynamics of covert and overt visual attention.

Ordikhani-Seyedlar, Mehdi

Publication date:
2017

Document Version
Publisher's PDF, also known as Version of record

Technical University of Denmark

Mehdi Ordikhani-Seyedlar

Electrophysiological dynamics of covert and overt visual attention

PhD thesis, June 2016

DTU Electrical Engineering
Department of Electrical Engineering

Abstract

Attention is a key neural function for choosing certain information to receive more processing than others. Attention is allocated either by directly looking at the target (overt) or without eye movement towards the target (covert). The current study was designed to extract relevant features by using steady-state visual evoked potentials (SSVEP) task.
SSVEP task was presented to subjects at the same time that the electroencephalography (EEG) signals were recorded by the scalp electrodes. Subjects were instructed to respond to a certain stimulus by pressing a button. This way attention was measure in continuous manner.

Results showed that the amplitude of SSVEP frequencies is higher in overt than covert attention. This indicates that by overt attention events are registered with larger power. However, exploring the harmonics of frequencies showed that covert attention generates larger 2nd harmonic (e.g. 12Hz) than the 1st harmonic (e.g. 6Hz). This pattern was not observed in overt attention. We suggest that covert attention increases the non-linearity in the visual system.

Results from the source analysis showed that SSVEP signals are extracted from the primary visual cortex in overt attention. However, when covert attention is allocated to SSVEPs, frequencies are extracted from parietal and frontal areas. This shows that covert attention recruits higher cognitive function.

To test how SSVEPs are represented in higher brain areas, we conducted an invasive multi-unit recording from rhesus monkeys. Monkeys were trained to perform similar SSVEP task. Recording was done from somatosensory (S1) and motor (M1) cortices. Results showed that the neuronal firing rates in S1 and M1 not only increased selectively to attended flicker stimulus, but also they were highly synchronized. Moreover, some SSVEP frequencies was enhanced in single neurons. These results showed, for the first time, that visual attention to repetitive stimuli is able to regulate neuronal activities in S1 and M1 regions.

Abstrakt

Det neurale grundlag for opmærksomhed er afgørende for hvor og i hvilken grad forskellige informationer processeres. Opmærksomhed tildeles enten ved at se direkte påmålet (åbenlys opmærksomhed) eller uden øjenbevægelse i retning af målet (skjult opmærksomhed). Dette studie var designet til at beskrive karakteristiske neurale aktiveringsmønstre ved henholdsvis åbenlys og skjult opmærksomhed. Til dette formål anvendtes et steady-state visual evoked potential (SSVEP) paradigme.

Elektroencefalografi (EEG) signaler blev registreret når SSVEP paradigmet blev præsenteret for forsøgsdyrene. De blev instrueret i at respondere pået bestemt stimulus ved at trykke påen knap. Således blev opmærksomhed målt påen kontinuerlig måde.

Reslutaterne viste, at SSVEP frekvensernes amplitude er større ved åbenlys end ved skjult opmærksomhed. Dette indikerer at ved åbenlys opmærksomhed blive begivenheder registreret med større amplitude. Men undersøgelse af harmoniske frekvenser viste at skjult opmærksomhed generer større 2. harmoniske frekvenser (fx 12Hz) end 1. harmoniske frekvenser (fx 6hz) Dette mønster blev ikke observeret ved åbenlys opmærksom. Vi foreslår, at skjult opmærksomhed forøger non-lineariteten i det visuelle system.

Resultater fra kilde analysen viste, at SSVEP signalerne udspringer fra primær visuel cortex (V1) ved direkte opærksomhed. I skjult opmærksomhed udspringer SSVEP signalerne derimod fra paritale og frontale områder. Dette viser, at skjult opmærksomhed rekrutterer højere kognitive funktioner.

For at teste hvordan SSVEP'erne er repræsenteret i højere cerebrale områder udførte vi en invasiv multi-unit måling pårhesus aber. Aberne blev trænet til at udføre tilsvarende SSVEP paradigmer. EEG signaler blev optaget fra somatosensorisk cortex (S1) og motorcortex (M1).

Resultaterne viste, at den neurale fyringsfrekvens i S1 og M1 øgedes selektivt ved opmærskomhed påen flimrende stimulus, men ogsåat de i høj grad var synkroniserede. Derudover var visse SSVEP frekvenser forstærkede i enkelte neuroner. Disse resultater viste, for første gang, at visuel opmærksomhed pågentagende stimuli er i stand til at regulere neural aktivitet i S1 og M1.

Contents

List of Figures

List of Tables

Abbreviations

AD	Anderson-Darling
ADHD	Attention-Deficit/Hyperactivity Disorder
AUC	Area-Under-the-Curve
BCI	Brain-Computer Interface
BDF	BioSemi Data Format
BESA	Brain Electrical Source Analysis
CNS	Central Nervous System
Cls	Cluster
EEG	Electroencephalography
EOG	Electrooculography
EPSP	Excitatory Post-Synaptic Potential
ERNS	Event-related neuronal synchronization
ERP	Event-Related Potential
ERSP	Event-Related Spectral Estimation
FEF	Frontal Eye Field
FFT	Fast-Fourier Transform
fMRI	Functional Magnetic Resonance Imaging
Hz	Hertz
ICA	Independent Component Analysis
IPS	Intra-Parietal Sulcus
IPSP	Inhibitory Post-Synaptic Potential
kΩ	Kilo-Ohm
LCD	Liquid-Crystal-Display
LGN	Lateral Geniculte Nucleus
M1	Primary sensory area
MAP	Multi-channel acquisition processor
MEG	Magnetoencephalography
ms	Milli Second
MT	Middle-Temporal
mV	Milli-Volt
μV	Micro-Volt
Na^+	Sodium
OC	Operating Characteristic
PC	Personal Computer
PCA	Principal Component Analysis

PMd	Dorsal premotor area
PN	Pulvinar Nuclei
PPC	Posterior parietal cortex
RDA	Random-Dot Pattern
RF	Receptive Field
RT	Reaction time
RV	Residual Variance
s	Second
S1	Primary somatosensory area
SD	Standard Deviation
SEF	Supplementary Eye Field
SMA	Supplementary motor cortex
SNR	Signal-to-Noise-Ratio
SPL	Superior Parietal Lobule
SSVEP	Steady-State Visual Evoked Potential
TE	Inferior Temporal
TEO	Temporo-Occipital
VEP	Visual-Evoked Potential

Preface

This dissertation is submitted in partial fulfillment of the requirements for the degree of Doctor of Philosophy (Ph.D.) at the Technical University of Denmark. The research was conducted under the supervision of Dr. Sadasivan Puthusserypady and co-supervised by Dr. Helge B.D. Sørensen at the Division of Biomedical Engineering at the Department of Electrical Engineering. I hereby declare that this work is original and the product of my independent work, except where acknowledgment and references were stated. Neither this, nor any other similar dissertation has been submitted for any other degree at any other university.

The project started in September 2012 and ended in July 2016. All data recordings were carried out in the ContAct EEG lab located at the Danish Research Center for Magnetic Resonance (DRCMR), Hvidovre Hospital. The author of this thesis has conducted a part of the work at the Department of Neuroengineering at Duke University between October 2014 and March 2015. The project was funded by the Technical University of Denmark, Radiometer and the Lundbeck Foundation for the duration of three years. In addition, the expenses relate to stay abroad was partially supported by *Otto Mønsteds foundation* and the *Fabrikejer, Ingeniør Valdemar Selmer Trane og Hustru Elisa Tranes Fond.*

Acknowledgments

First and foremost, I would like to thank DTU-Electrical Engineering, Lundbeck foundation and the Radiometer for the financial support I received during first three years of this study.

I would like to acknowledges my supervisors Dr. Sadasivan Puthusserypady (Technical University of Denmark), Dr. Helge BD Sørensen (Technical University of Denmark), Dr. Troels W. Kjær (Zealand University Hospital, Roskilde) and Professor Hartwig R. Siebner (ContAct EEG-lab located at DRCMR, Hvidovre Hospital).

My greatest appreciation goes to Dr. Miguel Nicolelis who hosted me in his lab and provided the stat-of-the-art facilities and supported me with his detailed feedbacks on the results. I also express my special thank to Dr. Laura M. Oliveira who was always kind and helpful in all steps from being admitted at Duke University till the end of my stay in USA. Accordingly, I would like to thank Dr. Mikhail A. Lebedev, the senior research scientist at Duke, a wonderful friend and my senior mentor for very constructive discussions during the project at Duke and his persisting feedbacks on the manuscripts. I thank Arjun Ramakrishnan, the postdoctoral researcher at Duke, for his day-to-day supervision, fantastic scientific discussion and extraordinary efforts during the project. This stay was possible because of the partial financial support by *Otto Mønsteds foundation* and the *Fabrikejer, Ingeniør Valdemar Selmer Trane og Hustru Elisa Tranes Fond.*

I would like to thank Dr. Markus Waser for his very helpful advices in statistical analysis and Mette Marie Gunnergaard for her kindness and commitment in translating some parts of the thesis into Danish.

Perhaps the Ph.D. thesis was an end by itself, but I had an endless honor to meet great people each played important roles during my academic and social life. I would like to thank them all:
Maritta and Norbert Doser, Paul Thompson, Oleksandr Rybalko, Sean Bowen, Thomas De Cooman, Darius Rohani, Bettina Bork and the anonymous participants in EEG experiments. Any missing names in this list is unintentional.

I am very grateful for my parents who brought me up, educated me and provided the best they could do to let me grow. Their role in my life is unforgettable. Also I thank my brothers Ahmad, Amin and Ramin whom I always had their faithful support.

Finally, my sincere gratitude goes to my wife Karoline, who provided a happy and peaceful life, supported me by her beautiful thoughts and emotional power and made me stronger again in all ups and downs. She is a wonderful person to share my life with.

Evaluation committee

- Chairperson: Assoc. Professor Thomas Sams (Department of Electrical Engineering, Technical University of Denmark)
- Professor Wlodzimierz Klonowski (Polish Academy of Science, Warsaw, Poland)
- Senior Assoc. Professor Henrik Karstoft (Department of Engineering - Signal Processing, Aarhus University, Denmark)
- **Ph.D. education started**
  September 1, 2012
- **Thesis submitted**
  June 1, 2016
- **Thesis defended**
  August 23, 2016

Chapter 1

Introduction

1.1 General

The visual system of the human brain has evolved to construct useful representation of complex input information. In everyday life, we constantly deal with vast amounts of visual information from our complex and dynamic environment. The brain starts the processing of incoming information by filtering out irrelevant signals. Only a tiny amount of the incoming information enters the higher-order processing levels and becomes available to consciousness[1,2]. Because the amount of information can only decrease during neural processing, it is crucial for the visual system to preserve only behaviorally relevant information[3]. For instance, when a driver approaches a busy intersection it is important to detect and respond to the relevant traffic light rather than any other light source in the visual scene. Our ability to block the irrelevant information to the current task and to enhance the processing of the important information is called attention. Attention is a unique function to flexibly select and enhance a subset of sensory input based on behavioral goal. Once way to identify this function is to measure the electrical currents under numerous signatures and features. These features have become a fundamental interest for developing assistive technologies.

Attention as a key neural function can deteriorate due to neurological disorders. Patients with impaired attention have disabilities to focus on single tasks, and they easily get distracted by irrelevant information. One of the most common disorders of attention, namely the attention deficit hyperactivity disorder (ADHD), is a mental condition characterized by inattention, hyperactivity and impulsivity. ADHD symptoms are dominant in childhood, and extend to adulthood in 15-40% of cases[4,5]. The disorder impairs behaviors relevant to academic, occupational and social interactions[6]. According to meta-regression analyses of published studies, ADHD has 5% prevalence worldwide[7–9]. To date, treatment strategies have been mostly pharmacological, such as prescription of psycho-stimulants. However, long-term treatment with pharmacological agents is complicated by side-effects[10,11]. Children may develop anxiety symptoms after being treated with psycho-stimulants for 6 months and longer[12]. Psychological therapy, an alternative approach, relieves ADHD symptoms in 30% of cases[13]. Overall, currently available therapies for ADHD are only partially effective. A complementary attempt to treat attention-deficiency syndrome also comes from the assistive devices seen as neurofeedback therapy[14–16]. Assistive devices decode neural signals using mathematical algorithms often utilizing templates of neural patterns. They are

defined based on prior knowledge of the characteristics of signals in healthy subjects. These templates play a critical role in how well the NF therapy performs on targeting a specific dysfunction.

1.2 Problem statement

The main goal of this Ph.D. thesis is to identify the normal EEG signature of visual attention and how attention manipulates SSVEP* frequencies. The main task is to identify these effects on two major attentional orientation systems as overt and covert attention. Several aspects led to the decision to focus on covert attention. First, covert attention has been reported to be severely impaired, along with other components of attention, in subjects with attention-deficiency[17–19]. Second, covert attention is the first to come when attention is to be allocated, i.e. covert attention allows us to select visual information and grant such information priority in processing[20]. And third, covert attention may carry unique information related to attention as it is less contaminated with other modalities such as simple physical responses by visual system or eye movement. Therefore, understanding the specific features related to covert attention and their scalp topographical distribution may provide a valuable information for follow- up studies to exploit these specific features.

1.3 Contribution of the thesis

The goal of the thesis is to find a consistent pattern of activation across subjects while observing an SSVEP frequency. The activity pattern considers:

- Output signal properties – manipulated by covert and overt attention – in the range of SSVEP frequency
- Differences in topographical distribution of different frequencies over the scalp
- SSVEP impact on monkey single-neuron level in non-visual areas in invasive recording

These findings will contribute to identify the specific features in different types of attentional shifts (covert and overt). Topographical distribution of different frequency bands indicating where to look for specific frequency. Intra-cortical single-neuron and LFP recordings gives a better insight on how externally-generated oscillations (e.g. SSVEPs) affect the firing rate as well as the synchronization of the population of neurons.

Understanding the features related to the EEG (macro-features) and single-neurons (micro-features) gives a better representation of SSVEP-based attention. These features can be used in assistive devices for higher precision in detecting when a person is focused.

1.4 Organization of the thesis

The current thesis has been organized in 7 chapters. Following the current chapter, some related theories will be explained in the chapter 2. Chapter 3 is specified for the preprocessing of EEG data. EEG experimental results have been partitioned in two subsequent chapters: chapter 4 includes the EEG results for SSVEP frequency-bands analysis by special focus on the harmonics; whereas, the topographical distribution of SSVEPs over the scalp has been discussed in the chapter 5. Finally, the experiments end in chapter 6 discussing

*Steady-State Visual Evoked Potential

the attention-induced representation of SSVEPs in the single-neuron level in the monkey. Chapter 7 concludes the entire thesis as the "general conclusion".

Chapter 2

Theory

2.1 Attention system

In every moment of visual stream an overwhelming amount of inputs (10^8-10^9 bits) enter through our eyes to the brain[21]. Such enormous amount of information sent by retina, encounter a processing bottleneck in the visual system. These information need to be efficiently filtered and only the most relevant information to the current aim and behavior must be registered in the brain. Human and animals are able to bias and choose such most important information and ignore the irrelevant ones using the attention system. Most often (but not always) our gaze or direction of eyes is spatially aligned to our focus of attention. This enables our brain to resolve the final details of fixated stimuli via a fovea, where visual acuity is in the highest level. The spatial alignment of eye gaze and attention is referred as "overt attention". However, this is not the only way we attend to the important information surrounding us. In a driving time, for example, the direction of our eyes are mostly to the front, yet we are able to detect changes in almost all direction without explicitly looking at them. This type of attention is known as "covert attention". The importance of covert attention has been acknowledged by Hermann[22] who found that he is able to remember the letters only appearing in the area of the screen where his attention was driven despite having his eye-gaze elsewhere. Later, his experiments showed that attention and gaze can be dissociated.

Much of our understanding from visual attention comes from studies in primates as the invasive experiment is possible. Intra-cortical recordings showed that while animals are attending to a specific target, the neuronal responses to attended stimuli increases compared to the unattended ones. These enhancements have been observed in different visual regions such as the V4 area. V4 is an extra-striate region where neurons are modulated by visual attention. Like all neurons in the visual system, V4 neurons have receptive fields (RFs) by which the stimulations to the visual field is received. V4 neurons responds stronger with higher number of spikes when the stimulus is located inside the RFs and attended rather than unattended (even though the stimulus is located within the RF). Furthermore, V4 neurons are also specialized for specific characteristics of the stimulus such as orientation stimulus (e.g. more response when a stimulus appears in the 90° of visual angle than in 0°) or the features (e.g. more salient features such as a red circle among several blue circles). During attention, V4 responses to stimuli of preferred characteristics are increased more

than responses to non-preferred stimuli.

Prior to identification of covert attention, it had been observed that when an animal targets a stimulus with eye movement, the neuronal responses of superior colliculus[23] and posterior parietal cortex[24] is substantially increased. Later researches showed that the pre-saccadic visual enhancement also affect V4 neurons[25] and in the inferior temporal cortex[26]. Moore and Chang[27] found that during covert attention, the presaccadic enhancement of V4 neurons is selective for the features of the saccade targets, just like it is in the initial response of the target in the receptive field. Again as in covert attention, pre-saccadic enhancement (which is assumed to take action in covert attention) was greatest to the target at V4 neurons. These evidence showed that RFs's rule works also for covert attention just by attending to the target and not even watching them directly.

2.1.1 Organization of visual attention

Visual system has extensively been studied in monkey. Monkey cortex contains more than 30 separate visual areas[28] in two functionally specialized pathways[29]. Both pathways are originated from the primary visual cortex (V1) and both are composed of several areas beyond V1. The ventral pathway (occipito-temporal) is important for identification of objects (what pathway); whereas the dorsal pathway (occipito-parietal) play a critical role in identifying the spatial relations (where pathway) among objects as well as the visual orientation toward objects in space[30].

The ventral stream consists of several important areas such as the V4, TEO* and TE†. There areas in the ventral stream have clearly shown a selective response to object vision such as texture, color and shape[29]. However, neurons in the middle-temporal (MT) area and other regions of the dorsal pathway does not contribute to the object recognition; rather, they are involved in responding to speed and direction of the motions[31]. Within the ventral pathway, the information processing is conducted in hierarchical way (figure 2.1). This means that low level information processing (e.g. brightness and contrast) is done by early visual area; whereas, complex feature analysis is conducted by higher-level visual areas (e.g. face recognition by TEO area)[29]. PLStudies have shown that all connections between successive pairs of areas within ventral stream are reciprocally interconnected. In other words, the projections from the first area to second are back projected from the second to the first area[28]. Furthermore, there is only feedback projections to areas in the ventral stream from both parietal and prefrontal cortices[32]. Feedback projections, both within the ventral stream and from other areas beyond this stream, forms the anatomical basis for top-down influences such as top-down attention (attention based on the internal will). These results from the monkey was later supported in human using functional magnetic resonance imaging (fMRI) techniques. In tasks which required the color and face recognition, V4 area as well as more anterior ventral stream areas turned to be activated[33] resembling neurons which were selective for features in monkey. Similarly, measures targeting the perception of motion often showed activations in the dorsal pathways.

*Temporo-occipital
†Inferior temporal

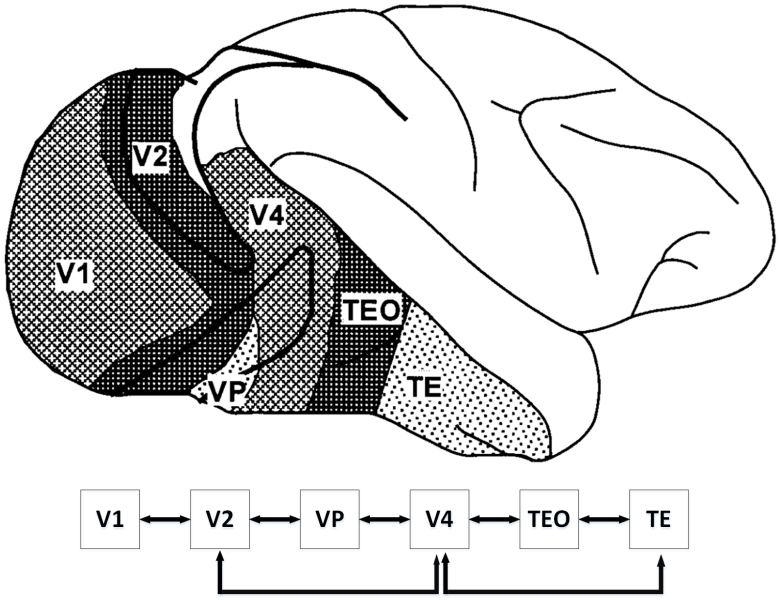

Figure 2.1: The object-vision pathway. Ventral stream (occipitotemporal pathway) is cruitial for object recognition. This pathway starts from visual cortex (V1) and is composed of multiple areas in occipital (V2, VP and V4) as well as in temporal cortex (TEO, TE). The anatomical organization of ventral stream areas, as shown here from the lateral view of the monkey brain, is highly hierarchical. Connections between regions are reciprocal. Therefore, the feed-forward projections from first area to the second is reciprocated by feedback from the second area to the first (see arrow). Image from Kastner and Ungerleider[34]

2.1.2 Visual attention networks

As visual attention is the main focus of the current study, we elaborate more the neural networks involved in visual attention. Our early understanding from the attentional networks in human comes from patients with unilateral brain lesions, particularly in the higher cortical areas which results in the hemi-neglect syndrome. Patients in severe state, neglect the half of the visual field usually contra-lateral to the lesion site[35].

A visuo-spatial hemi-neglect has been reported to appear due to lesions in temporo-parietal junctions and superior temporal cortex[36]. Neglect also happens due to damage in frontal lobe[37], superior parietal lobule (SPL), anterior cingulate cortex and pulvinar[34]. Neglect syndrome occurs more often in right-side lesions indicating the importance of right hemisphere in attentional modulation[34].

Imaging studies have declared more detailed information about the attentional networks in human. It has been shown that in attention the neural signals increase in fronto-parietal network including intra-parietal sulcus (IPS), SPL, supplementary eye field (SEF) and frontal eye field (FEF). This pathway known as the dorsal fronto-parietal network has been involved in numerous attentional tasks, whether the target is to be discriminated[38], detected[39] or tracked[40] in the visual field.

The fronto-parietal network modulates attention in accordance to the behavior. One mechanism that this network works is altering the synchrony of neurons. Studies in this line have shown that an increase of synchronization of inputs into a single neuron has a great effect on elevating the attentional state. Thus, modulation of synchronized activity of a population of neurons alters their downstream impacts. This indicates that increase of inter-neuronal synchronization is an efficient way to strengthen the impact of attended stimulus. Neural synchrony increased the high-frequency oscillations in the range of 40-80Hz while decreasing the lower frequencies ($< 10Hz$) in the neurons representing the attended location. Increased synchrony in neural population among different brain areas also changes the inter-regional communication where oscillations in the neural population causes increase and decrease in inhibition in a local network. Therefore, inter-regional neural synchronization causes a co-excitable state among those areas, being a possible model for enhancing the connectivity[41]. In a recent study, Bosman et al.[42] recorded from population of neurons in V1 with receptive fields for one of two stimuli. At the same time, neurons from V4 with the receptive field for both stimuli has been recorded. This study showed that when attention is driven to a single object, gamma oscillations (30-80Hz) were selectively synchronized between the V1 and V4 areas. The synchronization effects are not specific for the visual cortex and gamma-band, rather synchrony has also been observed between parietal and prefrontal cortices depending on weather attention was internally directed towards a remembered target or externally driven for a salient stimulus. In externally-driven attention or "bottom-up" attention[‡] gamma-band was synchronized between parietal and frontal cortices. Where in internally-driven or "top-down" attention, the information flow was through beta-band synchronization between prefrontal and parietal cortices. These studies indicate that attention acts through synchronizing or desynchronizing brain oscillations among different brain areas which in turn transmits these information to specialized regions to be recognized.

In addition to cortico-cortical communication, thalamo-cortical interaction also plays a critical role in focusing attention. Pulvinar, the largest nucleus in thalamus, mediates this interaction. Pulvinar establishes cortico-thalamo-cortical connections by making the input-output loops with cortical areas. The indirect connection between different cortical areas facilitate the information transfer between the connected regions. A recent study has shown that in a spatial attention task, alpha-band synchrony, enhanced between two interconnected regions (V4 and TEO), was the result of pulvino-cortical connection rather than cortico-cortical. Slow oscillations were couples to fast oscillations such as gamma-band in the communicated cortical regions. This frequency coupling is suggested to be a mechanism by which long-range communication is made feasible, where low-frequencies modulate the excitability of the neural population and facilitate the function of high-frequency oscillations in the target areas.

2.1.3 Overt & covert attention

Initial studies on the differential allocation of information processing resources has shown that there are two dissociable sub-domain of allocation as overt and covert attention. Overt attention is manifested by eye-movement and saccade towards the target object (stimulus) in order to place the visual information at the fovea where the sensitivity to details is highest. Covert attention, on the other hand, is manifested as the improvement in information processing of the stimuli in the absence of eye movements and without directly staring at the stimulus[43]. While overt attention can be seen by an observer, covert attention must be inferred from changes in phenomenological experience in a carefully-designed situation

[‡]A type of attention in which attention is driven by a stimulus due to its salience, e.g. a loud noise

in which individuals are required to fixate their eyes on a fixation point while other variables can be manipulated to solicit changes in covert attention. In the well-known Posner's task[44], individuals responded to targets that are located peripheral to the fixation point. Targets were preceded by cues to alert the subject where to attend. Subjects were instructed to give the response as soon as the target is detected. Posner observed that the responses to covert was faster than over attention (faster reaction time). Due to technical difficulties in studying covert attention on animals – as it is difficult to know exactly where an animal' focus of covert attention is[45] – this line of research has remained to be better understood. In-spite of these limitations, many researchers have been focused on the distinction between overt and covert attention.

2.1.4 Linkage between overt and covert attention

The link between overt and covert orientation of attention lies somewhere on a continuum from complete neural independence to identical neural circuitry. Literature suggested three possible scenario for this relationship; (1) Posner and Petersen[46] proposed that covert and overt shift of attention are completely independent of each other[47], (2) Corbetta[39] suggested that these two types of attentional orientation are two separate phenomenon but with interdependent neural mechanisms and (3) Rizzolatti et al.[48] argued that covert and overt shifts of attention are two completely independent phenomenon with different neural circuits. This theory has later been known as the premotor theory of attention.
Posner[44] suggested that "attention shifts are not an inevitable consequence of eye movements" which provided the early evidence for the dissociability of covert and overt attention[49]. Rizzolatti et al.[48] developed the idea of the 'pre-motor theory of attention'. This theory explains why subjects had more difficulty in covertly attending both sides of a vertical meridian. They suggested that covert attention might involve the preparation of an eye movement, but this movement is actually not executed.

2.2 Electrophysiology

One way to investigate the electrical activity of the brain is to use the technique of the electroencephalography (EEG). The first discovery of EEG in human was by Hans Berger of the University of Jena, Germany in 1920 for graphical representation of electrical currents of the brain. He hypothesized that the brain changes the voltage depending on different functional and behavioral status. His first report included the alpha rhythm as the major component of the EEG signals[50]. To understand the principals of EEG recording we need to know the neural activities.

2.2.1 Principals of brain electrical signals

The brain consists of two major cell types: *(1)* neural cells: as the fundamental units of the generation of the electrical signals; and *(2)* glial cells: located in between neurons and their role is to maintain the homeostasis of the neurons. Each neuron has three important parts: cell bodies, axon and dendrites. Nerve cells respond to stimuli and transmit information over long distances. In the cell body, most of the cellular metabolism takes place where the proteins are synthesized and transmitted to other parts of the cell. Synthesized proteins as well as the electrical signals are transmitted through axons. Dendrites are connected either to axons or dendrites from other cells and receive impulses from nerves or rely signals to neural cells[51]. In the brain, each neuron is connected to approximately 10^4 other neurons. The neural activity is mainly related to the synaptic currents transferred between the synapses. An action potential of -60 to -70mV can be recorded under the membrane of the cell body

(figure 2.2). Action potentials traveling along the axon, may end in two types of synapses: Excitatory and inhibitory. Excitatory neurons are followed by the depolarization of the cell membrane due to a sudden influx of cations and outflow of anions. This type of neurons are called excitatory post-synaptic potential (EPSP). Inhibitory neurons, on the other hand, occur due to outflow of cations and influx of anions which result in the hyper-polarization of the cell membrane, known as the inhibitory post-synaptic potential (IPSP).

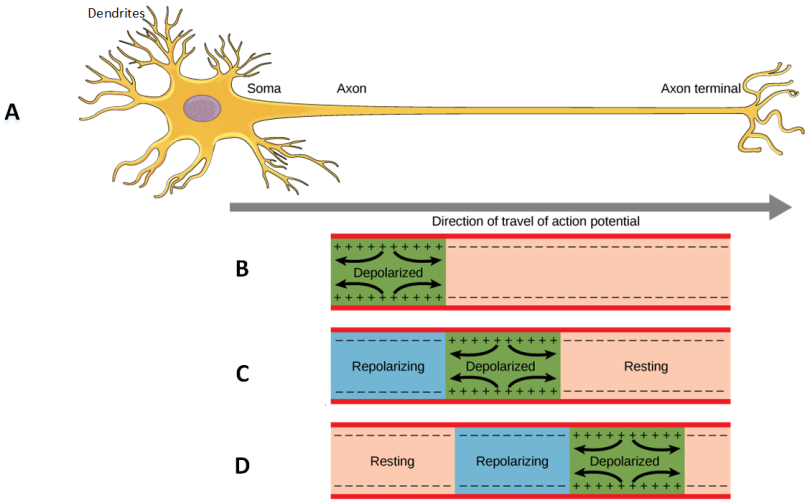

Figure 2.2: Illustration of a single neuron and generation of an action potential. *(A)* A nerve cell contains three major components of cell body (soma), axon and dendrites (axon terminal). Action potential is typically generate in the soma and travels throughout the axons till it reaches the dendrites in order to transmit the electrical signal to the next neurons through synapses. *(B)* The action potential is generated in the soma in response to a signal. This causes a sudden influx of cations (which have the highest concentration outside of the cell membrane in resting state) and depolarization of the membrane. *(C)* The depolarization spreads down the axon. Meanwhile the first part of the membrane starts to be re-polarized. The re-polarized section cannot be depolarized again just for a short time after the depolarization (refractory period) as the Na^+ channels are de-activated. *(D)* The action potential continues to travel down the axon to reach the dendrites. At the same time the previously re-polarized section turns into resting state which is excitable again. Image from Boundless[52]

Generation of EEG

An EEG signal is a measure of electrical currents that flow during synaptic activity of dendrites of large population of pyramidal cells in the cerebral cortex. When neurons become active, the synaptic currents are produced within the dendrites. These currents generate electrical fields which are measurable over the scalp. Differences of electrical potentials are caused by the summation of post-synaptic potentials from the pyramidal cells. At the synaptic site where an EPSP occurs, is an active current sink (when the cations rush into the neural cells) which create a negative charge outside of the neural membrane. In the meantime, at the distal part of the cell there exist a passive current source (flow of positive

charges outside of the cell). This phenomenon generates a dipole with another electrode located in a distance from the first electrode where opposite action is carried out in the neurons close to the second electrode (see figure 2.3).

The main source of EEG derives from the cerebral cortex. In principal, EEG provides a two-dimensional representation of a 3-dimensional reality. It takes a combined synchronized electrical activity of a population of neurons approximately from the cortical area of minimum 6 cm^2 to create a visible EEG [53].

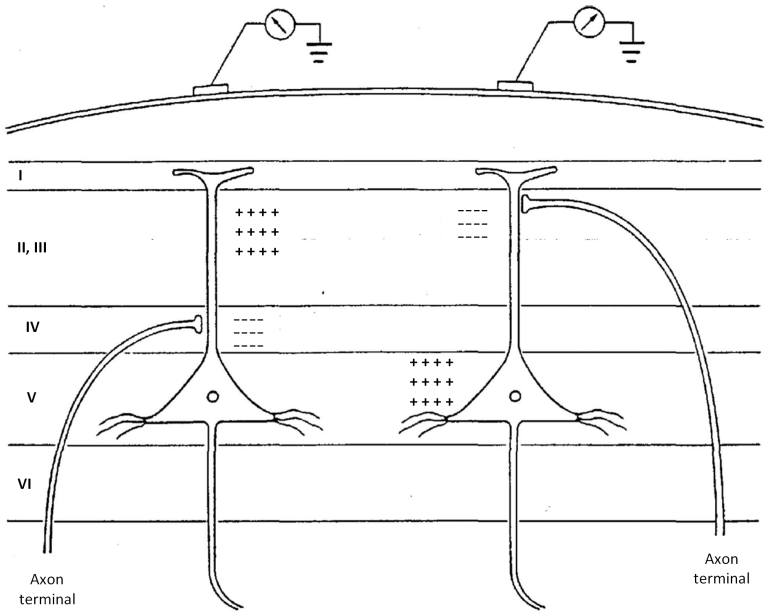

Figure 2.3: Generation of extra-cellular voltage field from graded synaptic activity. Two pyramidal cells are shown, each of which receiving excitation from other axons (axon terminals). Based on the location where the pyramidal cells are excited, the closest electrodes on the scalp record the dirrences in voltages. Image courtesy of Martin [54]

2.3 Steady-state visual evoked potentials and visual attention

The basic mechanism of visual attention has been widely studied by using visual evoked potentials (VEPs) [55]. VEPs generate an enhanced response in extra-striate visual cortex [56]. This enhancement of evoked cortical activities indicate that attention to specific location generates an amplification of sensory information. In spite of good applicability of transient VEPs to understand the brain's sensory systems in response to attended stimulus, this approach has some limitations to study the visual attention. One major issue is that transient evoked potentials are often presented in onsets with fairly large intervals (0.3-1.5s). This makes it difficult to maintain a state of focused attention for relevant targets and ignore the irrelevant stimuli [57].

Steady-state visual evoked potential (SSVEP) is defined as repetitive flicker (e.g. flickering light or images) to generate a continuous activity in cortical areas. These activities

can be recorded from the scalp as sinusoidal signals with the same fundamental frequencies (figure 2.4). SSVEP was first introduced by Adrian and Matthews[58] as a method to investigate the perception and sensation. When a repetitive stimulus, usually over 4Hz[59], with a certain frequency is presented to a subject, the oscillatory wave-response to the stimulus frequency can be observed in recorded data from the brain[60]. Several studies have shown that stimulus with low flickering frequency, in particular, below 30Hz can effectively generate strong responses[61–63]. SSVEP has been widely used in brain-machine interfaces, binocular rivalry, working memory and visual attention[62,64–68]. Furthermore, studies based on fMRI, magnetoencephalography (MEG) and EEG consistently revealed the SSVEP response in broadly distributed brain areas from occipital to parietal, temporal and prefrontal lobes[64,69–74]. The advantage of SSVEP over transient visual evoked potential is that the experimenter can easily vary the rate of flicker frequency. More importantly, SSVEPs are characterized by high signal-to-noise-ratio (SNR)[75].

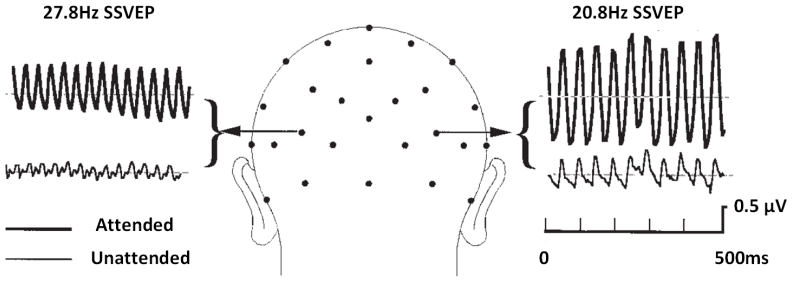

Figure 2.4: Schematic figure of how attention might alter SSVEP signals' amplitude. Subject was presented by two SSVEP frequencies of 27.8Hz and 20.8Hz. In the recorded signals, the attended (thick line) frequency has larger amplitude compared to unattended frequency (thin line) (the figure is adapted from Müller et al.[76])

Considering the origin of SSVEP signal in the brain, SSVEP is generated as a result of physical stimulation of retinal receptors by a sensory stimulus; however, the strength of this signal can be modulated by the internal will and cognitive system. When a single stimulus is presented periodically to the visual system, the evoked response generated by that stimulus follows the same pattern of periodicity[77]. One theory argues that the SSVEP is due to modulation at early sensory stages which represent the action of clustering of neurons influenced by a higher order control process[78]. In the current thesis, we have explored how SSVEPs are processed by different types of attention. Furthermore, we observed how SSVEPs act on single neuronal level.

Chapter 3

EEG pre-processing

3.1 Experimental setup

Pre-processing contains a series of mathematical operations to prepare the data for final processing. Pre-processing is an essential part of EEG data analysis in the current study. This is because the signals related to "*visual attention*", as a highly delicate cognitive function, can be easily confounded or masked by other brain functions. Attention-related signals naturally are difficult yo trace and this is the reason that we need pre-processing to remove or suppress any other irrelevant signals in order to be able to extract attention-related features.
Data collection was carried out by a *Biosemi* ActiveTwo EEG setup with 128 scalp electrodes and eight external electrodes. Data recorded at a sampling rate of 512Hz and referenced to a ground formed by the common mode sense (CMS) active and driven right leg (DRL) passive electrodes (Biosemi Inc.). Different parts of the EEG setup have been introduced as below:

1. AD box (analog-to-digital converter box): This box digitizes 128 sensor-signals with 24 bit resolution. The digital output of the AD box is transmitted to the PC visa a single optical fiber.
2. USB2 receiver: The receiver converts the optical data coming from the AD-box to a USB2 output. USB2 receiver has a trigger port with 16 independent trigger inputs and outputs. The trigger inputs allow the experimenter to send the event codes to the data.
3. Active electrodes: A number of 128 electrodes are used in this experiment. Each electrode is integrated with a sintered Ag-AgCl core.
4. External electrodes (figure 3.1): These electrode were used in order to detect non-brain activities which often contaminate the EEG signals. The order of electrodes placed on the skin was as follow:
    - Electrode #1: Reference electrode attached to the left mastoid
    - Electrode #2: Reference electrode attached to the right mastoid
    - Electrode #3: Reference electrode attached to the left earlobe
    - Electrode #4: Reference electrode attached to the right earlobe
    - Electrode #5: EOG electrode attached in the internal canthus
    - Electrode #6: EOG electrode attached in the external canthus
    - Electrode #7: EOG electrode attached below the lower eye lid

- Electrode #8: Pulse electrode attached to the left wrist

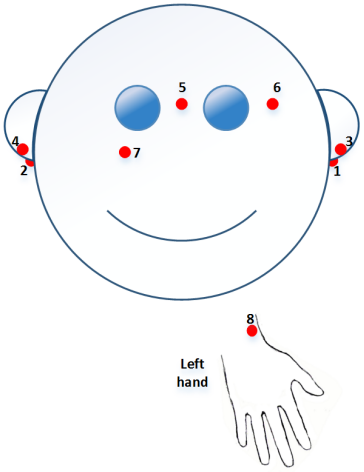

Figure 3.1: Location of external electrodes on the body: *(#1&2)* Mastoid reference: these electrodes were referenced in pre-processing stage. *(#2&4)* Ear-lobe reference: these electrodes were place to be considered as reference *just in case* mastoid electrodes had no proper contacts. *(#5&6)* Electrodes to measure the horizontal eye movements. *(#7)* Electrodes to measure vertical eye movements. *(#8)* Electrode to measure the pulse.

5. Head cap (figure 3.2): Provided in different head sizes.
6. Monitor with the refresh rate of $144Hz$
7. Stimulation PC where the visual task was executed
8. Data recorder PC

3.2 Participants

3.2.1 Healthy subjects

Neurologically healthy volunteers, above 18 years of age were recruited in this study. The participants were interviewed about their psychiatric history and any type of medication consumption before performing the experiments. Volunteers were allowed to bring their companion with them during the interview as well as the experimental sessions.

Inclusion criteria

- Age 18 years old or older
- Signed consent form

Exclusion criteria

- Known neurologic disorder
- Epilepsy or photosensitivity

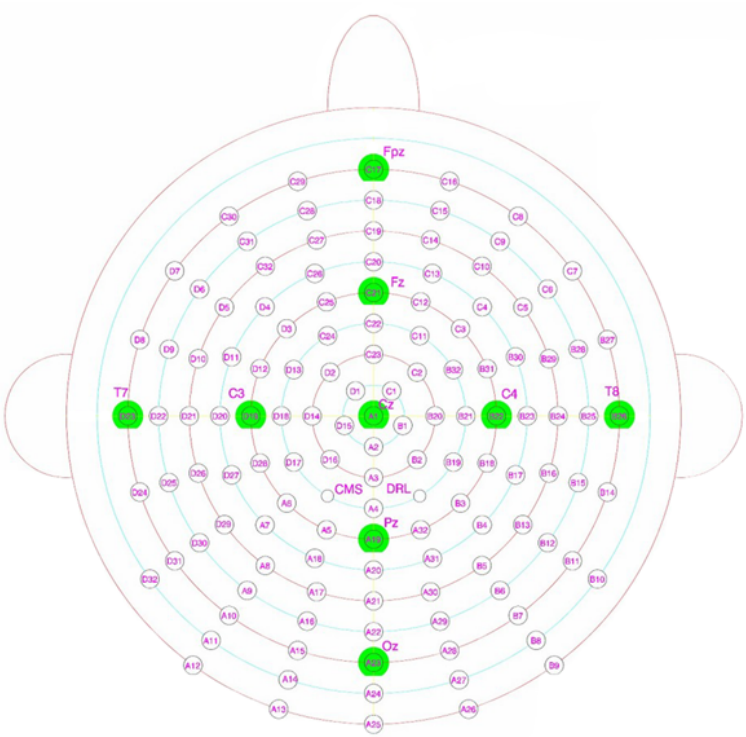

Figure 3.2: 128-channel EEG cap with active electrodes. Labeling system: ABC

- History of severe head trauma
- Pregnancy
- Inability to give informed consent
- Any restrictions which prevents subjects to be undergone EEG recording session
- Taking CNS activating medications

3.2.2 Call for subjects

Call for subjects was done through the official web-page `www.forsoegsperson.dk`. A total of 102 subjects applied to this experiment. They were immediately provided by written information with more details for the experimental procedure. Then they were invited to the EEG lab located at Hvidovre hospital where more information was provided to ensure that all inclusion and exclusion criteria are met. Participants signed a consent form before the experiment started. Subjects were compensated by monetary reward at the end of the experiment.

3.2.3 Ethical considerations

All participants had the freedom to withdraw from the experiments at any time without stating any reason. Confidential documents have been stored in a locked file. The electronic information have been stored in a password-protected computer behind secure "firewall" in accordance with the Privacy Act and notified to the *Datatilsynet*. Collected data has been linked to an individual by using `dateFictiousName`. All personally identifiable information

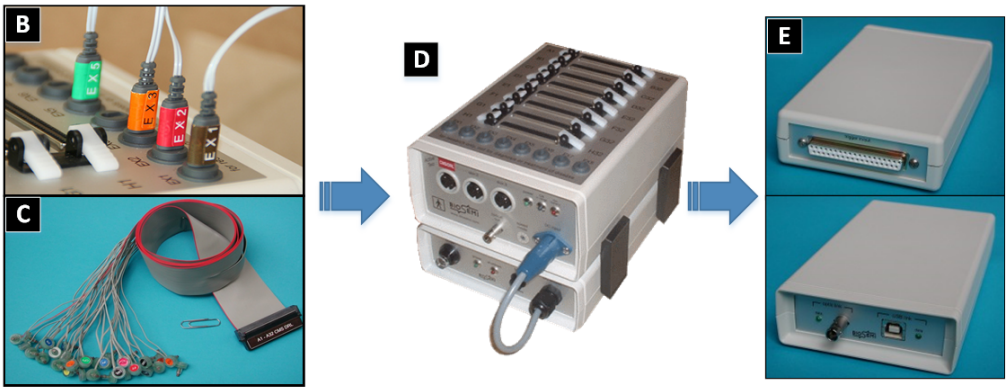

Figure 3.3: EEG setup used in human experiment. *(A)* 128-channel EEG cap with different sizes for various head-size. The electrode's locations were arranged based on *ABC* labeling system. Before placing electrodes, the conductive gel (Signa gel) was used to reduce the impedance to below 5KΩ. *(B)* External electrodes were located on different locations on the face and wrist (see figure 3.1) and connected to the AD-box. *(C)* Active flat electrodes are labeled as A1-A32, B1-B32, C1-C32 and D1-D32. Each set of 32 electrodes are grouped together to be connected to one port in AD-box. The dimension of each single electrode is 11mm width, 17mm length, 4.5mm height and is sintered with Ag-AgCl electrode pallet (4mm in diameter) to reduce noise. *(D)* The AD-box (upper) connected to the battery box (lower). The signals are digitized in AD-box and transmitted through a fiber-optic to the USB2 receiver box *(E)*. USB2 receiver (which is shown from the front and back view) transmit the data through a USB2 port to the acquisition computer. *(F)* Acquisition computer. Images are adopted from Corp.[79]

will be destroyed (corresponding to total anonymity) 15 years after project completion. The subject's name will never be used in scientific publications or presentations. Associate professor Sadasivan Puthusserypady was responsible to ensuring that all sensitive personal data will be stored under the *Lov om behandling af personoplysninger*. Subjects were asked in the informed consent if they would like to be notified in case something abnormal is observed in their brain function. Subjects were told that there is no immediate benefit to expect for participants, nor is there considered to be any significant risk associated with the study. Participants were provided taxable monetary reward at the end of the experiment. The participants were covered by the general national insurance of the health-care sector (*patientforsikringen*). No biological material was taken from the participants for the purpose of storage in a research bio-bank.

3.2.4 Preparation of participants for the experiment

Each subject was seated in an adjustable chair. The head size was measured in two dimension of inion-to-nasion as well as left-to-right preauricular points. The head-cap was located and centralized based on these measurements. The location of electrodes were filled by conductor gel and electrodes were located in place and were connected to the AD-box. External electrodes were also attached after cleaning the skin surface by alcohol wipes. The visual task was explained and a few training sessions were conducted which allowed the participants to learn the task.

3.3 Visual attention task

Subjects were seated in a dimmed room with a distance of $60 - 65cm$ from the screen and had a computer keyboard accessible. The visual attention task consists of one fixation point in the center of the screen (small square) and two larger squares in both sides. Side squares were flickering in different frequencies ($6Hz$ vs $7Hz$ and $8Hz$ vs $9Hz$). The choice of flickers was made based on previous literature[55,80] as well as the limitation of our experimental setup. The SSVEP frequencies were chosen within a range that is reliably presentable in our experimental computer (frequencies had to be shown homogeneously and with no delay). We experimented highly inhomogeneous light-flashes in frequencies higher than 10Hz in our system. In addition, we aimed to reserve higher harmonics for future analyzes.
Inside each flickering square, random numbers have been presented for a brief period of time ($280ms$). The participants were required to pay attention to either left or right square based on the indicator beside the central fixation square and press the space button on the keyboard as quickly and as accurately as possible whenever the number inside the attended flickering squares matches with the number already shown in the central square. In other words, the central square provides a cue, both in case of direction of attention and the digit to be responded. These cues flash for only $300ms$. The center cue was presented randomly every 8-12s. Therefore, this time represented the duration of each trial.

3.3.1 Visual task instruction

There have been two experimental protocols for the participants: Each experimental session included several blocks. The experiment was divided into four major blocks as covert and overt attention with and without flickers. In the first two blocks there were fours minor blocks presented the following flicker frequencies:
left vs right:
$6Hz$ *vs* $7Hz$
$7Hz$ *vs* $6Hz$
$8Hz$ *vs* $9Hz$
$9Hz$ *vs* $8Hz$
Each minor block was replicated two times (see Figure 3.5).

Instruction in overt attention: In overt attention, subjects were instructed to directly look at the flickering squares based on the cued direction and press the space key one the cued digit was appeared. As the subjects were not able to look at the central square to acquire the instruction for the next cue, the experimenter guided them for direction and the digit.

Instruction in covert attention: In covert attention, subjects were instructed to fix their eyes at the central square and attend covertly to either flickering squares in the left or right side of the fixation point. Similar to overt attention, the space button had to be pressed as soon as the target digit was appeared in the flickering object.

Instruction in overt and covert attention without flicker: The procedure in this block was very similar to the covert attention with a difference that the objects did not flicker.

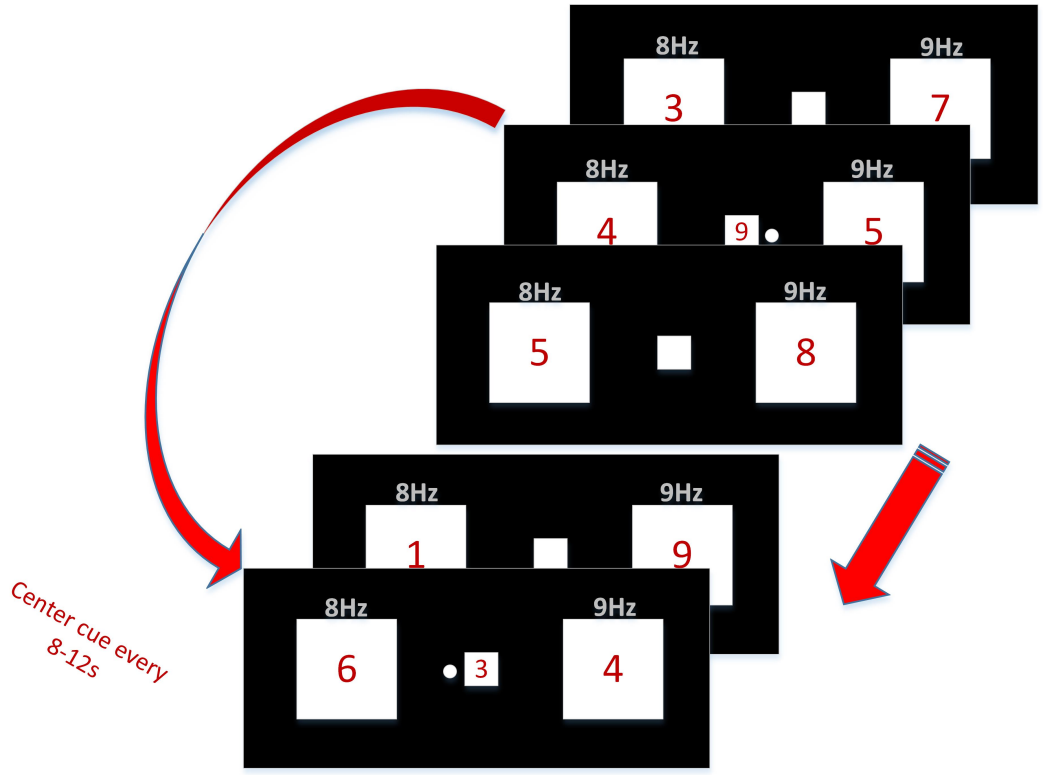

Figure 3.4: Steady-state visual evoked potential (SSVEP) task for visual attention. The task consists of two flickering squared in the left and right of the screen which flicker in two different frequencies. 8Hz and 9Hz are shown in this figure (the frequency values on top of the squares are not shown in the real experiments). Within each flickering square numbers (0-9) appear for 300ms randomly.

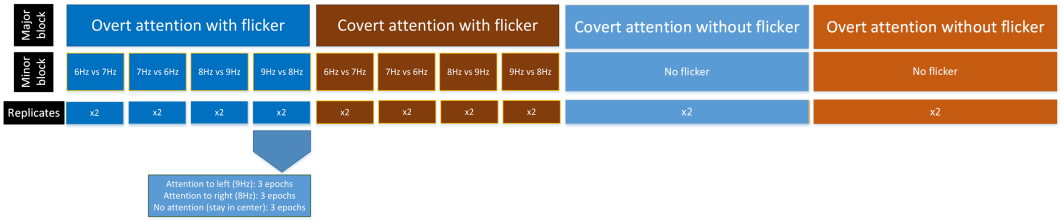

Figure 3.5: The visual task consisted of three major blocks: overt/covert attention with flickers, overt/covert attention without flickers. The first and second blocks contained of four minor blocks with different frequencies and flipped orders of flickers in the left and right side of the screen (e.g. $6Hz$ frequency flickered on the left in $6Hz$ vs $7Hz$ and on the right in $7Hz$ vs $6Hz$). Each minor block was replicated two times (*Replicates*). Within each minor block, subjects had to attend to either left or right (in random manner) or stay unattended while looking at the center of the screen (active rest). This was the same in all replicates, so that, only one box is shown in this figure for illustration purpose.

3.4 Data analysis

The data analysis was performed using EEGLAB toolbox[81] under MATLAB 2014b as well as customized functions and scripts. Below the analysis steps have been delineated.

Data type The data recorded by *Biosemi* EEG setup was saved as **.BDF* files.

Inserting channel locations The coordinates of channels provided by the *Biosemi* was added on the data. Therefore, the exact locations of the channels on the brain topography was identified.

Removing bad data EEG data is always prone to unexpected noise which in some cases can significantly affect all channels. Some example of these noises is moving the entire cap, major muscle contraction (e.g. yawning) or any kind of external major artifacts. These artifacts create a chunk of data which is often very unreliable even after strict filtering. Artifacts were detected in our dataset and removed from the rest of analysis.

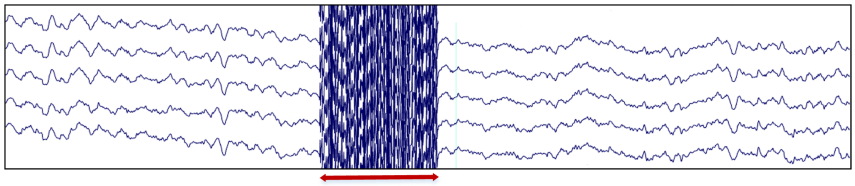

Figure 3.6: Huge noise (indicated by red arrow) which affected entire EEG channels were removed from the dataset

Removing bad channels Existence of noise in some EEG channels is inevitable. Some types of noise such as broken channel or improper contact to scalp persist over entire experiment. In some other cases the extreme noise starts while an experiment is performed which is usually hidden from the eyes of experimenter (e.g. detaching the electrode from the scalp due to dried gel). As this type of noise exist for a long period of time, the related channel(s) are identified and interpolated (using Spherical splines method) to generate a new dataset for the specific channel.

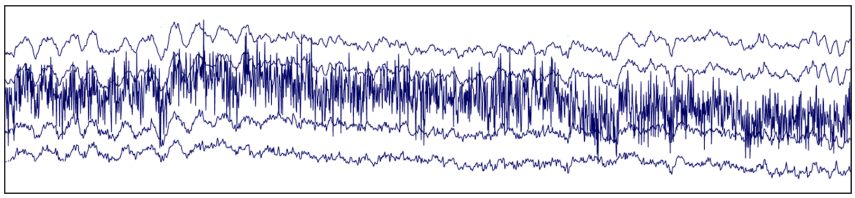

Figure 3.7: A chunk of data which represent a noisy channel among other normal channels

Re-referencing and average referencing In EEG, the recorded voltages in each electrode is relative to the voltages recorded in other electrodes. In principal, the reference electrode can be anywhere; however, it should be carefully chosen as any activity in reference electrodes are reflected in the activity of other electrodes. The best location for the reference

electrode should be far away from a place where the main brain activity comes from. Otherwise, we risk canceling out much of interesting information from the recording electrodes. As referencing is a linear transformation, it is possible to re-reference the already collected data to another electrode. In our experiments, all channels have initially been referenced to the vortex electrode (C_Z) in recording session. They were then re-referenced to mastoid electrodes (as mastoid region is considered to contain signals with least common properties with brain activity pattern). This solves the problem for keeping the signal patterns in each electrodes. In this project we used a modified "average reference" method of Nunez [82] to correct this problem. Since brain currents are dipolar, the integral over the closed head surface for any single- or multiple- dipole configuration is theoretically zero. This provides a basis for calculating a reference independent potentials which have better interpretation as they can be interpreted as potentials measure relative to infinity. This method uses the reference electrode (average of two mastoid electrode to be considered as 129^{th} channel) in addition to 128 electrodes to estimate the average reference. Clearly, V_{129} contains the voltage of the reference electrode relative to itself which is by definition zero.

$$\hat{V}_i = (V_i - V_{129}) - \frac{1}{129}\sum_{j=1}^{129}(V_j - V_{129}) \tag{3.1}$$

where $\hat{V}_i$ is the voltage of electrode after re-referencing; V_i is the voltage of each channel ($i = 1, 2, 3, ..., 128$). Because the sum runs over 129 values and is normalized by 129, V_{129} cancels exactly from this expression. Thus results is reference-independent. It is straightforward to verify that sum of all voltages is zero:

$$\sum_{i=1}^{129}\hat{V}_i = 0 \tag{3.2}$$

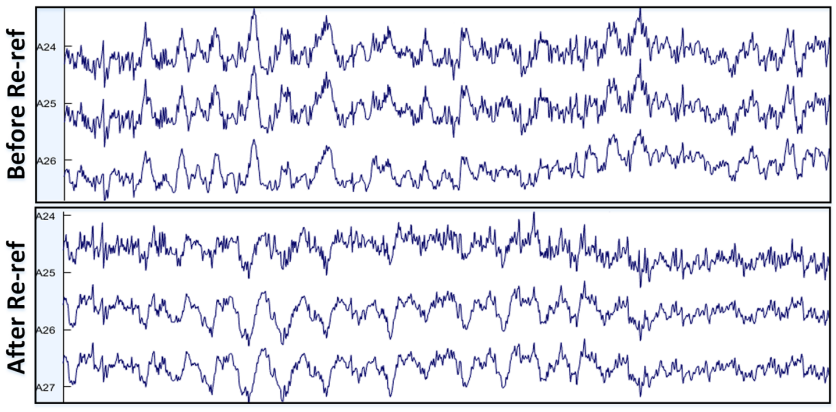

Figure 3.8: Data from all channels are re-referenced from C_Z to average of mastoid electrodes and average-referenced. Upper and lower figure shows the data before and after re-referencing, respectively.

Filtering the raw data During EEG recordings problems with non-physiological signals (artifacts) are common. Some of these artifacts could be eliminated or reduced during the experimental sessions. For instance, the most common artifact is the 50Hz power supply noise. Grounding the subject significantly reduces this alternative current artifact. Also, the length of the connectors and cables were kept short, use of communication devices (cell-phones) was restricted and more importantly the experiments were conducted in a Faraday cage. The artifacts were removed by digital filtering methods. Data from our recordings were band-pass filtered between $3Hz - 80Hz$ with the filter order of 846. Notch filter was not conducted as the 50Hz frequency was far away from our frequencies of interest. This way we also prevented distorting the data around this frequency.

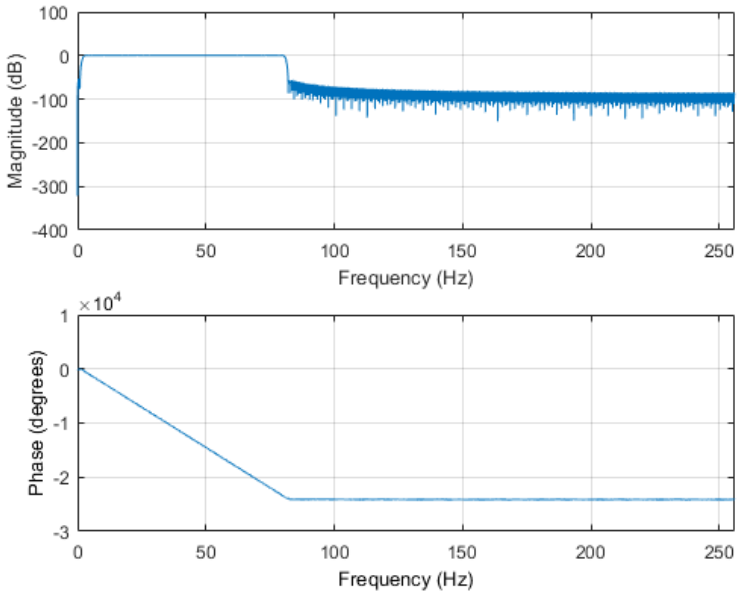

Figure 3.9: Band-pass FIR filter in EEG analysis in the range of 3-80Hz.

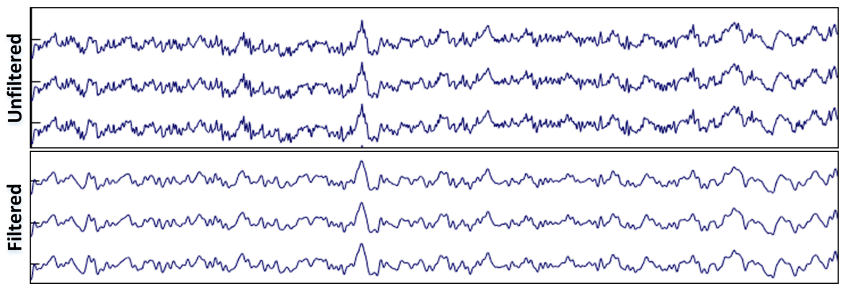

Figure 3.10: Unfiltered and filtered data are shown for the same EEG channels

Data concatenation As each experiment took only 2 min in duration, the data from one experimental day was saved in separate files. These data needed to be prepared for the next step of analysis e.g. independent component analysis that requires larger datasets.

For this aim, the dataset with similar experimental conditions were concatenated to obtain larger data per condition i.e. a single file of 8min duration for each experimental condition ($4 \times 2min$).

Re-filtering the cleaned data The concatenated data has created sharp edges in points where the data was concatenated. In order to smoothen these artificial edges over the entire data, low-pass filtering was conducted.

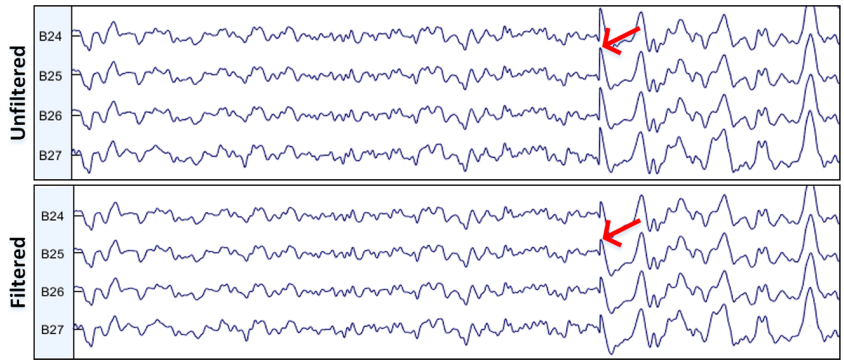

Figure 3.11: Concatenated data: *upper* shows the concatenated data before filtering. Sharp edges appear in point where the data are appended. As the lower figure shows, these edges were removed using a low pass filter.

Chapter 4

Covert and overt attention modulates SSVEP signals

4.1 Introduction

The SSVEP oscillations generate similar oscillations to the flickers in the visual system which can be read using high-temporal resolution recording methods such as the EEG. Numerous EEG studies have shown that SSVEP amplitudes are changed between attentive and inattentive states. Further, covert attention has become an interest for researchers in the field of neuroscience and biomedical engineers to understand its neural mechanisms and its application in assistive technology. Treder and Blankertz[83] explored overt and covert attention based on the event-related potentials (ERPs) task. Although ERPs and SSVEP share some fundamental characteristics, the interpretation of EEG features may vary substantially especially in case of time-course of ERPs and SSVEPs. Walter et al.[84] performed a study by which they explored the effect of covert and overt attention on SSVEP amplitude as well as the topography. They used a task with random-dot-arrays to the left and right of a central fixation point. Dots were flickering in two different frequencies (10Hz vs 12 Hz). Subjects were instructed to directly look at the targets or covertly pay attention to them. Findings showed that over SSVEPs, recorded during overt attention, possessed a higher amplitude compared to covert attention in conjunction with some topographical changes on the scalp. This study, however, disregarded the confounding effect of simple physical activity (see Xu et al.[85]). We argue that observing an enhanced amplitude in overt versus covert attention might be a trivial phenomenon due to foveation in overt attention, giving rise to more powerful stimulation of retinal receptors. Findings by Walter et al.[84] may only specify very few characteristics of covert attention. The same applies also for the study conducted by Kelly et al.[86] where the classification accuracy was reduced when attention is driven in covert rather than overt attention. However, amplitude differences provides only limited information regarding the nature of covert attention and how it can be deployed for different biomedical applications. Amplitude can be varied due to different factors rather than attention *per se*. Moreover, although these studies compared the electrophysiological features of covert and overt attention, none found unique features which characterizes the nature of *covert* attention. In another study by Kelly et al.[86], they aimed to understand the EEG signature of covert attention and when attention is driven by saccade (overt attention) for a spatial cueing task. They used the task with and without distracters. This study showed that although orienting signals during covert and overt attention might be similar in principle, their pattern of activities are very distinct when it comes to deal with distracters.

This indicates that there should be some degree of separability between these attentional orientation in EEG signals.

In this section of the thesis, the aim was to answer the question whether or not there is any measurable distinction between covert and overt shift of attention in human subjects. If positive, what is the specification of covert attention? It is hypothesized, that by identifying the pattern of activity in covert attention, this feature can be used to steer future research in the neuroscientific area. More importantly, this specific feature potentially can be implemented in assistive devices aimed to improve attentional capabilities.

4.2 Materials and methods

Experimental session: Subjects were seated in an adjustable armchair in a distance of 65cm in front of the screen. The circumference of the head was measured to use the proper cap-size on each individual. The electrodes (active electrodes) were mounted on the cap and the conductance was kept below 5kΩ using electrode gel (*Signa gel*). An SSVEP-based task was used in this study (see Figure 3.4 for details).

Analysis of the behavioral data: Subjects were asked to press a *key* on the computer keyboard as fast and as accurate as possible when the target number appeared in the attended flickering square. The reaction times (RTs) were calculated from the onset of the target number till the button is pressed. The RTs in each SSVEP frequency were concatenated across all trials. Therefore, there were two vectors for RTs, one for overt and the other vector for covert attention reaction times. The same way, the missed rates* in each SSVEP frequencies were calculated ($Accuracy = 1 - missedrate$). Unpaired t-tests were performed to compare the parameters (RTs and accuracies) in covert and overt conditions.

Analysis of the electrophysiological data: As we were interested in signal characteristics of the visual area, the data were chosen from three channels (O_1, O_2 and O_Z). The data from these three channels were averaged to enhance the SNR. Epochs of 8s were selected starting from 2s after the appearance of the central cue. The epochs were Fourier transformed and the power spectra was calculated for each trial.

$$X(f) = \sum_{n=0}^{N-1} x(n) e^{-j2\pi fn} \tag{4.1}$$

where $X(f)$ represents the frequency spectrum of the signal $x(n)$, and N is the length of signal. The power of the signal is obtained by:

$$Y(f) = |X(f)|^2 \tag{4.2}$$

From each spectrum, the area-under-the-curve (AUC) for the SSVEPs' fundamental frequency as well as its second harmonic were calculated to quantify the power in those specific frequency bands. The AUC for each selected frequency was calculated as follows:

*Missed rate refers to the number of trials in which the target stimulus was not detected by the subject.

$$A_f = \sum_{m=-l}^{l} \left[Y\left(m + f\frac{L}{f_s} \right) \right] \tag{4.3}$$

where A_f is the AUC of the flicker frequency or its harmonics. l is the number of bins taken to the left or the right side of the frequency of interest (*e.g.* if the window-length of 5 bins is desired, then $l = -2$ which picks the bins of $m = -2 : 2$ centered in the desired frequency. f is the desired frequency (flicker frequency or the 2^{nd} harmonic), f_s is the sampling frequency of the signal and L is the FFT length. This was performed on both harmonics resulting in two vectors of A_{h1} (AUC of the 1^{st} harmonic) and A_{h2} (AUC of the 2^{nd} harmonic) for each trial (8s duration) in which the subject was attending to a certain SSVEP frequency.

Trial-by-trial AUCs were acquired in covert and overt condition in each subject. Therefore, a total of maximum 12 AUCs existed for each condition. These were compared to each other in the 1^{st} and 2^{nd} harmonics.

$$r = \frac{A_{f_{h2}}}{A_{f_{h1}}} \tag{4.4}$$

where $A_{f_{h2}}$ is the AUCs for the 2^{nd} harmonic, and A_{f_1} is the corresponding AUCs for the 1^{st} harmonic. These column vectors exist for each SSVEP frequencies (6Hz, 7Hz, 8Hz and 9Hz) in both overt and covert. If our hypothesis is valid and covert attention generates higher power in the 2^{nd} harmonic than the 1^{st} harmonic, then the ratio of these harmonics should be higher in covert compared to overt condition.

4.3 Results

Results of this study has been partitioned in two section: behavioral and EEG results.

Behavioral results Figure 4.1 shows RTs for all subjects in both attentional condition (overt and covert) and their comparisons. Unpaired t–tests were performed to compare two groups in each subject. Results showed that only in three subjects (subjects number 4, 10 and 14) the RTs were significantly higher with the p-values = 0.013, 0.001 and 0.049, respectively.

Similar to RTs, the accuracies from trials consisting all frequency bands were concatenated in each conditions. The accuracy of performances are also shown in figure 4.2 where each bar indicates the accuracy of button-presses in one subject in all trials within overt and covert conditions. The accuracies are found in two conditions of overt and covert. The means accuracy level across all subjects was 95.02% for overt and 93.87% for covert attention.

Comparison of missed rates – within subjects – between the covert and overt condition showed that the accuracy was lower ($p<0.05$) in covert compared to overt in subject number 4. Opposite result was observed in subject number 14. The accuracies in other subjects did not differ substantially between covert and overt conditions.

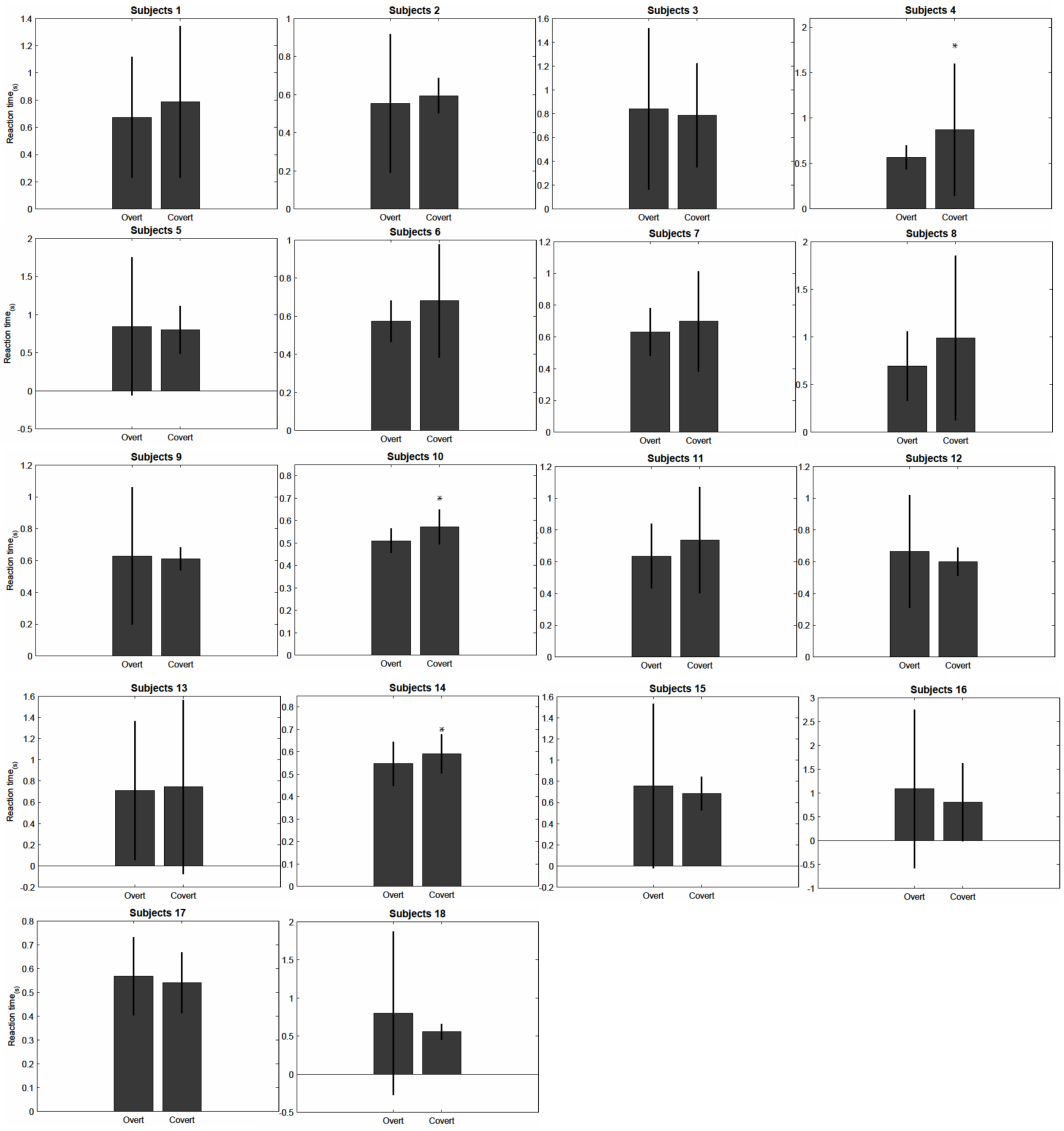

Figure 4.1: **Reaction times:** Subjects were instructed to press the *Space key* as soon and as accurate as possible upon appearing the targets. Reaction times here are acquired when subjects responded to stimuli both in the left and right flickering objects. The mean value of reaction times in each subjects were calculated and the error bars were estimated. Each bar plot is specified for these values in each subject in response to stimuli for overt and covert attention. X-axis indicates for reaction time (s) while y-axis is for type of attention allocated to stimuli (overt vs covert). The reaction times between overt and covert attention were compared using unpaired t-tests. Only in subjects 4, 10 and 14 a significant difference have been observed between two attentional orientation (p-values = 0.013, 0.001, 0.049 for subjects 4, 10 and 14, respectively). * significant ($p<0.05$).

EEG results: higher power of flicker frequencies in overt attention The power of signals were obtained in each trial and the AUCs from the 1^{st} and 2^{nd} harmonics

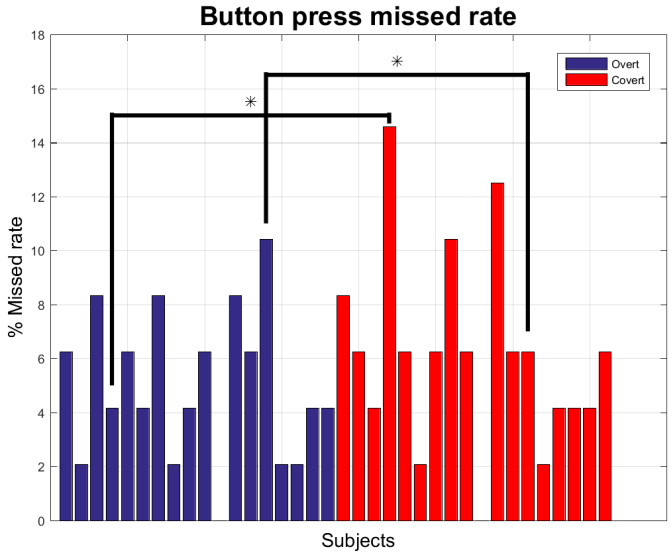

Figure 4.2: The figure shows the percentage of missed stimuli which were ignored or not seen in the attended sides. Each bar indicates a subject (18 subjects). Notice that subject number 11 had 0% of missed rate and it is why it is not shown in the graph. Blue and red bars correspond to overt attention and covert attention, respectively. In an unpaired t−test comparison between overt and covert attention within each subject, only two subjects showed a significant difference: in subject 4 the miss rates increased (p–value = 0.0421) and in subject 14 the miss rate decreased (p–value = 0.0406) in covert attention. * significant ($p<0.05$)

were calculated in the width of 5 bins covering the desired frequency. Comparison of overt and covert conditions in their trial-by-trial AUCs showed that the power of SSVEPs is higher ($p<0.05$) in overt compared to covert attention. This increase was observed in both the 1^{st} (figure 4.3) and 2^{nd} (figure 4.4) harmonics.

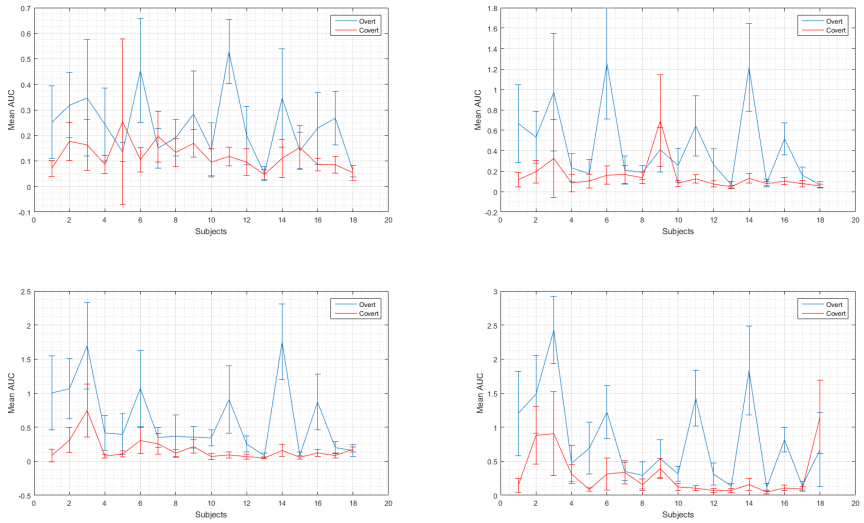

Figure 4.3: AUC differences between covert and overt attention in the 1^{st} harmonic: The mean values (y-axis) of standard deviations of AUCs in each subject (x-axis) is demonstrated. The blue and red graphs correspond to covert and overt attention, respectively.

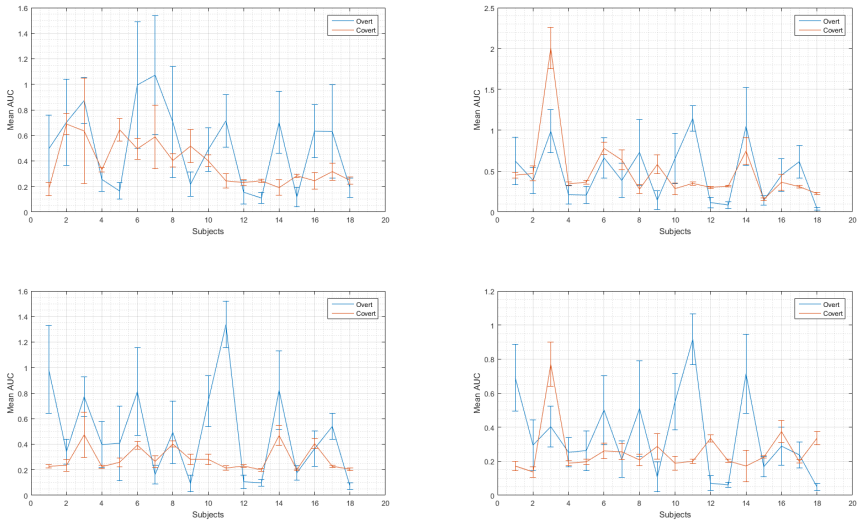

Figure 4.4: AUC differences between covert and overt attention in the 2^{nd} harmonic: The mean values (y-axis) of standard deviations of AUCs in each subject (x-axis) is demonstrated. The blue and red graphs correspond to covert and overt attention, respectively.

EEG results: the 2^{nd} harmonic is greater than the 1^{st} harmonic in covert attention We observed that the amplitude of the 2^{nd} harmonic is consistently larger than the 1^{st} harmonic across subjects. In order to validate this difference, the ratios (4.4) were obtained across both covert and overt trials. We observed that when comparing the ratios between covert and overt conditions, the significant differences occur in considerable number of subjects.

If covert attention could truly enhance the level of second harmonic, then eliminating the flicker would remove this effect. No-flicker trials were used for this aim. The AUCs were acquired in the same frequency bins as control AUCs. The the ratios were acquired in similar way as for the flicker trials. Results showed that the magnitudes of ratios has changed substantially but in less number of subjects compared to flicker trials (figure 4.6). Importantly, in all of these changes, the ratio of overt condition was larger than covert. As there was no flicker in these trials, such variations may be due to spontaneous fluctuations with no link to flicker frequencies. Therefore, the SSVEP frequencies were processed in different ways based on the type of attention allocated to the stimulus.

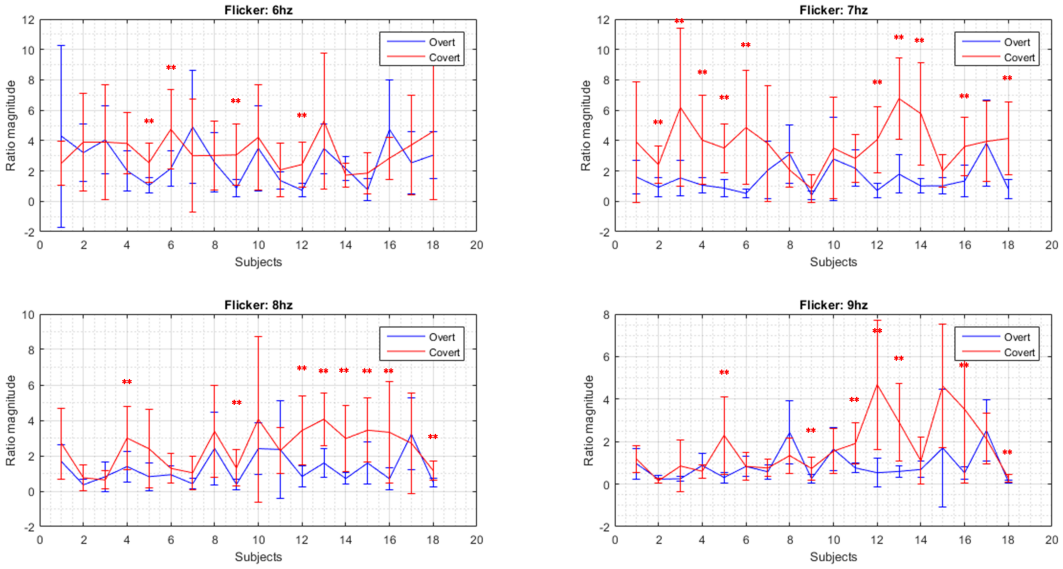

Figure 4.5: The figure shows the ratios of the 2^{nd} to the 1^{st} harmonics in overt and covert trials. This was performed in overall flicker frequencies (6, 7, 8 and 9Hz). Red and blue graphs correspond to covert and overt trials, respectively. x-axes are the number of subjects and y-axes are the magnitude of ratios. * significant ($p<0.01$)

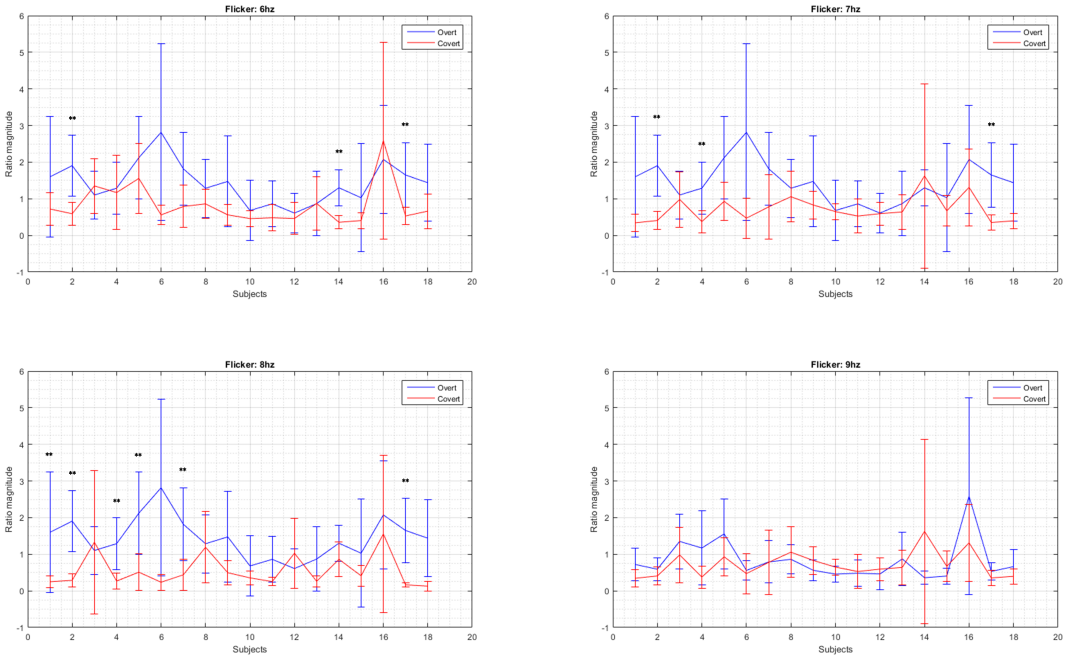

Figure 4.6: The no-flicker trials were taken as control groups. The AUCs of the same frequency bins similar to the flicker were obtained. This figure shows the ratios of the 2^{nd} to the 1^{st} harmonics in overt and covert trials. This was performed in overall frequencies (6, 7, 8 and 9Hz). Red and blue graphs correspond to covert and overt trials, respectively. x-axes are the number of subjects and y-axes are the magnitude of ratios. * significant ($p<0.01$)

4.4 Discussion

The results of this study showed that the frequency response in overt attention is higher in the fundamental frequency and the 2^{nd} harmonic when compared to the responses in covert attention. However, when comparing the magnitude of the 2^{nd} to 1^{st} harmonics covert attention enhanced the 2^{nd} harmonics substantially than the fundamental frequency. A discussion of different aspects of the findings is following below:

Behavioral results: The focus of this study was to find the electrophysiological features. However, also behavioral results were obtained related to RTs and accuracy of responding to target stimuli. The aim of implementing the behavioral section in our task was as a proof of performance for the subjects to make sure that the subjects are well-involved in the task. Results from the RTs indicate that although three subjects showed significantly slower RTs in covert compared to overt attention, the overall vigilance in majority of subjects was similar in both conditions. Although in covert attention eyes are fixed in a location apart from the location of stimulus, yet attention is cued to the right direction in both cases, and therefore, the RTs stayed very similar.

Furthermore, the accuracy level of button-press in response to the onset of target stimuli was significantly higher in *only* two subjects in overt compared to covert attention. The overall accuracies did not vary significantly across the two conditions. The high accuracy level in both conditions indicates that subjects were well-involved in the task and detected

the majority of targets.

Higher power of frequency response was obtained in overt attention: First to be discussed is the higher power of frequency responses in overt attention. This study clearly showed that oscillatory signals are indeed registered much stronger when the person directly watched the flicker stimulus. Some previous studies supported this finding by showing that there is larger amplitude for the presented flicker frequencies when they are attended overtly[59,84,87]. Kelly et al.[87] showed through a similar experiment using flickering checkerboards in different frequencies in the left and right of the fixation cross that the classification accuracy was 20% higher in overt than covert attention. This was due to larger amplitudes of SSVEP frequencies in overt attention. Walter et al.[84] performed an experiment by using random dot arrays (RDAs) distributed within a rectangular aperture. Rectangles were located in the left and right side of the central fixation point. RDAs flickered with 10Hz in the left rectangle and with 12 Hz in the right one. Subjects had to detect a slight change in the luminance of the objects in the attended side and ignore the unattended objects. They showed that stimuli generate the largest amplitude when the stimulus is attended overtly. Overt attention to the objects, recruits the foveal fixation[85,88]. It is well-known that receptors in the fovea have the highest resolution in the visual cortex[89]. This means that the sensitivity to the light is very high. Comparing this characteristic with covert attention which includes the peripheral vision[55] explain the signal strength between these two attentional modulations. With these evidences one could ask to what extend we could rely on signals directed by foveating on the flickering objects as *attention*-modulated signals? This was challenged by previous studies[85,90,91] who induced SSVEP on anesthetized animals. The study by Liang et al.[91] revealed that topological network features in response to SSVEP can still be maintained even in anesthetized brain[90,91]. Further confirmation came when Xu et al.[85] anesthetized rats in their experiment to understand the multiple brain areas that handle the generation of SSVEP in the brain. They examined the link between SSVEP amplitude and the network topological properties for different flickering frequencies. Considering these evidences, we suggest that overt attention may not be a proper feature-generator for the visual attention. This may lead to concerns regarding the interpretation of signals when implementing assistive devices such as BCIs for improving the attention.

The power of harmonics are affected by type of attentional orientation: The present findings showed that different attentional orientation manipulates the output signals differently. Covert attention has little effect on the amplitude of the fundamental frequency; instead, raises the power of the 2^{nd} harmonics substantially.

It has already been shown that the SSVEP responses contain activities not only at the fundamental frequency, but also at the respected harmonics[77]. A response in harmonics of specific frequencies occur at the exact integer multiple of the stimulus frequency ($2f, 3f$, etc.). Norcia et al.[77] argues that if the system generates a perfect sine wave, it contain only the fundamental frequencies. In linear system, only the phase and/or amplitude varies. However, when the system is non-linear it will be manifested in the response of higher harmonics. In this case the time waveforms are not sinusoidal but periodic. It is proposed that because the visual system is non-linear, responses will often be present at multiple harmonics of the stimulus frequency[77]. Regan and Regan[92] suggested that each type of non-linearity has its own pattern of output frequencies and from this pattern one can understand the type of non-linearity within the system. Current study was conducted using the linear methods (Fourier transformation). This method of analysis was widely used in many literature for the similar purposes[93–98]. We suggest that the non-linear methods such as fractal dimen-

sion[99,100] in order to explore specifically the non-linear properties of the SSVEP signals. However, the comparison of linear and non-linear methods of analyzes was out of scope of this thesis. In the section we only compared the signal characteristics between covert and overt attention by keeping exactly the same type of analysis in all conditions.
If we consider the non-linearity principal into the consideration, one could argue that covert attention increases the non-linearity of the visual system. Indeed, the amount of harmonic distortion is a quantitative measure of non-linearity which was used by Tranchina et al.[101]. Our findings showed that distortion occurs in the 2^{nd} harmonic of the SSVEP frequency. This leads one to ask how attention can affect this specific characteristics of the visual system? How attending covertly to an stimulus increases the non-linearity of the system compared to overt attention? One argument could be that this happens due to the nature of response generated by the visual cortex. The cortical cells in visual system are responsible for representing the different aspects of the visual scene. In order for the visual cortex to perform this, it has been equipped with two types of cells: simple and complex. If the cellular responses depends on the stimulus in a linear fashion, the corresponding cell is termed 'simple' and otherwise 'complex'[102]. Simple and complex cells were known for the first time by Hubel and Wiesel[103] and were then confirmed in macaque monkey V1 by Hubel and Wiesel[104] and then De Valois et al.[105]. Later on, the existence of these cells were also found in other mammals[106–108]. The existence of simple cells that selectively respond to the contrasts is necessary for the representation of perceptual organization and the target properties. Furthermore, researches on color vision implicitly assumed the existence of *simple cells* is necessary due to their necessity for numerical computation of edge contrast[109]. These types of neural computations require the linearity that only the simple cells provide. Therefore, one can conclude that the visual system needs simple cells to recognize and represent the basic functions. This explains our findings why overt attention acts more linear than covert attention. When subjects are instructed to move their eye gaze on the flickering stimulus, the physical features dominate in the visual perception. This may cause the simple cells to be activated and generate linear responses. However, when the stimulus is attended covertly, the simple physical features become less important as the stimulus is seen peripherally. The speculation would be that when the attention becomes covert, complex cells start being activated. The role of complex cells in attentional processes is not a novel topic. Ito and Gilbert[110] showed that attention influences the activities of the complex cells in the superficial layers of the visual cortex. McAdams and Reid[111] argued that complex cells have larger receptive fields than simple cells. This is yet another indication that in overt attention, when the target is directly gazed by the subjects, the target fall into smaller receptive fields and therefore, detected by the simple cells. Rather, covert attention with the peripheral vision require larger receptive field, and therefore, recruit complex cells. Our study adds more information based on the continuous stimulation of the visual system using SSVEP. Importantly, one should consider that based on our experimental design, both stimuli (attended and unattended) have fallen into the same receptive field when only one of them was attended covertly. Our results clearly show, how two different orientation of attention may incorporate different neural networks in the brain.

Chapter 5

Spatial distribution of SSVEP activity in covert and overt attention

5.1 Introduction

Because the human visual system is continually exposed with an overwhelming amount of input information, it is extremely crucial to have an effective selection mechanism for filtering out the irrelevant information. This is partly achieved by allowing the visual system to process information which are relevant to the current intention and disregard the non-interesting stimuli (distracters). These information compete to take the behavioral control of the organism at every moment. Competition can be affected by the type of attentional shifts which is conducted in two ways. From the neural structural point of view, it has been suggested that the two types of attentional shifts are very similar. This has been explained by the premotor theory of attention, where covert shift of attention is conducted by similar brain areas, with a difference that the eye-movement is not taken place when attention is driven covertly[48]. Accordingly, the overlapping networks for these two attentional shifts have been shown in electrophysiological[112] and neuroimaging[39,113] studies. Some single-unit studies demonstrated that there is a distinct neural population, *e.g.* within frontal eye field which responds differently in covert attentional processes than in attention which is followed by saccades[114,115]. Beauchamp et al.[116] showed that overt shift of attention engages higher level activation in fronto-parietal cortices compared to covert attention. Moreover, overt attention has been shown to be modulated by cerebellum; whereas, such an indication has not been shown for covert attention[117]. A single unit recording study in monkey showed that even subcortical regions such as intermediate layer of superior colliculus are part of a shared network for covert and overt attention[118]. Although the activation of subcortical areas are not directly measurable by EEG, it is expected that the outcome of the complex activities in subcortical areas is summed up in EEG measurements. In a recent study by Walter et al.[84], fourteen human subjects performed a flickering random dot point visual task. During the task, the luminance of the flickering dots was decreased/increased occasionally for a short time. Subjects were instructed to respond to luminance decrements at the attended side. This study found that the topographical distribution in overt attention was more located in the early visual areas compared to covert attention. In addition, despite the fact that different studies have used various task to measure the topographical signature of these two types of attentional orientation, to our knowledge there was no other study -

by the time of starting this project - using continuous external oscillatory stimulus in order to track the scalp distribution of covert and overt attention.

One method to measure the representation of external stimuli in the nervous system in a continuous way is to use frequency tagging. In this technique, two or several objects on the computer screen flicker in different temporal frequencies generating the SSVEP. These temporal frequencies can be detected using the EEG [119,120]. It has been shown that the power of SSVEP frequencies in the brain varies as a direct function of allocated level of attention[55,121–123]. The amplitude of a specific SSVEP frequency is enhanced when this frequency is attended by the subject. Using different temporal frequencies is a sophisticated method to measure the sustained attention based on how strong these frequencies are represented in the corresponding neural substrates.
As a primary aim in this part of the project, we hypothesized that covert, unlike overt attention is less contaminated by the physical characteristics of the flickering stimuli. Therefore, the detected changes in activity over the scalp may be a better representation of attention function rather than the stimulation by simple physical features. The representation of SSVEP frequencies in covert attention are most likely to be gated through high-level cognitive functions. As in covert attention the eyes are fixed in a location away from the main stimulus, the input of physical features (in our case light intensity) are equalized from attended and unattended stimuli in covert attention, and therefore, the power increment/decrement of attended/unattended flickers depends on subjects' ability to gate the information mentally. Thus, scalp distribution of activities during covert attention may have higher association with brain processes which are specifically conducted in attention.

The second aim of this study was to observe the overall pattern of activation in different neural networks regardless of frequency tagging (SSVEP frequency detection). While the primary indications of SSVEP responses are expected from visual cortex, yet some studies showed that SSVEP representation can also be seen in other brain regions [124]. Ding et al. [64] argued that several networks are involved based on factors such as the range of flickers and type of spatial allocation of attention. However, in a latter study, the stimuli was located in several concentric circles with varying positions. Subjects were instructed to look for a certain target (triangle) among several non-targets, all located within a circular ring. However, it is possible that the activity of different brain regions shown in Ding's study may be contaminated due to the *search function* by moving eyes around the circle. Other studies have shown that attention-modulated SSVEP power is distributed more broadly over the scalp with least lateralization. Dipole modeling indicated that attentional modulation of flicker frequencies was taking place in ventral and lateral extra-striatal visual areas in occipital-temporal cortex[55,125].

5.2 Materials and methods

5.2.1 Experimental session

A total of 21 subjects participated in the experiment. From this the data from three subjects was discarded from further analysis due to high noise contamination of majority of channels, low precision in response to target stimuli or any other reasons that made data useless for the analysis. Out of the 18 subjects (11 females) none was left-handed and their age-range was between 24 to 41 years.

High-resolution 128-channel EEG (*Biosemi*) was used for the data recording. Electrodes

were positioned according to the ABC system (figure3.2). Impedance of the recorded channels were kept below 5kΩ. Signals were digitized at 512Hz and referenced to the vertex in the recording session. In addition to scalp electrodes, eight external electrodes (figure 3.1) were used for the purpose of reference electrodes and recording the EOG and pulse data (see section 3.1 for details).

Participants were seated in a quiet room with dimmed light. EEG cap was mounted consistent with the head-sizes. The quality of channels were double checked before the experiments and bad connections were corrected to the best. Subjects were advised that they could pause the experiment for break or discontinue without giving reasons. As participants were involved in a visual task, we made sure that their sight was normal or corrected to normal. Individuals with contact lenses were provided Saline solution (Sodium chloride 0.9%) to prevent dry eyes. The task was designed based on the SSVEP protocol and programmed in Cogent toolbox under MATLAB 2013b,thoroughly explained in the section 3.3.

5.2.2 Data analysis

Independent component analysis: ICA was applied to parse EEG signals into their spatially static, maximally independent components (ICs) [126]. Before performing the ICA, all artifacts (possible eye movements, EMG, etc.) were removed from the EEG recordings from all channels. In addition, the channels with persistent artifact (e.g. broken channels) were removed and the data was recovered by interpolating the surrounding channels. In ICA, finding N stable components from N_c-channel data requires more than θN^2 sample points in every single channel. N_c is the number of channels. A value of $\theta \geqslant 30$ is recommended to obtain an optimal ICA decomposition:

$$\theta = \frac{N_p}{N_c^2} \tag{5.1}$$

where N_p is the number of points in each channel which is fed to ICA decomposition. In order to increase the value of θ, we concatenated the data after artifact removal to obtain a larger dataset. Therefore, ICA would return more stable decomposition with larger datasets. Having components with common spatial maps also makes it easier to compare different component behaviors across different groups. We merged the data containing both flickering frequencies presented simultaneously in one session (e.g. 6&7Hz *or* 8&9Hz) in the same condition (overt *or* covert attention). Once ICA was performed on the merged data, epochs were extracted based on the flicker frequencies. In this study we focused to compare the topographical distribution of oscillations in overt and covert attention. For this aim, we were not interested in splitting the data to each single flicker frequency and in each overt and covert condition to prevent generation of too many redundant possibility in statistical comparisons. Four major datasets that used are:

- Overt 6&7Hz
- Covert 6&7Hz
- Overt 8&9Hz
- Covert 8&9Hz

The length of each epoch was 8s starting at the onset of the *central cue*. Epoched ICA data was then used to feed the equivalent current dipole computation.

Event-related spectral perturbation: The ICA-ed data were examined to detect the stimulus and response-induced changes in the EEG spectrum using event-related spectral perturbation (ERSP) transform[127] for each clustered independent data component by means of EEGLAB[128]. ERSP shows changes (in dB) from the baseline in spectral power across a certain frequency range (3-45 in this experiment). In time-frequency analysis, we used Hanning windowed sinusoidal wavelets of 3 cycles at lower frequencies (3Hz), rising linearly to about 15 cycles at higher frequencies (45Hz). This pattern of wavelet transform was chosen to optimize the trade-off between the temporal resolution at lower frequencies and stability at higher frequencies[129].

Equivalent current dipole modeling: This is a source modeling method providing a sophisticated estimation of the location of relevant brain activity recorded by the EEG. The EEG records small changes in the electrical currents caused by transmission of ions among a large population of neurons. Therefore, the amount of possible current distributions that leads to signals and can be picked up by by EEG channels are theoretically infinite. So, although the signals are seen in the EEG recordings, their sources are yet unclear. Equivalent current dipole modeling is a method to reconstruct the sources. It provides a single theoretical current with certain directions at specific parts of the brain that would most likely indicate the real source of the brain activity. In other words, when the local coupling density of both excitatory and inhibitory neurons in the cortex is high, local field potentials become synchronous and create measurable EEG signal. These local field potential currents tend to extend through a compact spatial domain - roughly speaking, a patch of cortex of unspecific extend. The partially synchronized activities within the cortical sources, produce far-field potentials throughout the entire brain which eventually extend to the scalp. The distribution of the scalp electrical field produced by cortical sources is similar to a small dipolar potential elements whose geometry is like a miniature battery oriented perpendicular to the cortical surface. This small battery is termed as equivalent dipole for the cortical sources[129].

`DIPFIT` functions within EEGLAB[130] were used to compute an equivalent current dipole model of epoched data that best explained the scalp topography of each IC using a four-shell spherical head model for each component (BESA). If the best-fitting equivalent current dipole model had more than 15% residual variance (RV%) from the spherical forward-model scalp projection (a total of 128 electrodes) or if the topography of the IC was clearly reflecting the non-brain activity (e.g. eye-movement artifact) they were removed from further analysis. Next, electrophysiological sources were clustered across subjects using k-means clustering method on vectors which code differences in equivalent dipole locations and power spectra. The resulting joint vector was reduced to 10 principal dimensions using principal component analysis[131,132].

Source analysis across subjects: Our interest was to find the common pattern of activities across subjects. We compared only those dipoles whose RV $\leqslant$15%. This was done once the current dipoles were uploaded into the `STUDY design` of EEGLAB (see Appendix: Figure 7.1). The study were then designed to enable us to compare overt and covert groups across all subjects (see Appendix: Figure 7.2). Based on the `STUDY design` we ran the pre-computation on the dipole data. The pre-computation measures different parameters such as power spectrum, ERSPs and scalp maps in all subjects and all groups (overt or covert) (Appendix: Figure 7.3). Following the pre-computation, the data were pre-clustered. This is because following ICA or any other linear decomposition method, there is no easy way to identify and compare one component from one subject with that of from another subject. Two ICs from two subjects might vary or resemble in many ways depending on different measures like power spectra, scalp map, ERSP, etc. Therefore, there are several possible

distance measures of similarities and many ways to combine the activity measures into a global distance measure to estimate the similarities between different components. The aim of the pre-clustering was to establish a global distance matrix (5.2) specifying the distances between components which will be later on used by the clustering algorithm.

$$M = \begin{pmatrix} a_{1,1} & a_{1,2} & \cdots & a_{1,n} \\ a_{2,1} & a_{2,2} & \cdots & a_{2,n} \\ \vdots & \vdots & \ddots & \vdots \\ a_{m,1} & a_{m,2} & \cdots & a_{m,n} \end{pmatrix} \tag{5.2}$$

where M is the global distance matrix with distances between components which is used by the clustering algorithm. m corresponds to the number of selected components in all subjects and n is the dimensionality.

As the distances are arbitrary, to estimate how far different measures (power spectrum, ERSPs, dipole models and scalp maps) are from each other, principal component analysis (PCA) was used to reduce the dimensionality of selected parameters (Appendix: 7.4). This way we reduced the dimension of the data by maximizing the variances. The principal dimensions were normalized to the location and activity measures in order to have their matrices equivariant across the measures. Finally, as we were interested in topography of the activations based on the dipole positions and orientation, the location of the current dipoles were assigned with higher weights in pre-clustering. Different parameters for pre-clustering were as follow:

- **Spectra:** The power spectrum is calculated based on the subtraction of the mean spectral values of point-by-point spectrum in selected frequency range (in our case 3-45Hz)

$$X_{(out)} = X_{(in)} - \left| \frac{1}{N.k} \sum_{i=1}^{N} \sum_{j=1}^{k} |X_{(in)i,j}|^2 \right| \tag{5.3}$$

  where X_{out} is the mean-reduced power spectra for one subject in one trial and X_{in} is the original power spectrum of the same subject, N is the number of subjects, k is the number of trials and $X_{(in)i,j}$ is the Fourier transform of the signal.

- **Scalp map:** This option in EEGLAB includes the information from scalp map in the component cluster location.

- **ERSPs:** This computes the time-frequency decomposition of each component.

Clustering: Following the pre-clustering, the data was processed using the k-means clustering method. In this step, the algorithm first estimates the number of clusters by taking the mean of number of elements of the vector which indicates the selected components for clustering (this selection has already been determined in the pre-clustering step):

$$C = \left\lceil \frac{1}{NM} \sum_{i=1}^{N} \sum_{j=1}^{M} |P_{ij}| \right\rceil \tag{5.4}$$

where C is the estimated number of clusters, N is the number of subjects, M is the number of groups (covert and overt in our case) and $|P|$ is the cardinality of the vector containing the selected components (number of selected components).

5.3 Results

The equivalent current dipole modeling extracted the locations of dipole for all ICs projected into a standard brain space (Figure 5.1). Each dipole shows the possible location where the activity most likely come from and the orientation of those activities. Figure 5.1 illustrates an example outcome of equivalent current dipole modeling on the head model.

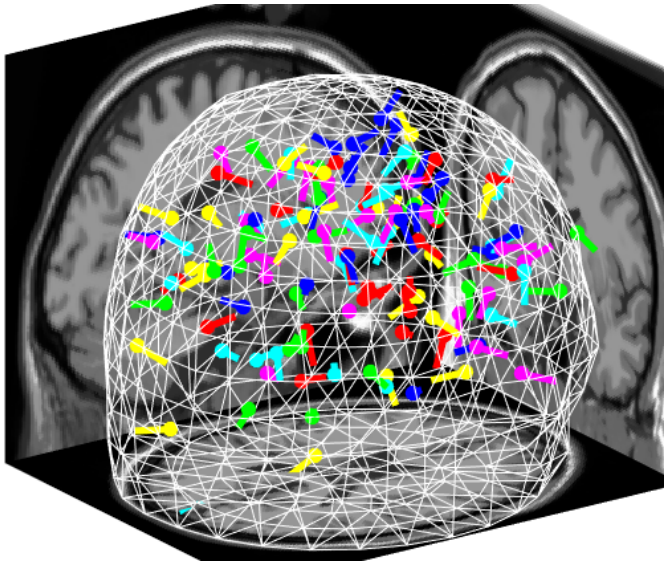

Figure 5.1: All dipoles with residual values of less than 15% are demonstrated on the head model. Each dipole corresponds to one independent component (maximum 128 dipole in this case) which indicates the possible source of brain activity. Dipoles' orientations is also been shown.

Each dipole in figure 5.1 corresponds to one IC. ICs which were selected based on their RV% (RV $<$ 15%) were included in the clustering step. Figure 5.2 shows an example of selection criteria for all dipoles in one subjects.

The parameter measures from the selected components were collected in one global matrix where the rows indicate for all selected components in all subjects and columns indicate the 10 dimensions we chose for our pre-clustering. Then the principal components (PCs) of selected components across groups (covert & overt) and subjects in multiple dimensions were obtained to find the largest variability. The k-means clustering was then performed on the data with PCs. These components are then projected on the head-model:

5.3.1 Topographical results

The components were clustered by their similarities in 3D dipole locations as well as features of scalp maps, power spectra and ERSPs. We had two major groups for comparisons: (1)

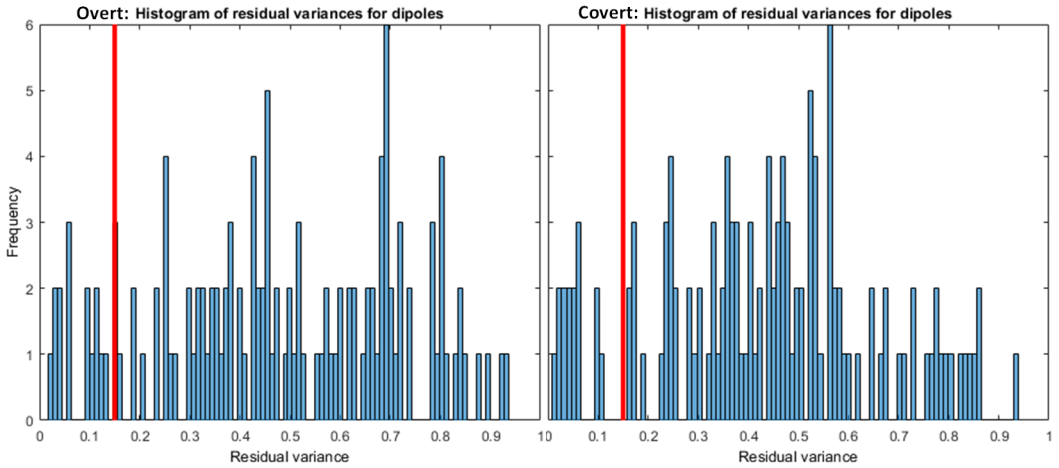

Figure 5.2: Histogram of residual variances (RVs%) for different dipoles (the number of dipoles is equal to the number of independent components). The red line (RV = 15%) shows the threshold for the component selection for clustering. Figure corresponds to the overt (left) and covert (right) attention when attending to 6&7Hz across all subjects. The number of selected components for the clustering was 9 for overt group and 8 for covert group.

Covert *vs* overt in merged 6&7Hz data, and (2) Covert *vs* Overt in merged 8&9Hz data. The first and the second groups consisted of a total of 24 and 23 clusters, respectively. In both cases, the first cluster correspond to pre-clustering and the second cluster was the outliers which did not fit into any other cluster or simply was located outside of the brain.
We identified 4 clusters for 6&7Hz (Cls 5, 13, 14 and 18) and 5 clusters for 8&9Hz (Cls 4, 5, 19, 22, 23) which covered the frequencies of interests. Results from different analyzes have been illustrated in figure **??** through figure 5.13. To initiate interpretation of the results following the clustering, first the power spectra were visually inspected to observe their behavior in response to the SSVEP frequencies or other prominent and consistent activities. We clearly observed the SSVEP frequencies along with their second harmonics in the power spectral analysis in data acquired from 6&7Hz and 8&9Hz. Each graph of power spectrum corresponds to the mean of the number of $trials \times subjects$. The maximum number of trials was 24 whereas the number of subjects varied based on the cluster selection (See table 5.3.1). The same averaging was also done for ERSPs in each cluster.

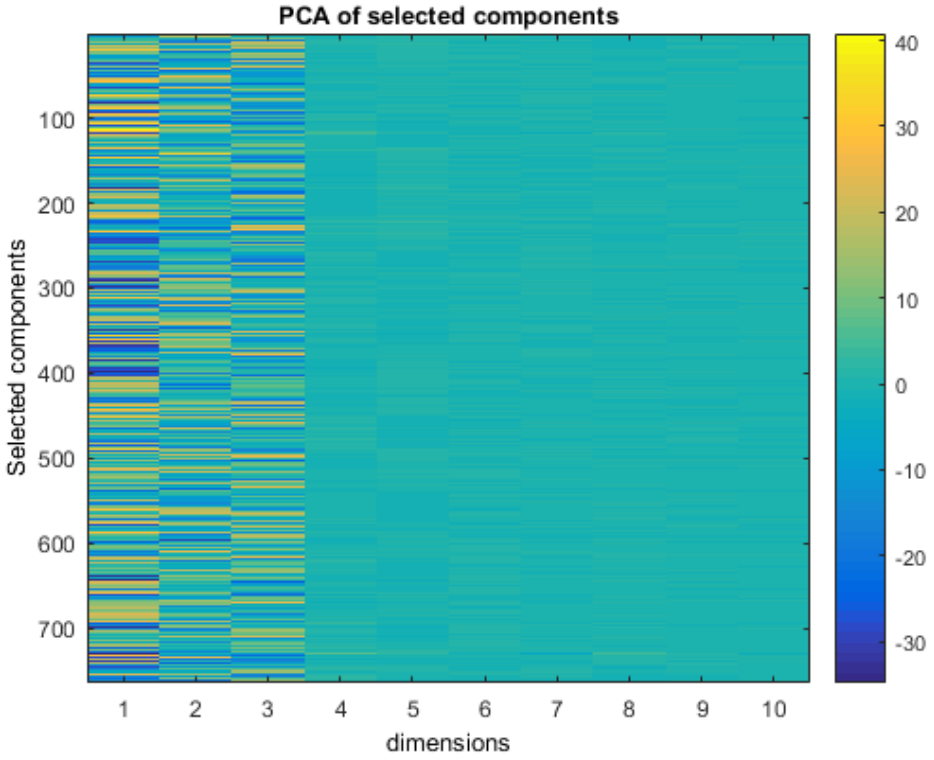

Figure 5.3: Result of PCA from all selected components across subjects. The matrix of 764×10 above y-axis corresponds to the data for the number of selected components in all groups (overt & covert) and all subjects; whereas the x-axis is the number of dimensions defined in the pre-clustering. Following PCA, the first three components (first three columns) show the highest variances.

Number of subjects (out of 18) in selected clusters		
Cluster number	No. of subjects (6&7Hz)	No. of subjects (8&9Hz)
Cls04	–	13
Cls05	14	14
Cls13	11	–
Cls14	13	–
Cls18	11	–
Cls19	15	12
Cls22	–	14
Cls23	–	15

- Cluster 5, 6&7Hz shows larger response on SSVEP frequencies in overt attention in both harmonics (figure ??.A). However, due to α-wave domination, the power appears

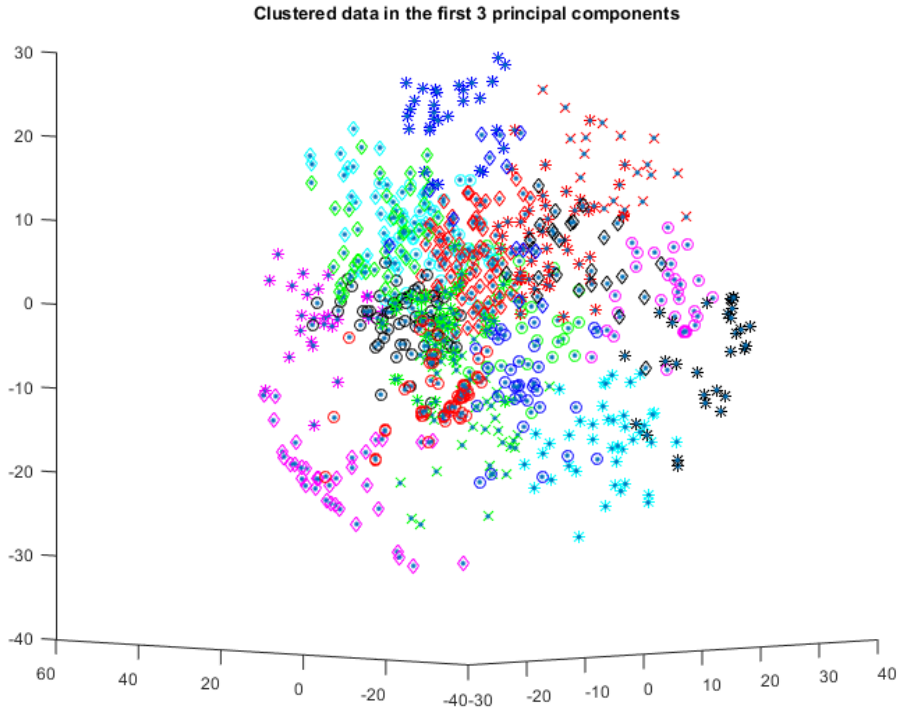

Figure 5.4: An illustrative figure for k-means clustering. The data is drawn from the first three principal components of all selected components across subjects . Data are clustered into 20 clusters illustrated by different colors and symbols.

higher in ERSP (figure ??.B). In this figure the power of the fundamental frequencies (6&7Hz) are clearly higher in overt attention although it is not significant. The significant difference ($p<0.01$) corresponds to the frequency range of 9-14Hz which is higher in covert attention. The dipole is very similar in both attention types which covers the occipital regions with MDC* of $X = 21, Y = -91, Z = -16$ for covert and $X = 22, Y = -92, Z = -17$ for overt.

- Cluster 14, 6&7Hz: Power spectral analysis (figure 5.7.A) in this cluster shows a peak in α-range in both covert and overt attention along with the SSVEP frequencies and their harmonic. In ERSP (figure 5.7.B) overt attention shows stronger ($p<0.01$) frequencies in the range of 6Hz and 7Hz than covert attention. In addition, some high frequency oscillations is also observed significantly higher in overt compared to covert attention. These oscillations are shown to be originated from similar sources (figure 5.7.C-D) in dipole modeling (covert:$X = 39, Y = -67, Z = 25$; overt: $X = 32, Y = -60, Z = 11$) as well as the scalp map distribution covering the right occipital area.
- Cluster 18, 6&7Hz: In this cluster (figure 5.8.A-B), flicker frequencies and their harmonics are obviously seen in both spectrum for covert and overt attention. The oscillations in the α-range shows a prominent peak where the second harmonics of the flicker frequencies (12&14Hz) are mounted on it. In ERSP, the frequency range

*mean dipole coordinates

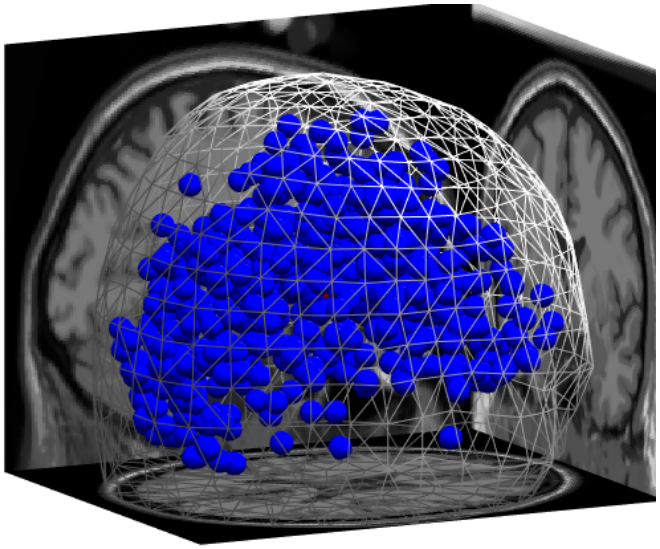

Figure 5.5: The selected clusters in the pre-clustering step was overlaid on the 3D head-model. A total of 752 ICs (each blue sphere denotes for one IC) has been shown here.

of 8-13Hz has been increased significantly ($p<0.01$) overall the block in the covert than overt attention. Exploring the source of activity in dipole positions (figure 5.8.C-D), indicates that sources of activities are located more superficially in the visual cortex ($X = 13, Y = -80, Z = 32$) located in covert attention. Whereas, it originates from deeper structures of visual cortex such as cuneus and precuneus ($X = -15, Y = -51, Z = 5$) in overt attention. The representation of activity on the scalp map is more local in the visual cortex when attending covertly and more distributed over larger area of occipital region in overt attention.

- Cluster 13, 6&7Hz: This cluster has been collected based on the α-activity (figure 5.9.A-B). The increase in this frequency band (*app.* 8-12Hz) is shown in both covert and overt attention. The ERSP analysis showed the persistence of this activity over all the block of 8s in both attentional conditions with no significant different in bootstrap of $p<0.01$. Source localization analysis, however, indicates different sources of activities between covert and overt attention. The mean dipole position (figure 5.9.C) for covert attention shows that activity comes from parietal regions stretched in some subjects to central sulcus ($X = -23, Y = -11, Z = 60$); whereas, this activity drifted into deeper layers around thalamus ($X = 29, Y = -37, Z = 16$). The scalp map investigation shows that the α-oscillations are projected on the left parietal region in covert attention while these oscillations are summed up and represented on the right visual cortex in covert attention.

- Cluster 4, 8&9Hz: This cluster demonstrates the spikes in the flicker frequencies (8&9Hz) and their second harmonics (figure 5.10.A). The intensity of these frequencies appear to be non-significant over the time-period of 8s blocks across subjects. Corresponding activities are located (figure 5.10) in the deeper structures ($X = 20, Y = -1, Z = 2$) – associated with the thalamic area – in the covert attention; whereas, the activation source is estimated on the calcarine cortex ($X = -24, Y = -91, Z = -18$) in overt attention. The scalp distribution is demonstrated in the lower row of figure 5.10 in which the outcome of covert attention is shown in the right frontal regions,

whereas in overt attention the scalp distribution is focused more on the occipital region.

- Cluster 5, 8&9Hz: Spectral analysis of cluster 5 indicates larger power (figure 5.11.A-B) for the flicker frequencies and their harmonics in overt compared to the covert attention. An increase of α-oscillations is also obvious in both attentional conditions although it is more prominent in covert attention. Unpaired t-tests of ERSPs for both conditions showed that attending overtly increased the power of second harmonics significantly ($p<0.01$) compared to the covert attention. In α-range, the difference was restricted to a few seconds at the start of the block which is significantly higher in covert attention ($p<0.01$). The location of dipoles *figure **??** and scalp distributions are similar in both attentional conditions located on the visual cortex.
- Cluster 19, 8&9Hz: The power spectral analysis in the cluster 19 shows a similar spectrum to the cluster 4 (8&9Hz) in the range of SSVEP frequencies (figure 5.12.A-B). However, the difference appears in lower and higher frequencies with significantly ($p<0.01$) higher power in overt compared to covert attention. The sources corresponding to activities in covert attention is cuneus ($X = -27, Y = -74, Z = 19$) and in overt is in deeper structures ($X = 24, Y = -21, Z = 25$) – the across subjects' mean dipole position indicates the cingulate gyrus (figure 5.12.C-D).The scalp map representation shows the activity in the parietal area for covert and frontal-parietal areas in overt attention.
- Cluster 22, 8&9Hz: We observed identical results for the power spectral analysis as well as ERSP analysis in both covert and overt attention where the SSVEP frequencies were obviously present in both conditions (figure 5.13.A). Plotting the data in time-frequency domain (ERSPs) shows high power in the frequency range of 7-13Hz with dominant intensities in 8Hz and 9Hz of flicker frequencies (see color coded ERSPs in figure 5.13.B). However, the intensity of these frequencies did not differ significantly between the two attentional conditions. The location of the activities was also identical in both conditions with distribution in the occipital-parietal area.

Table 5.1: Mean dipole coordinates and their RVs (covert vs overt 6&7Hz)

	Covert				Overt			
Cluster No.	X	Y	Z	RV%	X	Y	Z	RV%
Cls 05	21	-91	-16	5.98	22	-92	-17	8.10
Cls 13	-23	-11	60	7.29	29	-37	16	8.37
Cls 14	39	-67	-25	7.07	32	-60	11	4.20
Cls 18	13	-80	32	8.60	-15	-51	5	8.59
Cls 19	-6	-63	38	7.63	10	-27	-9	10.26

Table 5.2: Mean dipole coordinates and their RVs (covert vs overt 8&9Hz)

	Covert				Overt			
Cluster No.	X	Y	Z	RV%	X	Y	Z	RV%
Cls 04	20	-1	2	8.37	-24	-91	-18	5.00
Cls 05	19	-94	-9	8.29	17	-96	-2	7.82
Cls 19	-26	-74	19	8.37	24	-21	25	9.48
Cls 22	38	-70	2	6.04	53	-48	-2	8.47

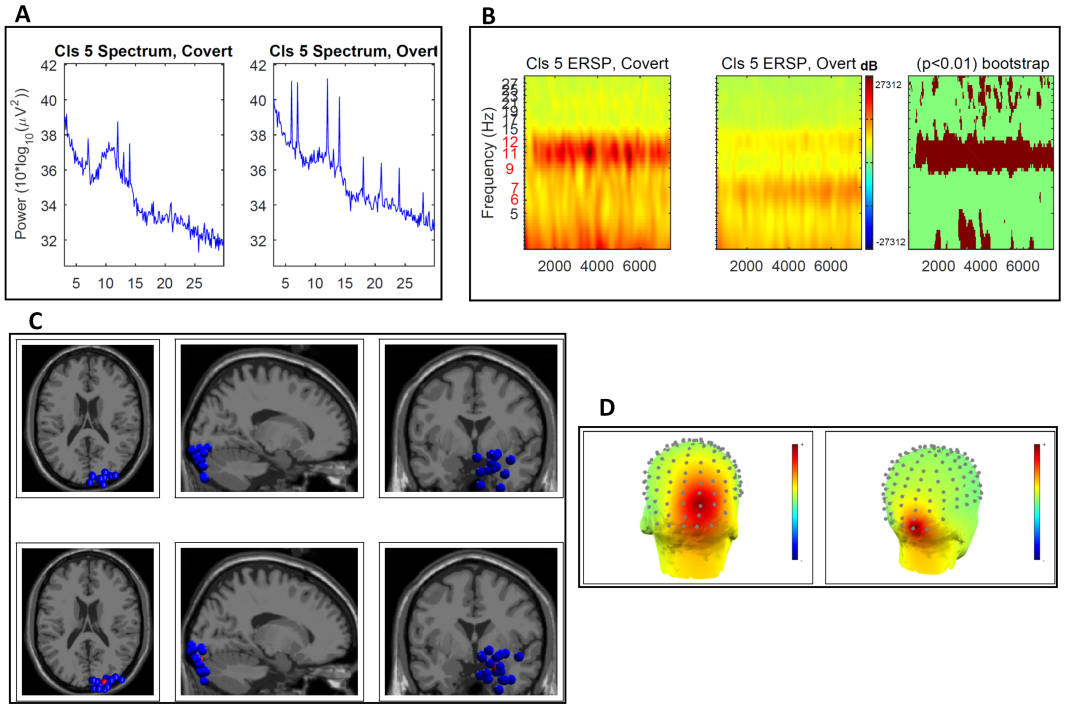

Figure 5.6: Cluster 5; covert *vs* overt attention to 6&7Hz: ***(A)*** The grand average of the spectral analysis of covert (left) and overt (right) attention. The X-axis is the frequency displayed in the range of 3-30Hz; the Y-axis is the power of frequencies. ***(B)*** Mean ERSP across 14 subjects during covert (left) and overt (middle) attention. Bootstrap in $p<0.01$ level (right) shows significant difference between ERSPs in two adjacent windows. Red pixels in the lower right figure show the significant points in corresponding time and frequencies between covert and overt conditions across subjects. Overt attention shows some activity in the range of 1^{st} harmonic (6&7Hz); however, the activity in the α-range was significantly higher in the covert compared to overt attention. Time points (blocks of 8s) are shown in the X-axis while the frequencies in the range of 3-30Hz is demonstrated in the Y-axis. ***(C)*** Equivalent current dipole models when subjects attended 6&7Hz flickering stimuli *covertly* (upper row) and *overtly* (middle row). The location of dipoles are shown in horizontal (left), sagittal (middle) and coronal (right) sections. Each blue sphere corresponds to a single equivalent current dipole for a single IC. The red sphere is the mean coordinate of all dipoles. ***(D)*** 3D scalp topography of the activity in covert (left) and overt (right) attention. This figure is the scalp-map projection of the activities most probably originated from the dipoles shown in this figure. The sources of activities in both dipole models and 3D scalp maps were consistent across 9 subjects in covert and 13 subjects in overt attention. Electrodes are demonstrated over the scalp which are located based on the *ABC* system.

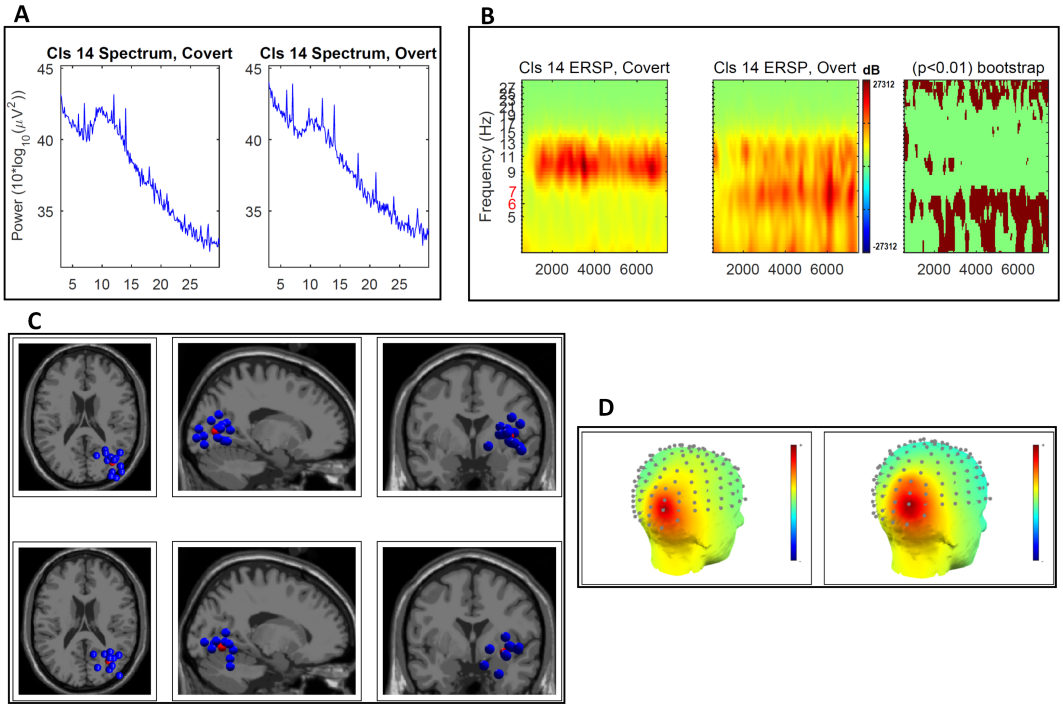

Figure 5.7: Cluster 14; covert *vs* overt attention to 6&7Hz: ***(A)*** The grand average of the spectral analysis of covert (left) and overt (right) attention. The X-axis is the frequency displayed in the range of 3-30Hz; the Y-axis is the power of frequencies. ***(B)*** Mean ERSP across 13 subjects during covert (left) and overt (middle) attention. Bootstrap in $p<0.01$ level (right) shows significant differences between ERSPs in two adjacent windows. Red pixels in the lower right figure show the significant points in corresponding time and frequencies between covert and overt conditions across subjects. The power of frequency in the range of 6 and 7Hz was higher in overt than in covert attention. Time points (blocks of 8s) are shown in the x-axis while the frequencies in the range of 3-30Hz is demonstrated in the Y-axis. ***(C)*** Equivalent current dipole models when subjects attended 6&7Hz flickering stimuli *covertly* (upper row) and *overtly* (middle row). The location of dipoles are shown in horizontal (left), sagittal (middle) and coronal (right) sections. Each blue sphere corresponds to a single equivalent current dipole for a single IC. The red sphere is the mean coordinate of all dipoles. ***(D)*** 3D scalp topography of the activity in covert (left) and overt (right) attention. This figure is the scalp-map projection of the activities originated from the dipoles shown in this figure. The sources of activities in both dipole models and 3D scalp maps were consistent across 13 subjects in covert and 8 subjects in overt attention. Electrodes are demonstrated over the scalp which are located based on the *ABC* system.

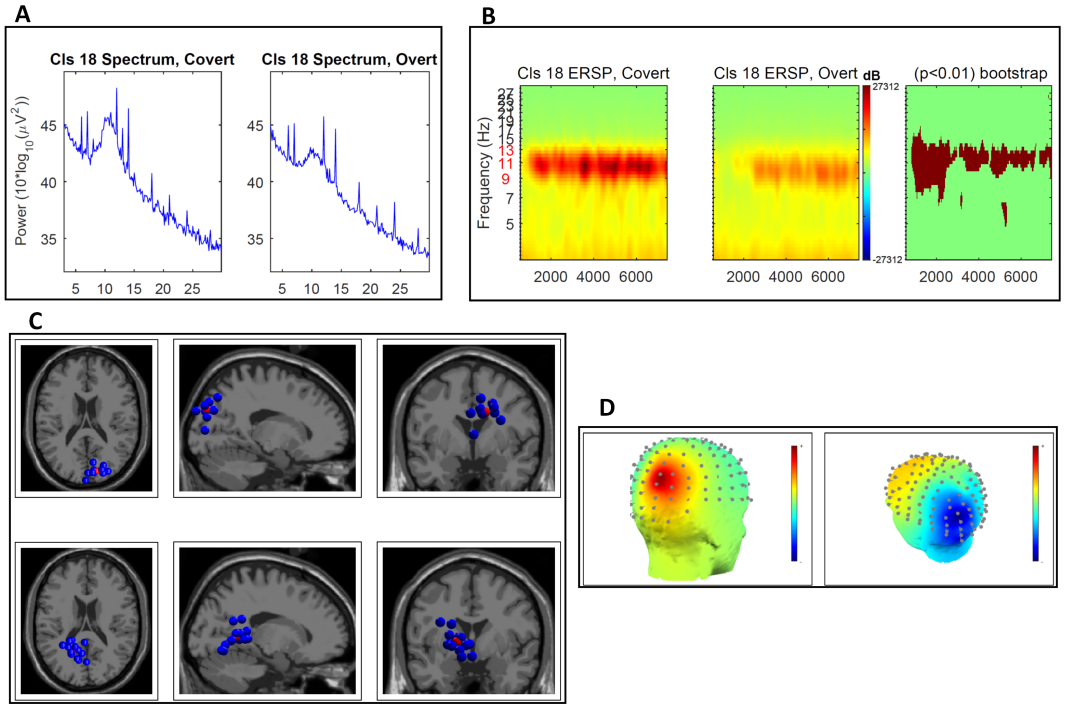

Figure 5.8: Cluster 18; covert *vs* overt attention to 6&7Hz: ***(A)*** The grand average of the spectral analysis of covert (left) and overt (right) attention. The X-axis is the frequency displayed in the range of 3-30Hz; the Y-axis is the power of frequencies. ***(B)*** Mean ERSP across 11 subjects during covert (left) and overt (middle) attention. Bootstrap in $p<0.01$ level (right) show significant differences between ERSPs in two adjacent windows. Red pixels in the lower right figure show the significant points in corresponding time and frequencies between covert and overt conditions across subjects. The significant frequencies ranges (9-13Hz) are shown in red. Time points (blocks of 8s) are shown in the X-axis while the frequencies in the range of 3-30Hz is demonstrated in the Y-axis. ***(C)*** Equivalent current dipole models when subjects attended 6&7Hz flickering stimuli *covertly* (upper row) and *overtly* (middle row). The location of dipoles are shown in horizontal (left), sagittal (middle) and coronal (right) sections. Each blue sphere corresponds to a single equivalent current dipole for a single IC. The red sphere is the mean coordinate of all dipoles. ***(D)*** 3D scalp topography of the activity in covert (left) and overt (right) attention. This figure is the scalp-map projection of the activities most probably originated from the dipoles shown in this figure. The sources of activities in both dipole models and 3D scalp maps were consistent across 8 subjects in covert and 11 subjects in overt attention. Electrodes are demonstrated over the scalp located based on the *ABC* system.

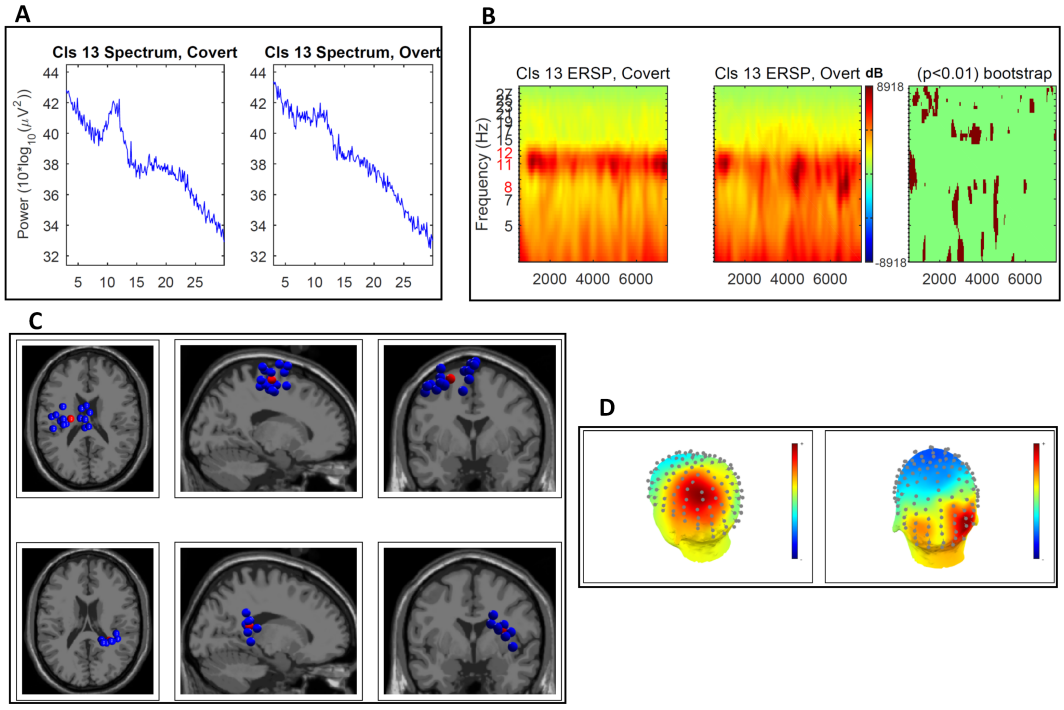

Figure 5.9: Cluster 13; covert *vs* overt attention to 6&7Hz: ***(A)*** The grand average of the spectral analysis of covert (left) and overt (right) attention. The X-axis is the frequency displayed in the range of 3-30Hz; the Y-axis is the power of frequencies. ***(B)*** Mean ERSP across 11 subjects during covert (left) and overt (middle) attention. Bootstrap in $p<0.01$ level (right) show significant differences between ERSPs in two adjacent windows. Red pixels in the lower right figure show the significant points in corresponding time and frequencies between covert and overt conditions across subjects. The activity in both covert and overt attention showed similar intensity (8-12Hz). Time points (blocks of 8s) are shown in the X-axis while the frequencies in the range of 3-30Hz is demonstrated in the Y-axis. ***(C)*** Equivalent current dipole models when subjects attended 6&7Hz flickering stimuli *covertly* (upper row) and *overtly* (middle row). The location of dipoles are shown in horizontal (left), sagittal (middle) and coronal (right) sections. Each blue sphere corresponds to a single equivalent current dipole for a single IC. The red sphere is the mean coordinate of all dipoles. ***(D)*** 3D scalp topography of the activity in covert (left) and overt (right) attention. This figure is the scalp-map projection of the activities most probably originated from the dipoles shown in this figure. The sources of activities in both dipole models and 3D scalp maps were consistent across 11 subjects in covert and 8 subjects in overt attention. Electrodes are demonstrated over the scalp which are located based on the *ABC* system.

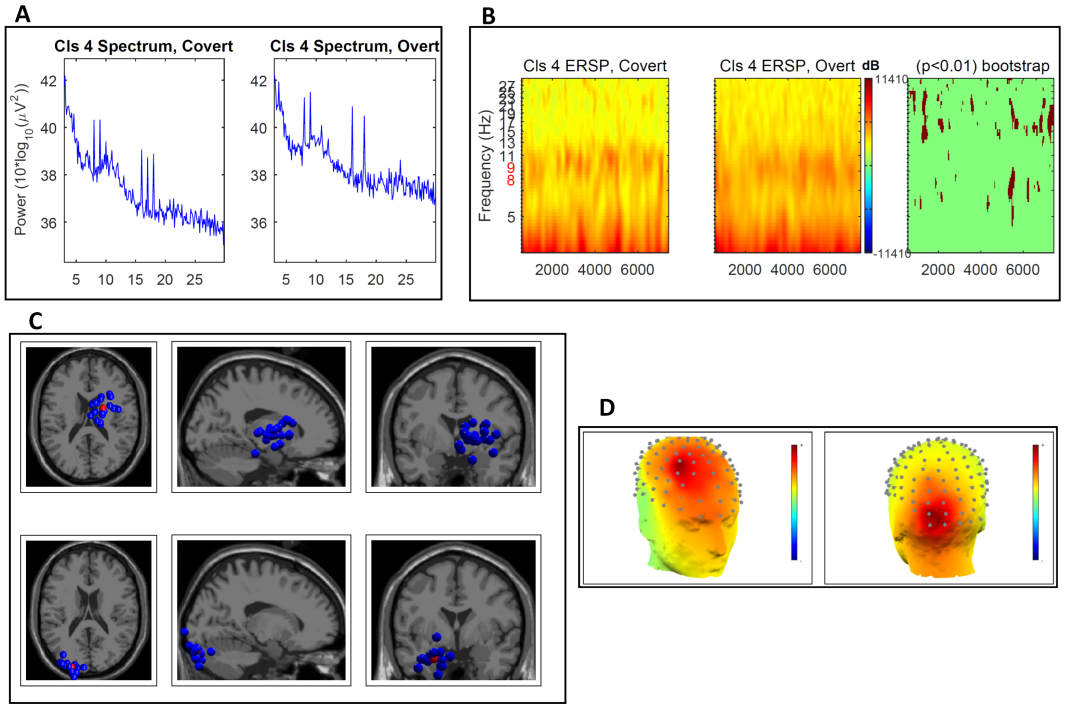

Figure 5.10: Cluster 4; covert *vs* overt attention to 8&9Hz: ***(A)*** The grand average of the spectral analysis of covert (left) and overt (right) attention. The X-axis is the frequency displayed in the range of 3-30Hz; the Y-axis is the power of frequencies. ***(B)*** Mean ERSP across 13 subjects during covert (left) and overt (middle) attention. The bootstrap in $p<0.01$ level (right) show significant differences between ERSPs in two adjacent windows. Red pixels in the lower right figure show the significant points in corresponding time and frequencies between covert and overt conditions across subjects. Covert and overt attention showed similar activation in the frequency-range of 8Hz and 9Hz (shown in red). Time points (blocks of 8s) are shown in the X-axis while the frequencies in the range of 3-30Hz is demonstrated in the Y-axis. ***(C)*** Equivalent current dipole models when subjects attended 8&9Hz flickering stimuli *covertly* (upper row) and *overtly* (middle row). The location of dipoles are shown in horizontal (left), sagittal (middle) and coronal (right) sections. Each blue sphere corresponds to a single equivalent current dipole for a single IC. The red sphere is the mean coordinate of all dipoles. ***(D)*** 3D scalp topography of the activity in covert (left) and overt (right) attention. This figure is the scalp-map projection of the activities most probably originated from the dipoles shown in this figure. The sources of activities in both dipole models and 3D scalp maps were consistent across 11 subjects in both covert and overt attention. Electrodes are demonstrated over the scalp which are located based on the *ABC* system.

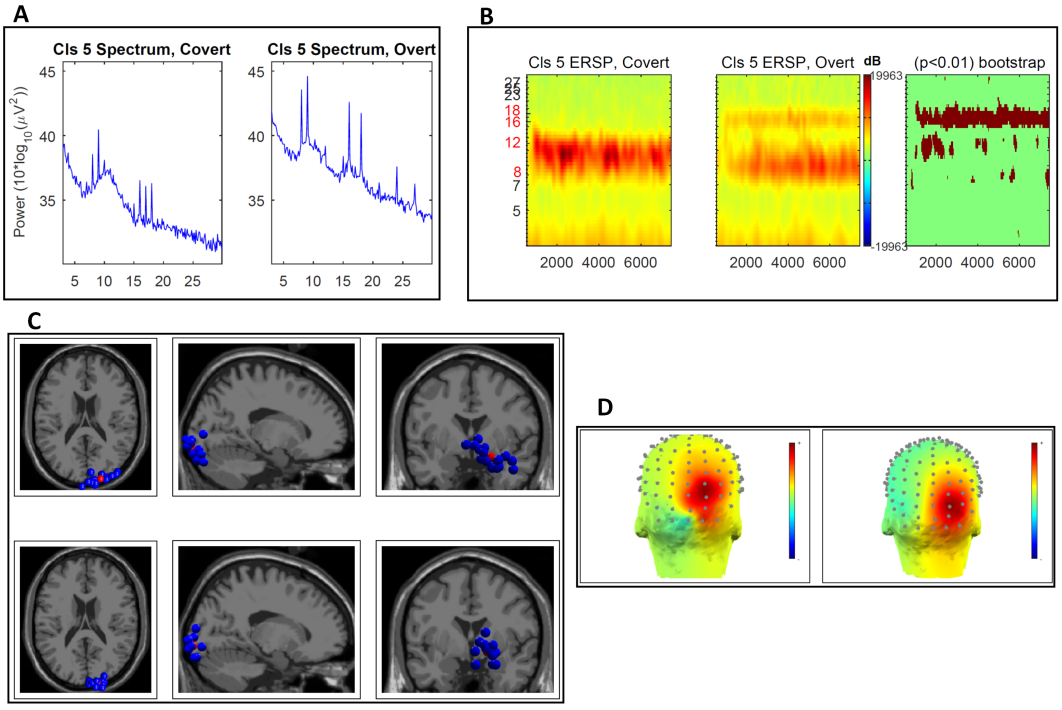

Figure 5.11: Cluster 5; covert *vs* overt attention to 8&9Hz: ***(A)*** The grand average of the spectral analysis of covert (left) and overt (right) attention. The X-axis is the frequency displayed in the range of 3-30Hz; the Y-axis is the power of frequencies. ***(B)*** Mean ERSP across 14 subjects during covert (left) and overt (middle) attention. Bootstrap in $p<0.01$ level (right) shows significant difference between ERSPs in two adjacent windows. Red pixels in the lower right figure show the significant points in corresponding time and frequencies between covert and overt conditions across subjects. Time points (blocks of 8s) are shown in the X-axis while the frequencies in the range of 3-30Hz is demonstrated in the Y-axis. The α-band frequencies (8-12Hz) as well as the 2^{nd} harmonics have been shown in red. The 2^{nd} harmonic showed larger amplitude in overt compared to covert attention. ***(C)*** Equivalent current dipole models when subjects attended 8&9Hz flickering stimuli *covertly* (upper row) and *overtly* (middle row). The location of dipoles are shown in horizontal (left), sagittal (middle) and coronal (right) sections. Each blue sphere corresponds to a single equivalent current dipole for a single IC. The red sphere is the mean coordinate of all dipoles. ***(D)*** 3D scalp topography of the activity in covert (left) and overt (right) attention. This figure is the scalp-map projection of the activities most probably originated from the dipoles shown in this figure. The sources of activities in both dipole models and 3D scalp maps were consistent across 10 subjects in covert and 9 subjects in overt attention. Electrodes are demonstrated over the scalp which are located based on the *ABC* system.

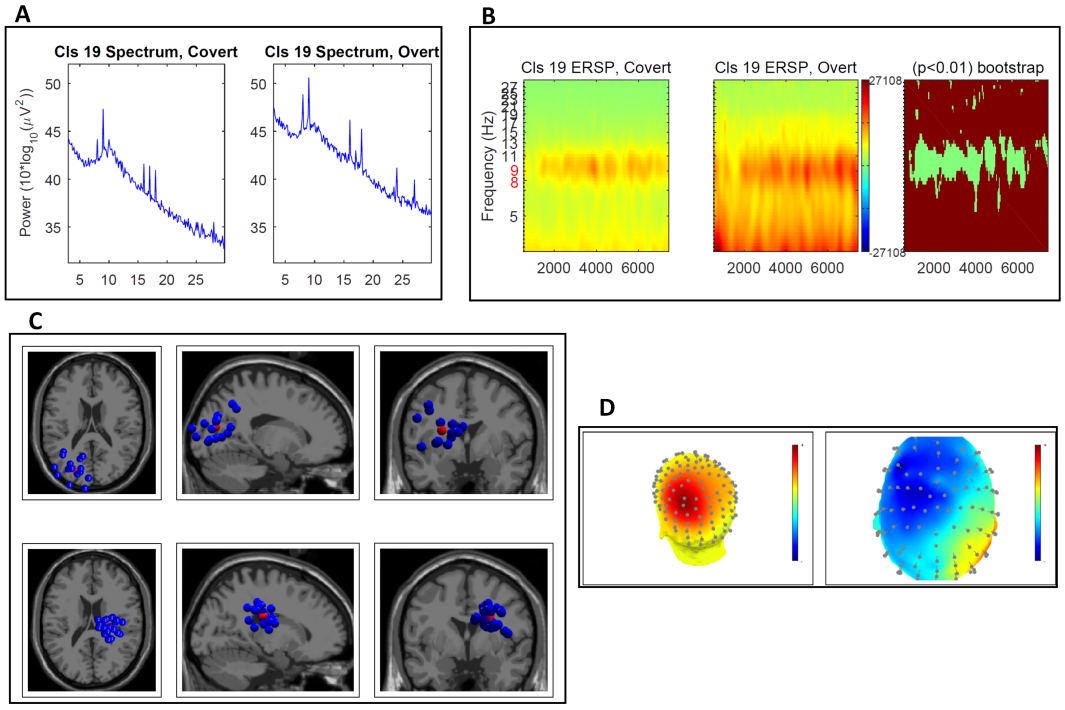

Figure 5.12: Cluster 19; covert *vs* overt attention to 8&9Hz: *(Upper row)* The grand average of the spectral analysis of covert (left) and overt (right) attention. The X-axis is the frequency displayed in the range of 3-30Hz; the Y-axis is the power of frequencies. *(Lower row)* Mean ERSP across 12 subjects during covert (left) and overt (middle) attention. Bootstrap in $p<0.01$ level (right) show significant differences between ERSPs in two adjacent windows. Red pixels in the lower right figure show the significant points in corresponding time and frequencies between covert and overt conditions across subjects. Time points (blocks of 8s) are shown in the X-axis while the frequencies in the range of 3-30Hz is demonstrated in the Y-axis. The activity in the frequency band shown in red is similar in both covert and overt attention. ***(C)*** Equivalent current dipole models when subjects attended 8&9Hz flickering stimuli *covertly* (upper row) and *overtly* (middle row). The location of dipoles are shown in horizontal (left), sagittal (middle) and coronal (right) sections. Each blue sphere corresponds to a single equivalent current dipole for a single IC. The red sphere is the mean coordinate of all dipoles. ***(D)*** 3D scalp topography of the activity in covert (left) and overt (right) attention. This figure is the scalp-map projection of the activities most probably originated from the dipoles shown in this figure. The sources of activities in both dipole models and 3D scalp maps were consistent across 10 subjects in both covert and overt attention. Electrodes are demonstrated over the scalp which are located based on the *ABC* system.

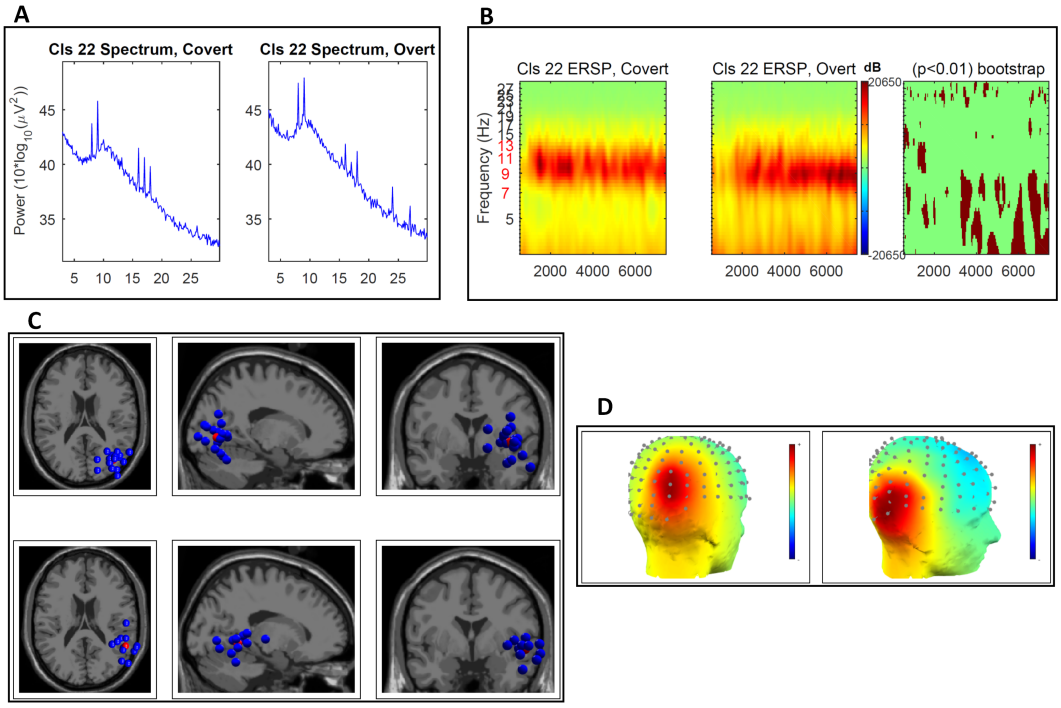

Figure 5.13: Cluster 22; covert *vs* overt attention to 8&9Hz: ***(A)*** The grand average of the spectral analysis of covert (left) and overt (right) attention. The X-axis is the frequency displayed in the range of 3-30Hz; the Y-axis is the power of frequencies. ***(B)*** Mean ERSP across 14 subjects during covert (left) and overt (middle) attention. Bootstrap in $p<0.01$ level (right) shows significant difference between ERSPs in two adjacent windows. Red pixels in the lower right figure show the significant points in corresponding time and frequencies between covert and overt conditions across subjects. Time points (blocks of 8s) are shown in the X-axis while the frequencies in the range of 3-30Hz is demonstrated in the Y-axis. The frequencies in the range of 7-13Hz (shown in red) had the highest activity in both covert and overt attention. ***(C)*** Equivalent current dipole models when subjects attended 8&9Hz flickering stimuli *covertly* (upper row) and *overtly* (middle row). The location of dipoles are shown in horizontal (left), sagittal (middle) and coronal (right) sections. Each blue sphere corresponds to a single equivalent current dipole for a single IC. The red sphere is the mean coordinate of all dipoles. ***(D)*** 3D scalp topography of the activity in covert (left) and overt (right) attention. This figure is the scalp-map projection of the activities most probably originated from the dipoles shown in this figure. The sources of activities in both dipole models and 3D scalp maps were consistent across 11 subjects in covert and 10 subjects in overt attention. Electrodes are demonstrated over the scalp which are located based on the *ABC* system.

5.4 Discussion

The results from the current study showed that the flicker frequencies are extracted consistently across all subjects. When comparing the power of flicker frequencies in covert and overt attention, it is higher when the subjects' attention was allocated overtly. Topographical distribution showed that the activities are mostly originated from visual areas in both covert and overt attention. However, other brain areas are also involved in different conditions. When subjects attended covertly to flickering stimuli, the activity in their parietal cortex (figure 5.9.C-D and 5.12.C-D) was higher compared to overt attention in the same cluster-levels (cluster 13 and 19 in 6&7Hz). In addition, the frontal cortex was involved in some clusters when attending covertly (cluster number 4 in 8&9Hz; figure 5.10.D) while attending overtly in other clusters (cluster 19 in 8&9Hz; figure 5.12.D). We also observed other consistent pattern across subjects: while covert attention recruits the superficial layers of the brain (cluster 13 and 18 in 6&7Hz; 5.9.C, 5.8.C, and cluster 19 in 8&9Hz; figure 5.12.C); overt attention is originated from deeper (sub-cortical) brain regions. Although the latest pattern was in some case observed also in overt attention, but this was only in one cluster (cluster 4 in 8&9Hz; figure 5.10.C). Finally, in the majority of the clusters, we observed a dominant α-wave (8-12Hz) activity which had a higher power in covert compared to overt condition.

We found that the flicker frequencies are well detectable in their fundamental frequencies as well as their harmonics in both attentional stages. Similar results were obtained by Muller and colleagues through a series of studies[76,121,124] where they experimented the brain response to SSVEP by successively presenting the target and non-target flickers. The frequency response was higher in attended stimulus. Additionally, they showed the increased power to the target flicker even when target and non-target flickering stimuli are located in the same spatial position and superimposed on each other. These studies show that even when the flickering objects are located in the same visual field, the representation of the attended object is *gated* by means of attention. These studies only explored the effect of attention as a "holistic concept" on the SSVEP signals and had least contribution in identifying the role of different components of attentional shifts on SSVEP signals. The response comparison to different SSVEP frequencies has not been considered in this study as the primary objective of the current study was to map the topographical distribution of flicker frequencies and for this aim the data for both attended flickering frequencies were merged. Regarding the anatomical distribution of SSVEP activities, our results are partly consistent with Müller et al.[121] and Müller et al.[76], showing that extra-striate cortex of the occipital lobe is involved in the representation of SSVEP signals. In a other study, Ding et al.[64] showed that based on the SSVEP frequency range, the read-out of these oscillations can be extracted from frontal, temporal and occipital areas. Although these studies were topographical-oriented, their focus was mostly the physical parameters of stimulus such as the choice of flicker frequencies[64], spatial frequencies, modulation depth, color[133], etc. In a pioneering study subjects were asked to maintain their gaze on the central fixation point. In each trial, a centrally presented arrow cued the subjects to attend an alphanumeric character sequence in either left or right visual field and respond to an specific letter as target stimulus. Letters were superimposed on flickering stimuli with the frequency of 8.6Hz and 12Hz. The EEG activity was recorded from 13 scalp electrodes in frontal, central, parietal, occipital and temporal areas. Results of this study showed that the enhancement of the flicker frequencies appeared in the right cerebral hemisphere as compared to the left. On the other hand, Müller et al.[121] used higher frequencies in the SSVEP task, and the site of maximum modulation was identified on the hemisphere contra-lateral to the attended stimuli. In the current study, we explored the attentional modulation with no lateralization

as the lateralization may indicate the representation of visual response to physical features of the stimuli. This has been also shown by Ales et al.[134] and Luck[135] where polarity-changes in the primary visual area changes as a function of location of stimulus in the visual field; whereas the source of attentional activities are known to be regardless of the visual field of the external stimulus[55]. We flipped the orientation of flicker frequencies in each trials, so that the lateralizations which were generated by the direction of attention *per se*, were canceled out across the analyzes. Therefore, the topographical findings in this study reflect the common pattern of activity across subjects regardless of orientation of the attended stimuli. Yet, our results indicated that the occipital area is the region which is commonly active in both covert and overt attention consistently with the results by Andersen et al.[136] who reported that selective attention to a feature facilitates the neural responses elicited in the visual cortex by attended flickering feature. The occipital region has been reported in several other literature for being be responsive to SSVEP frequencies[55,125,137,138]. Representation of SSVEP signals in the visual cortex sounds trivial for a visual stimulation and this is why the activation in occipital region was observed in both type of attentional shifts (covert and overt) in the current experiment.

In a similar study to ours Walter et al.[84] used SSVEP signals to map the brain activity over the scalp. They used dot-pattern flickering stimuli in the left and right of the central fixation points. The entire experiment was divided into equal trials of covert and overt attention where subjects were instructed to press a button for changes in the illumination of the flickering dots. The recording was performed by 64 channels on 256Hz sampling rate. Then SSVEP amplitudes were estimated by Fourier transformation of the 3s windows and the mean topographies for each flicker frequency as well as attentional state (covert *vs* overt) was calculated. Results of this study[84] showed that the occipital area registered the highest amplitude in both covert and overt attention with a difference that in covert attention the active region was slightly drifted to the contra-lateral side of the stimulus side. However, the source localization method used in their method[139] differed from ours in a way that our algorithm was able to estimated the sources of activities in the superficial layers or the gray matter activation[139–141]. By using the current dipole model in this study, we were able to estimate the activities originating their sources most likely originated from the deeper structure (involvement of subcortical structures will be discussed later in this chapter). The chosen dipole modeling has been widely used in determining the origin of scalp recorded potentials with various applications in clinical neurophysiology and neuroscience, such as the localization of epileptogenic foci aiding pre-surgical planning[142–144].

Our study confirmed the previous neuroimaging results[39] that covert and overt attention are originated from similar areas. However, single-unit studies on macaque monkey suggested that there is a distinction at the level of cell populations, with some cells in the frontal-eye field (FEF) being active in overt attention and a distinct but overlapping population of cells involved in covert attention[115,145]. The cell population responsible for covert attention also seemed to hold the location of cues during delay interval[146]. These two cell populations are mixed in FEF but they have never been identified distinctly in macroscopic level such as in functional MRI or EEG. Yet, physiological results show that covert attention is distinct from the motor system controlling eye movements, even though they are clearly interact[147]. We observed the similar activity in some regions such as frontal area in both overt (figure 5.12.C) and covert (figure 5.10.C) attention in response to the SSVEPs. This highlights the facts that the covert and overt attention have some similar site of activation. Our findings add more to this concept that in overt trials of our experiment, subjects moved their eyes once on the flickering object and kept their eyes fixed for the entire block. This suggests that relevant sources are probably involved in functions more than preparing

saccades and moving eyes. One would argue that in our results the SSVEP frequency is mounted on the α-range peak and it is α-oscillation which is represented on the dipoles as well as the scalp map. However, even if this argument is true, it seems that the α-wave is specifically generated by the covert attention procedure. This is evident in comparing covert and overt attention in different clusters in their power spectrogram (*e.g.* see clusters 5, 13 and 14 for SSVEP frequency of 6&7Hz in figures ??.A, 5.9.A and 5.7.A, respectively, and cluster 19 for 8&9Hz in figure 5.12.A). Despite the presence of α-peak, the role of SSVEP (which clearly have higher power in spectrograms) should not be underestimated as they clearly posses higher power in most clusters. The role of frontal cortex in spatial attentional deployment has been identified[148,149]. Moreover, the contribution of frontal region to the SSVEP response has already been demonstrated for the purpose of BCI application by Hsu et al.[150]. They measured the SSVEP oscillations from the frontal area and found that the frontal SSVEPs, just like occipital SSVEPs can be well characterized in their frequencies and amplitudes. In the meantime, frontal SSVEPs have lower amplitude and SNR compared to occipital's[150]. This is the case also in our ERSP analysis (figure 5.10.B and 5.12.B) where the presence of other frequencies (especially low frequency oscillations) are obvious during the block. Despite this, the averaged power spectrum in the same clusters indicate that SSVEP frequencies are quite distinct. One characteristic that we found in our results was that the SSVEP representation on the frontal area is distributed over a broad scalp region (figure ??.D lower-left and 5.12.D). Investigating the dipole locations corresponding to the frontal scalp distribution showed that the source of activity is originated from the deeper structures. Due to distant activity from the recording sites on the scalp, the sum of activities are spread over the larger part of the frontal region. Therefore, for applications like neurofeedback therapy it should be considered that the frontal SSVEP may not be a focus signal.

With regards to the SSVEP-induced activation depth, dipole models showed that overt attention involves more of the deeper layer of the brain; whereas, superficial layers are more active in covert attention. The role of subcortical structures such as superior colliculus (SC), lateral geniculate nucleus (LGN) and pulvinar nuclei (PN) in visual attention is known through plethora of literature[151–154]. Casey et al.[155] performed an experiment to understand the role of subcortical area in attention modulation. In each trial, three geographic shapes were presented to the subjects. In each set of figures, one was unique, either in the case of color or shape and subjects' instruction was to identify this uniqueness. Their results showed the role of subcortical regions in attention switching task, suggesting that switches of attention between simple attributes, such as color or shape, require minimal cognitive modulation. This function recruits the subcortical rather than cortical areas. Thus, the subcortical activation in our study occurring mostly in overt attention, could be explained by this phenomenon. In our experiment, since flickering objects in overt attention are directly observed by the subjects, the simple physical attributes activate the subcortical regions. Whereas, covert attention is more demanding to perform, since it requires higher cognitive involvements and more cortical processes. Subcortical modulation of attention has also been confirmed by invasive studies in monkeys, where micro-stimulation was used to stimulate some parts of the brainstem and to see whether the activation of these regions contributes to the attentional shifts[156]. With this stimulation, monkeys were able to easier detect changes in the visual task and had shorter RT, both indicating the improvement of shift of attention. It should be noted that the activities originated from the deeper structures are projected in a wider scalp areas, while the superficial activities are concentrated in a smaller scalp area.

Our study showed that the parietal cortex is specifically active in covert attention, where no such implication for overt attention was observed. Our visual task was based on

the spatial shift of visual attention; whereas, other literature has reported similar patterns of activation in non-spatial visual attention. In their experiment, Zhang et al.[157] devised a different strategy for allocating the covert attention,where the visual stimuli were located within the visual field. This was different in our study, as the stimuli were located in the peripheral vision. Stimuli were designed as moving dots in two colors (blue and red) each were flickering in different frequencies. The subjects were instructed to fixate their eyes to the central fixation point and covertly attend to either flickering dots. Their results showed that the attended SSVEP frequency was represented over the parietal and occipital areas. Ding et al.[64] performed a thorough study in order to understand the attentional modulation of SSVEP oscillations based on different brain networks. They used 15 different SSVEP frequencies in the range of 2.5Hz-20Hz. Results showed that in addition to enhanced activity in occipital and frontal responses, robust SSVEP signals were recorded from channels over parietal cortex close to midline, especially at the flicker frequency of 9.2 and 10Hz. However, this study has not considered the type of attentional allocation into the comparison. Our study consistently showed that there is an obvious parietal activation in the left parietal scalp area when subjects in covert attention to 8&9Hz frequencies (figure 5.12.D). No such activation was observed in overt attention in any cluster. Neither, we saw any parietal involvement in lower SSVEP frequencies was seen. This shows that the parietal region acts specifically to certain frequency range (as explained by Ding et al.[64]). Our study adds to this by highlighting that this region may also act specifically in response to covert attention. This can be an interesting signature for later BCI applications to extract attention-specific signals.

In our results we also observed that the power of α-oscillation increases in many clusters with largest peak in covert compared to the overt attention. This increase in α-activity was present in different areas such as occipital, frontal and parietal. Our finding was opposing some previous literature on the primary sensory-motor cortices suggesting that α-band oscillations decrease with attention and movements[158,159]. Also there is evidence that inhibitory α -power precedes the involvement of cortical regions in task-related functions[160,161] in which this oscillation appears to be inversely proportional to the performance of the subjects. Other studies showed that pre-stimulus α power in the parietal cortex has positive correlation with the performance[162] and also increased the amplitude of the ERP† [163] following the stimulus. These controversial reports already alerts the different role of α-band oscillations based on the type of experiments, or the allocation of attention. The inhibitory theory or α-oscillation has been proposed by Klimesch[164]. According to this theory, the α-enhancement causes an active top-down inhibition of task-irrelevant stimuli[165]. Therefore, the α-power is associated with inhibition of visual areas to suppress the processing of irrelevant information. The latter statement is supported by other studies[166–168] showing that the α-oscillation is increased over occipital area contra-lateral to the position of distracter in the spatial cuing attention. In a recent study Benedek et al.[169] performed an experiment to understand the role of alpha activity on different types of attention. In each trial subjects were shown a four-letter word by which subjects either had to make sentence or think of its application in the real-life. The former task was sensory-dependent as the subject needed to observe the word all over the time that he/she is trying to make sentence. The latter task, however, was sensory-independent as they could register the word immediately and think about its application in the real-life. They tested both tasks once by keeping the four-letter word on the screen for the entire time to perform the trial (low-internal attention) and once with a brief flashing the word for only 500ms (high-internal attention). They found that the enforcement of internal attention increased α-power only in the sensory-dependent task.

†Event-related potential (ERP) has been used as a measure of brain response to specific stimulus

This means that the α-power increases as a function of internal attention demands. Previous studies[170,171] also showed that internally focusing attention increase the α-oscillations much more than external attention. Based on this rationale, one can probably infer that the α-band power increases when an internal and effortful action takes place. Covert attention turns out to be an effortful task compared to the overt attention, as subjects observed both attended and unattended stimuli while trying to block the unattended stimulus by an internal (top-down) action. This requires that the irrelevant stimulus is suppressed by increasing the α-oscillations. Furthermore, the origination of α-band oscillations from different brain areas may be a rational indication that these regions are in cross-talk communication during covert attention in order to enhance attentional capability[172]. The difference in α-power in different brain areas is an interesting feature to distinct covert from overt attention and perhaps a very applicable feature in implementing the attention-based BCI systems in the later phases.

Chapter 6

Intra-cortical representation of SSVEP in monkeys

6.1 Introduction

The idea of "body schema" was introduced in early 1900 by Head and Holmes[173] describing that the spatial model of the body in the brain based on the sensory inputs from the skin and muscles as well as the visual information. First evidence that the motor cortex receives visual input comes from the study by Gastaut and Hunter[174]. These findings were supported by later studies[175–178] who found that most peri-cruciate neurons in cats (typically receiving the cutaneous receptive field) also respond to light stimuli. These responses occurred in about 50-70ms, but mostly within 10-20ms following the optical stimulation[179]. To understand the mechanistic pathways and how the visual-related signals travel to the sensory and motor areas in the brain, Dubrovsky and Garcia-Rill[177] recorded the neuronal responses in different paths and measured the response latency. It was found that neurons in peri-cruciate cortex respond 9±2ms after the stimulation of the superior colliculus and 16±3ms after the stimulation of the occipital cortex. Therefore, pre-cruciate gyrus* may perform the function once the visual information is already processed. An increasing number of studies indicated that the body schema is plastic and can even incorporate artificial tools[182–184]. A good example of body schema plasticity is the rubber hand illusion. In this concept, subject's hand is hidden from the vision and a rubber hand is shown instead. Then the subject's hand is touches at the same time that the rubber hand is touched. It is observed that after a few trials, the subject perceives the rubber hand as her/his own hand and the brain responds to the touch of rubber hand only[185–187]. Shokur et al.[188] investigated the cortical basis of such an embodiment through simultaneous recording from S1 and M1 cortices, while monkeys were observing an avatar arm being touched by a virtual ball. Following a period when virtual touches occurred synchronously with the physically brushing monkeys' arms, neurons in S1 (primary somatosensory cortex) and M1 (primary motor cortex) started to respond to virtual touched alone. They observed that the response to the virtual touch occurred 50-70ms later than the response to the real physical touch. This indicates the possibility of visual representations in the somatosensory cortex. This project was the first to our knowledge which explored the SSVEP representation in S1 and

*Peri-cruciate gyrus represents the feline homologue of the premotor area[180,181]

M1 neurons. Based on the existing evidence on the polysynaptic pathways linking the visual cortex to somatosensory and motor areas, we hypothesized that the repetitive light may modulate neuronal activities in these regions. We aimed to verify our hypothesis in several steps as follows:

1. Repetitive stimuli (SSVEPs) alters the neuronal activities. This modulation is manifested as increased firing rates.
2. SSVEP-induced neuronal modulations may be manifested as the event-related neuronal synchronization (ERNS).
3. The temporal frequencies of SSVEP can be extracted from the S1 and M1 neuronal cells in the level of multi-electrode single-unit recording.

6.2 Experimental setup

6.2.1 Multi-electrode cortical recording implantation

Electrodes were arranged in the grid-array of 4×10, resulting in a total of 40 shafts. Each shaft contained three electrodes (42μm in diameter each) which were offset by 400μm to different depth (figure 6.3). This was designed to record the neuronal activity from different cortical layers. The electrodes were stainless steel 304 with polyimide insulation. The end parts were clipped to expose the conductive materials to the brain tissue. Electrodes were custom-made at the Department of Neuroengineering, Duke University, by the lab engineer. Streotaxic coordinates and cortical surface landmarks were used to identify the cortical locations. Electrodes had been inserted into the cortex through an exposed craniotomy sites across the skull. To fixate the electrodes on the scalp, dental cement was used around the electrodes. In addition, Cerasorb was added to the implant sites which stimulates osteogenesis in the operated location. A headcap to cover the operated region had been fixated on the skull in the 6-locations with T-bolt screws. The headcap restricted the access to the region, thus, allowing better recovery. A few days after the surgery, Omnetics output connectors (Omnetics Connector Corporation, Minneapolis, MN, USA) were located inside the headcap and fixated with dental cement. These connectors had been used to plug in the recorder connectors in day-to-day experiments. The layout of these connectors are shown in the figure 6.2.

Figure 6.1: Monkeys were implanted by intra-cortical electrodes. The entire set was mounted on the head as a cap and fixed using dental cement (Image courtesy of Ifft [189]).

Figure 6.2: **Top view of the head-cap:** Electrodes were implanted and coded for different cortical areas. Sockets were coded for their regions. The cables were connected to these sockets in the recording sessions (Image courtesy of Ifft [189]). (SMA: Supplementary Motor Area; M1: Primary Motor Cortex; PMd: Dorsal Premotor Area; S1: Primary Somatosensory Area; PPC: Posterior Parietal Cortex)

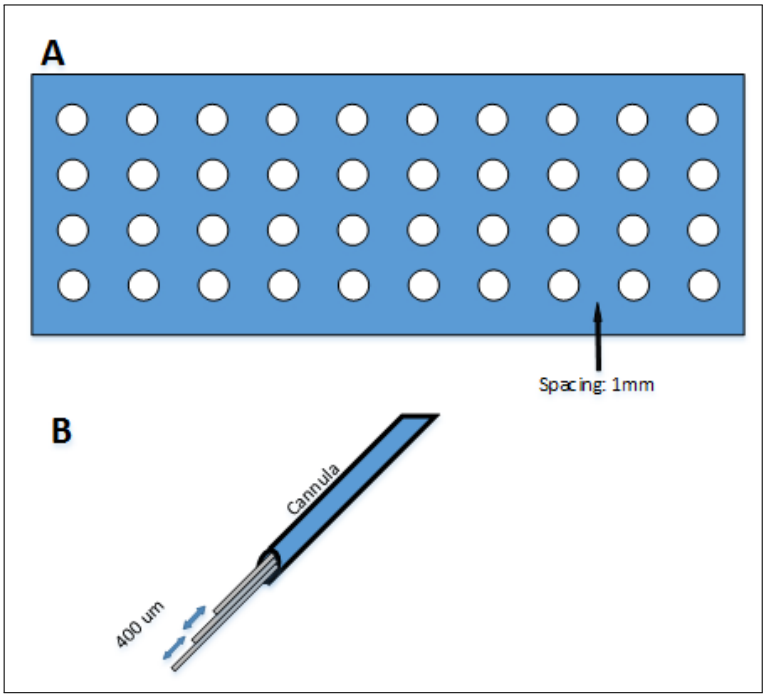

Figure 6.3: A grid of 4×10 cannulae is shown in *A*. Each cannula had up to three micro-wires offset at various depths. The lateral spacing between cannulae was 1mm and the vertical distance between micro-wires was 400μm. (Image courtesy of Ifft [189]).

6.2.2 Eye-tracker

To date, eye-tracking systems had been used in experiments which required no joystick during the trials. While the visual task was highly conservatively designed in a way that required monkeys to strictly look at the screen, we still preferred to use information from eye tracker to avoid analyzing data from trials in which there was no direct observation by monkeys. The precision level of this eye-tracker was not to detect the saccades [190], but yet sophisticated enough to follow the pupils and detect when monkeys were not attending the task. The eye tracking system (figure 6.4) was built by a former Ph.D. student Peter J. Ifft Ifft [189] at the Department of Neuroengineering which was a low-cost system. The eye-tracker algorithm was trained during the first few minutes of experiment when the animal is highly attentive to the screen. This way, the algorithm enabled us to customize the eye-tracking quality based on each monkey and the unique room condition in each particular session (e.g. lighting of the room, etc.).
Once the tracking was initiated, a frame was appeared in the video stream which had to be adjusted by the user on the left eye of the monkey (only one eye was required to be tracked). This adjustments had to be done when monkey was staring at the screen. In case the monkey redirected the gaze at any other point or closed the eyes, it was detected as 'not watching' (figure 6.4).

Figure 6.4: *left:* A firewire monochrome camera was installed on the wall facing the monkey's face. *Right:* Snapshots of the tracking windows. The pre-defined area in which monkey's eye is expected to be within that area is shown by a dashed red window. The yellow window indicates the real position of eye in real-time. *Right-top:* The tracked eye is located within the "watching" area; *Right-bottom:* The tracked eye is outside of the watching area. (Image courtesy of Ifft [189]).

6.2.3 Primate chair

The primate chair used in this experiment was originally designed for bimanual experiments; which in our case enabled monkeys to use both their hands in the experiments. As we needed only one arm during the experiment, the other arm (randomly switched in day-to-day experiments) was restricted inside the chair. The chair provided a comfortable place for the experiment duration of 45-60 minutes. The restricted arm was immobilized in the natural position. Furthermore, the chair was suitable for different arm sizes as we used two monkeys with relatively different sizes. All points of contact with monkey was foamed to provide a comfortable and safe place during the experiment. The restraint slide was inserted in the waist part of the monkey to prevent rotation of whole body which may have caused twisting and damaging the connector wires on the head.

6.2.4 Experimental sessions

During the experiments, monkeys were positioned in the primates' chair. Recording systems were connected to the head. The head was not restrained but the body movement was limited by a curved plate around the belly to prevent the rotation of monkeys. An analog joystick (with two degrees of freedom as right-left and forward-backward) was mounted vertically in front of the monkey at the waist level. The joystick was 30cm in length and had a maximum deflection of 12cm. A touch sensor was implemented on the joystick handle which measured weather or not the monkey is holding the joystick.

6.3 Center-out SSVEP task

The visual task was designed in accordance to the human SSVEP task with some adjustments to make it suitable for animal application. The task included three circular objects: a single middle circle as a starting point and two side circles as target objects (see figure 6.5). The

task starts with a central circle in the middle of the screen. Monkey has access to a joystick during the entire experiment and can freely move the cursor on each object on the screen. Once the cursor is moved into the central circle, two side circles appear. These circles flickered in two different temporal frequencies (8.18Hz *vs* 12Hz). To make the task more demanding, there were smaller circles within the large flickering circles. Only if the cursor was located within the small circle in either flickering objects, and was held for 2s, the juice was delivered as reward to the monkey. When the cursor was held into the right location, the other flickering object was disappeared from the screen for two purposes: *(1)* as an indication to monkey that the cursor is in the right position for juice disposal, and *(2)* to prevent interaction by the other flicker frequency later in the analysis. Two flickering objects were surrounded by two different marginal colors (blue and red). Colors indicated which type of juice to be disposed. We prepared two different juice, one of which was more favorable (we called it 'good juice') to monkey than the other one (so called 'bad juice'). Good and bad juice were coded by the marginal color, so that monkey learned, after a few trials, that which color corresponds to which juice. However, to balance the number of *goes* inside the target, the type of juice was switched between the left and right objects over the experiment. With this strategy they were urged to at least change the direction based on the juice differences. Juice was disposed for $500ms$ (approximately $\frac{1}{2}ml/s$) which was increased to $700ms$ at the end of the experiments to keep the monkeys motivated. During the juice disposal a *beep* sound was played to make monkeys aware of the juice. The juice was disposed through a stainless steel pipe located in front of the mouth. If they failed to move the cursor into the flickering targets for more than 10s, the trial ended and a new trial started again. As a control trial, approximately 30% of trials consisted of *no-flicker* targets, where targets appeared as before but they were filled by a bright color with no flickering. These trials were implemented to observe the neuronal activity when there is no SSVEP.

6.4 Methods

6.4.1 Participants

Monkey C: The monkey C (female; $6.4 \pm 0.2kg$) was implanted with electrode arrays in bilateral SMA[†], PMd[‡], M1[§], S1[¶] and PPC[‖]. Electrodes were grouped into 16 pairs. The separation between each adjacent pairs was $1mm$. Each pair consisted of two micro-wire electrodes placed tightly together.

Monkey M: Monkey M (male; $10.6 \pm 0.3kg$) was implanted by micro-electrode arrays in M1 and S1 bilaterally.The arrays consisted of a 4×4 uniform grid of 16 triplets. The separation between adjacent triplets was 1mm within each grid and 2mm across the gap separating the grids (figure 6.3).

6.4.2 Data acquisition

At the time of recording, due to the times passed from the surgery, some electrodes were no longer functional. A total of 218 electrodes could be recorded simultaneously. All neuronal data were amplified $8\times$ by headstages and $1000\times$ by 64-channel pre-amplifiers. Three

[†]Supplementary Motor Area
[‡]Dorsal Premotor Area
[§]Primary Motor Area
[¶]Primary Sensory Area
[‖]Posterior Parietal Cortex

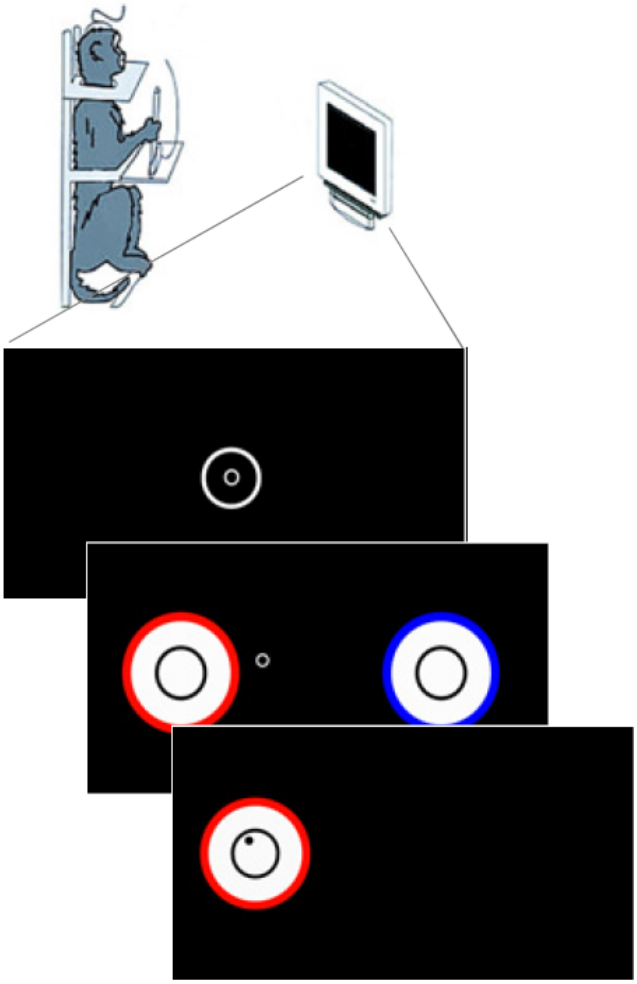

Figure 6.5: Monkey task: A visual task was designed in which monkeys were trained to drive their attention to either flickering stimuli. The monkey was seated in front of an LCD screen and has access to the joystick. The task starts with a cursor located inside the central circle. As soon as the flickering objects appeared on the screen, monkey had to move the cursor to either targets. Each target was indicated by a color which corresponds to the type of juice. Once the cursor is located inside the inner circle of the target, the other target was disappeared and the juice was delivered after 1s of holding the cursor inside the target. The process (which established one trial) was repeated as long as the monkey's performance dropped substantially.

128-channel *PLEXON* (PLEXON Inc., Texas) multi-channel acquisition processors (MAP) received input from the pre-amplifiers and digitized at 20kHz. Signal from MAP were then sent to the spike sorting software. An external sync feature was responsible for temporal synchronization of the data across the recording systems. The recorded signals were displayed by PLEXON Sortclient software (figure 6.7) in which multiple recordings on each channel were shown. Typically 3-4 units (neurons) per channel could be isolated for further analysis. Further data analysis was carried out in Matlab (MathWorks).

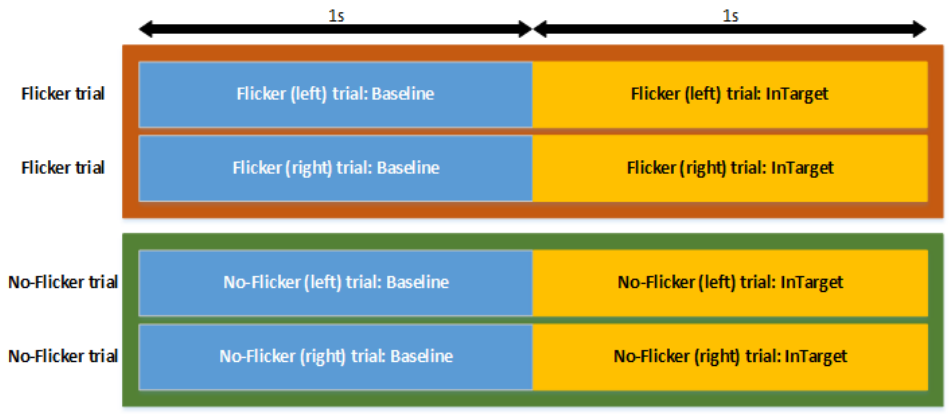

Figure 6.6: Structure of the data epochs: Epochs of 1s-duration was extracted from the data in the pre-processing. The *baseline* epoch corresponds to the time when the cursor is still out of any of target stimuli; whereas, the *InTarget* trial is when the cursor is located inside any of the left or right targets. These epochs were extracted in the same way in both flicker (red box) and no-flicker (green box) trials and for the left/right stimulus.

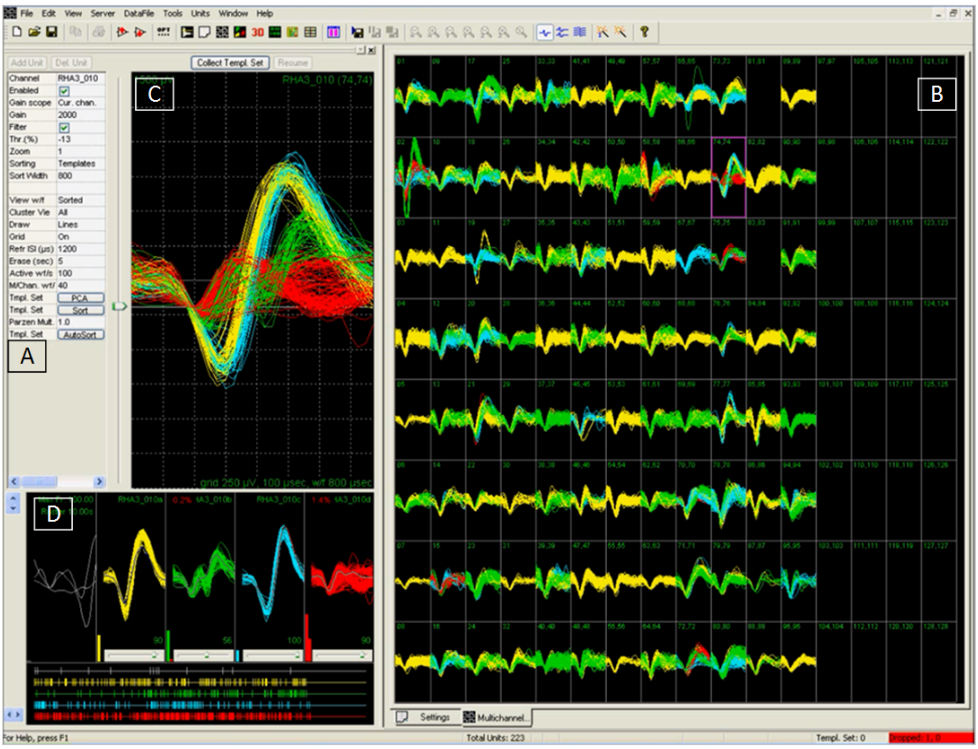

Figure 6.7: SortClient interface: Data acquisition from the implanted multi-unit electrodes was conducted using PLEXON system. *.plx*-files recorded with PLEXON system is associated to *SortClient* application where the neuronal templates could be chosen and sorted out by the user. SortClient contains several sections to be adjusted before the recording. *(A)* contains the information regarding the display adjustments. *(B)* demonstrates the recorded information from each channel located intra-cortically. Each channel may contain several neurons. By clicking on each channel, the action potentials can be observed in a window *(C)*. Only in this window, the user is allowed to define the parameters such as amplitude and width of the template in order to select the desired action potentials. Only action potentials which fall into this template will be recorded. A total of four templates can be defined for each channel. The action potentials which are compatible with selected templates, are shown in window *(D)*. Each color represents a single neuron.

Using the joystick, monkeys had to move the cursor with 1.6mm in diameter. The coordinates of the cursor movement was translated into x- and y-axis as forward-backwards and left-right, respectively. Information from x-axis (figure 6.8) was the most useful coordinates for the current experiment as the flickering (target) stimuli were located horizontally in the left and right side of the initiation point. These coordinates was used for pre-processing step when the data needed to be epoched based on when the cursor entered the target stimulus (experiment epoch) and the epoch of 1s prior to entering the target (baseline epoch).

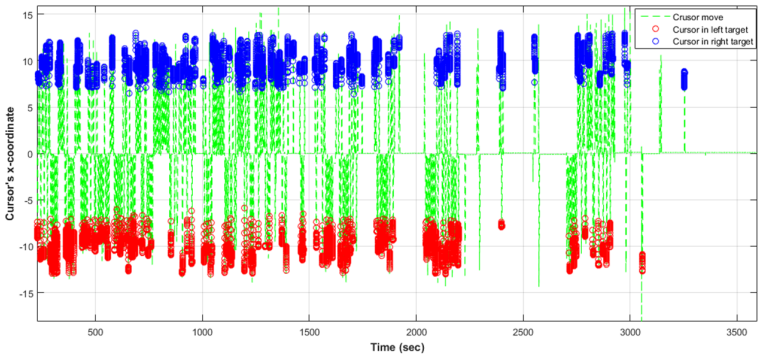

Figure 6.8: Cursor trajectory: This figure shows the trajectory of joystick movement in x-axis. The joystick was used by monkeys to take a computer cursor on the target stimulus. Dashed green lines show the cursor moves. The coordinates were recorded to find out when the cursor entered the target stimulus. Red and blue circles are to illustrate the time elapsed in the left or right target, respectively.

6.5 Data

Data from the neuronal activity was collected from 22 sessions of recording from the monkey M and 5 sessions from the monkey C. All sessions contained multi-unit recording from single neurons. The data from each unit and channel which were encoded based on their location in the cortex were sorted out into two grand sections of sensory and motor neurons. The raw data consisted of spike-trains representing the action potentials.The recorded activities from multiple electrodes were sorted out using *Sort client* software. For this purpose, templates were defined by the user by giving the lower and higher limits for different neuronal activities (shown in upper-left window in figure 6.7). Each time the neuronal activities matched these templates, they were considered as one spike (shown in lower-left window in 6.7). This template was set for each individual channels (channels are shown in the right window in figure 6.7). Once the data was acquired, as the first step in pre-processing, the firing rates were calculated as the summation of spikes in bins of 10ms (figure 6.9).

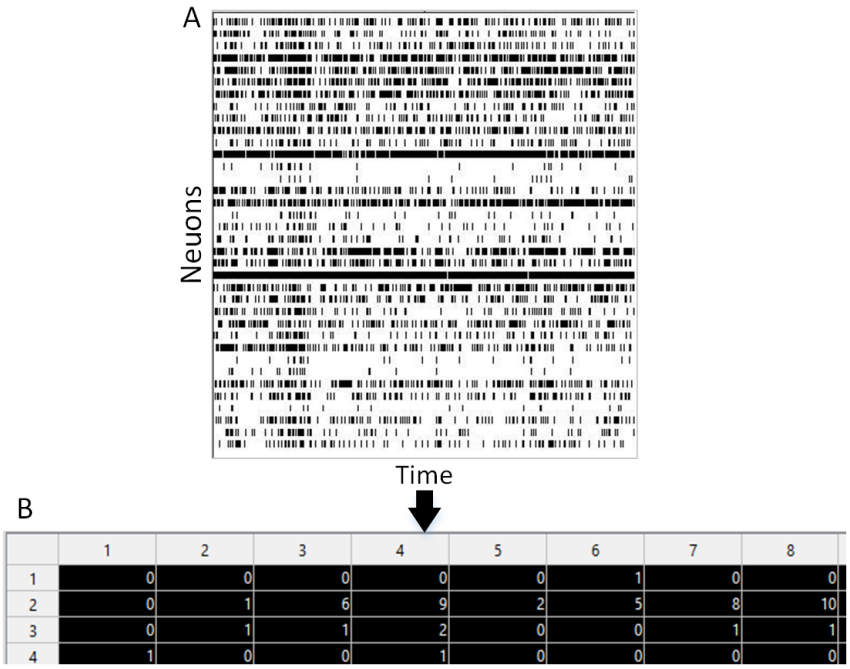

	1	2	3	4	5	6	7	8
1	0	0	0	0	0	1	0	0
2	0	1	6	9	2	5	8	10
3	0	1	1	2	0	0	1	1
4	1	0	0	1	0	0	0	0

Figure 6.9: Raw-data structure: Raw data (A) acquired from intra-cortical multi-electrodes were in the form of spike-trains, where each dot indicates an action potential. X-axis corresponds to the neurons and y-axis is the time. Spikes-trains were then converted into the firing rates (B) where each time-point (columns) indicates the total number of spikes in the duration of one bin (10ms).

6.6 Data analysis

6.6.1 Firing rate alteration due to visual flickering objects

In the first part of analysis, it was of interest to test whether the neuronal firing rate is affected by the presentation of flicker stimulus. Firing rates were calculated per bins of 10ms. As firing rates varied a lot across different neurons, for displaying purpose, they were normalized in the range of (0,1) in each neuron (figure 6.14 A-D 1,2). However, the statistical analyses were performed in non-normalized data.

In this section, it is hypothesized that *(1)* only some neurons will be affected by the flickering stimulus, *(2)* affected neurons would show an increase in the firing rates upon the appearance of the flickering stimulus rather than the baseline (before appearing the flickering stimulus); and *(3)* this increase of firing rates in response to flickering stimulus should be absent in no-flickering stimulus.

To examine whether or not flickering objects had any effect on the neuronal firing rates, the analysis was performed in two steps. In the step 1, only the responsive neurons were sorted out. i.e. the firing rate was either higher or lower in experiment epoch compared to baseline epoch. For this aim, two epochs were compared in each single neuron using paired

t-test.

$$t_0 = \frac{\bar{FE}_a - \bar{FB}_a}{\sigma_{FE_a.FB_a}\sqrt{\frac{1}{n}}} \tag{6.1}$$

$$\sigma^2{}_{FE_a.FB_a} = \sigma^2{}_{FE_a} + \sigma^2{}_{FB_a} \tag{6.2}$$

where $\bar{FE}_a$ and $\bar{FB}_a$ are the mean firing rates of neuron a in *experiment* and *baseline* epochs, respectively; $\sigma_{FE_a.FB_a}$ is the common standard deviation; $\sigma^2{}_{FE_a}$ and $\sigma^2{}_{FB_a}$ are the variance of *experiment* and *baseline* epochs, respectively, in neuron a. Neurons which showed a significant difference – either increased firing rate in experiment epoch than baseline (*positive response*) or decreased firing rate in experiment epoch (*negative response*) – were identified among all neurons.

In the second step, to test whether or not the presentation of flicker stimulus significantly increased (or decreased) the firing rate, flicker and no-flicker trials were compared (paired t-test) bin-wise (each bin consists of firing rates of all neurons in that specific bin). With this strategy, the bins with significantly different firing rates between flicker and no-flicker trials showed up.

6.6.2 Firing-rate synchronization

It is hypothesized that the flicker stimuli may have some indirect effect in which the firing rate may be synchronized instead of (or besides) directly being increased. For this aim, the firing rates in the time-units (bins of 10ms) of each neuron were correlated with all other neurons in the same condition (correlation within neurons in *sensory neuron (left)* or within *sensory neuron (right)*, etc.). The data structure before calculating the correlation coefficients is shown in figure 6.10.

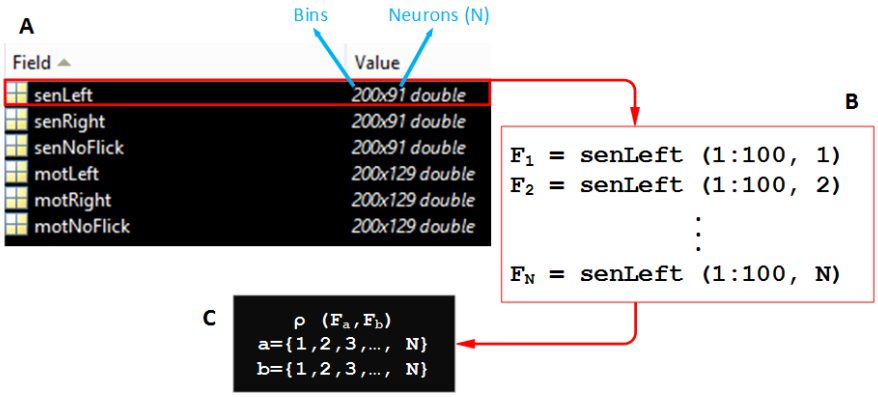

Figure 6.10: Data structure for correlation of firing rates: *(A)* variable table where the *Field* column consists of different experimental conditions and the *Value* columns indicates the data size and type. The data size of `200×  91` is for 200 rows of bins (`1:100` for baseline epochs and `101:200` for experiment epoch) and 91 columns of neurons. *(B)* Epochs extraction. *(C)* Correlation of firing rates between neurons. sen: sensory; mot: motor; Left: left flicker; right: right flicker; F: firing rate; N: number of total neurons in one condition

The Pearson correlation coefficient was calculated by:

$$\rho(F_a, F_b) = \frac{1}{k-1}\sum_{i=1}^{k}\left(\frac{F_a i - \bar{F}_a}{\sigma_{F_a}}\right)\left(\frac{F_b i - \bar{F}_b}{\sigma_{F_b}}\right) \tag{6.3}$$

$$\begin{cases} \text{a: } 1,2,3,\ldots,N \\ \text{b: } 1,2,3,\ldots,N \end{cases} \tag{6.4}$$

where N is the total number of neurons; $\rho(F_a, F_b)$ is the Pearson correlation of firing rates (F) of two neurons a and b (F_a and F_b); k is the number of bins (in our case $k = 100$); and σ_{Fa}, σ_{Fb} are the standard deviations of firing rates in neurons a and b, respectively. An schematic outcome of correlation coefficients is illustrated in the Matrix 6.5. As the same experimental condition was correlated to itself (auto-correlation) the number of neurons (N) is the same.

$$M = \begin{pmatrix} 1 & \rho(F_1,F_2) & \rho(F_1,F_3) & \cdots & \rho(F_1,F_N) \\ \rho(F_2,F_1) & 1 & \rho(F_2,F_3) & \cdots & \rho(F_2,F_N) \\ \rho(F_3,F_1) & \rho(F_3,F_2) & 1 & \cdots & \rho(F_3,F_N) \\ \vdots & \vdots & \vdots & \ddots & \vdots \\ \rho(F_N,F_1) & \rho(F_N,F_2) & \rho(F_N,F_3) & \cdots & 1 \end{pmatrix} \tag{6.5}$$

6.6.3 Frequency-band analysis

Besides possible effects of flickering objects on the firing rates or the neuronal synchronization, it is possible that temporal frequencies induced by flickers are also represented in the single-neuron level. The data acquired from this experiment was the firing rates which represented the number of spikes per 10ms (bin size). Spectral analysis was performed on each trial (baseline and experiment epochs) in both flicker and no-flicker trials as well as baseline and experiment epochs. The length of each section was 1s. Then, the area-under-the curve (AUC) was obtained in the width of 5 bins centered at the desired frequencies (8.18Hz and 12Hz). After this step, each neurons contains a single values of AUC for each trial (figure 6.11). The existence of outliers was identified based on the standard deviations (SD) of AUCs across trials in each epoch and neuron, where each data points which were greater or smaller than 2× SD were removed from the dataset.

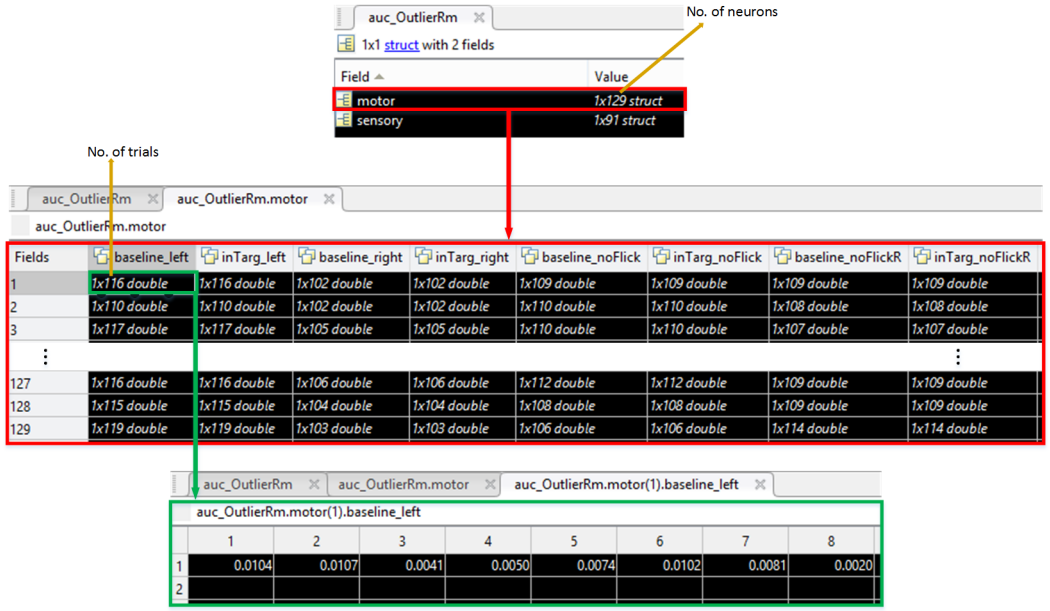

Figure 6.11: **Pre-processed data structure:** figure illustrates the structure of data following the pre-processing. The upper box demonstrates two major types of neurons as motor (×129) and sensory (×91) neurons. Each neuron of a type consists of eight conditions *(*middle box). *Baseline* refers to 1s-epoch when the cursor was not entered the target stimulus. *inTarg* refers to 1s-epoch when the cursor was located inside the target stimulus. *Left* and *right* refers to the stimulus located in the respective direction with different frequencies. *No-flicker* and *no-flickerR* refers to the left and right stimuli, respectively, when the stimuli were not flickering. Each neuron in a single condition, consists of a number of trials (*lower box*). The corresponding value for each trial demonstrates AUC of the desired flicker frequency.

It was interesting to compare the in-target (experiment) epoch of flicker trial *vs.* in-target (experiment) epoch of no-flicker in each neuron (see figure 6.6 for epochs and trials). By this way we know if the flicker stimulus increased the amplitude of the corresponding frequency in neurons. A normality test, Anderson-Darling (AD) test, was performed to observe whether or not the AUCs' distribution followed a Gaussian distribution. The datasets with

non-Gaussian distribution were log-transformed. From a single sample (*single neuron* in our case) consisting of a number of trials (e.g. a total of between 106 to 116 trials shown in figure 6.11), only one estimate of t-score can be obtained. In order to reason about the population, some sense of variability of the t-values was needed. i.e. if two groups are significantly different, what would have happened if we had a lot more trials instead of e.g. 106-116? Would higher sample size change the results? For this aim, it is decided to re-sample the data and obtain the t-score in each iteration (bootstrap method) of re-sampling. However, first the number of iterations (N) had to be determined. This was calculated by finding the sample size which indicates the number of replicates for each sample. The number of replicates define N for bootstrapping.

To compute the sample size, the operating characteristic (OC) curve was used. OC curve is a plot of type II error probability (β) of statistical test for a particular sample size versus a parameter that reflects the extent to which the null hypothesis is false[191].

$$\beta = 1 - P\{Reject\ H0 \mid H0\ is\ false\} \tag{6.6}$$

The OC-curve evaluates the probability statement in equation 6.7 and indicates the probability of type II error (β) against a parameter Φ,

$$\Phi^2 = \frac{n\sum_{i=1}^{a}{\tau_i}^2}{a\sigma^2} \tag{6.7}$$

where n is the sample size (replicates), $\tau_i^2 = \mu_i^2 - \bar{\mu}$, μ_i is the mean of AUCs in each epoch; $\bar{\mu}$ is the mean of no-flicker epoch to which the flicker epoch is compared to; a is the number of groups to be compared ($a = 2$ in our case corresponding to two groups of *flicker* and *no-flicker* epochs), and σ^2 is the variance of the samples in the flicker epoch.

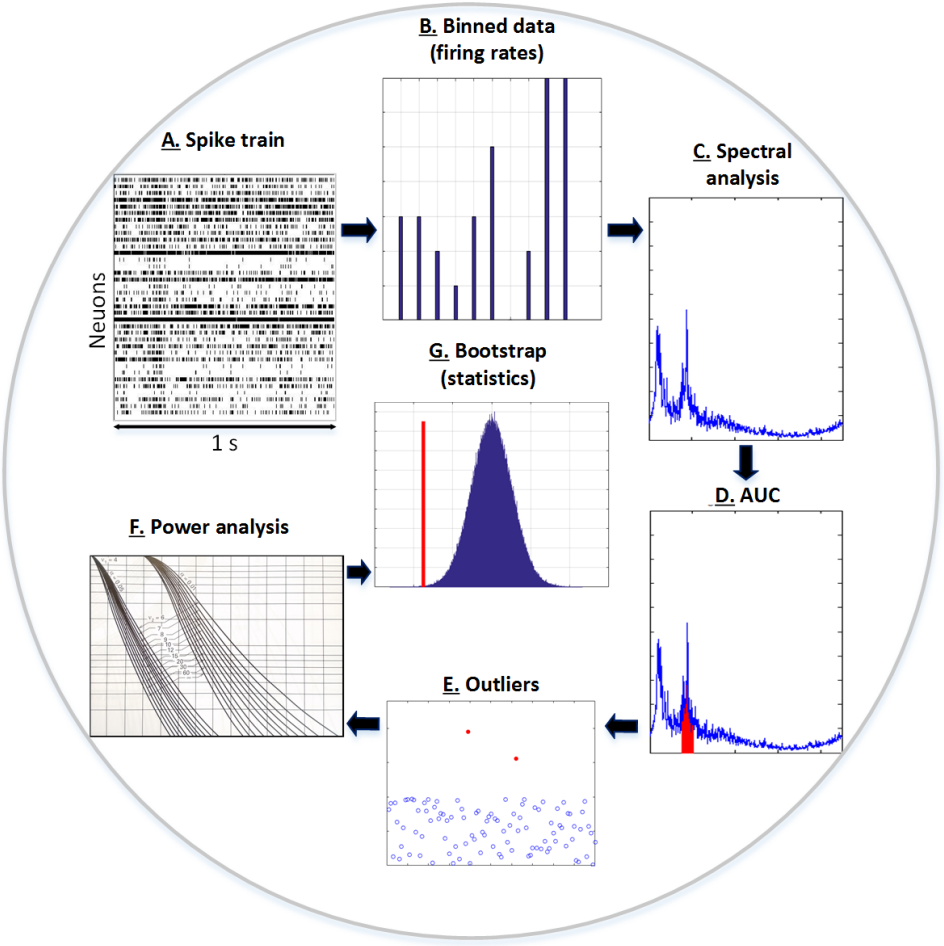

Figure 6.12: Analysis steps: Illustration of analysis steps in the frequency domain. Data acquired from the multi-unit electrodes were the spikes trains (A). The firing rate was calculated from the spike train (B). The spectral analysis was performed on each single trials (C). Area-under-the-curve (AUC) was found from the frequencies on interests (D) in all trials. Outliers were removed from the AUCs across the trials (E). Power analysis was performed on the clean AUC data (F) and based on that the appropriate statistics was performed (G).

Bootstrapping the statistical parameter: Following the estimation of sample size (n), this value was used as a number of iteration on re-sampling the original dataset from two comparison groups. Groups which were compared were as follows:

- Motor neuron, experiment epoch, left object: flicker trial *vs.* no-flicker trial
- Motor neuron, experiment epoch, right object: flicker trial *vs.* no-flicker trial
- Sensory neuron, experiment epoch, left object: flicker trial *vs.* no-flicker trial
- Sensory neuron, experiment epoch, right object: flicker trial *vs.* no-flicker trial
- Motor neuron, baseline epoch, left object: flicker trial *vs.* no-flicker trial

- Motor neuron, baseline epoch, right object: flicker trial *vs.* no-flicker trial
- Sensory neuron, baseline epoch, left object: flicker trial *vs.* no-flicker trial
- Sensory neuron, baseline epoch, right object: flicker trial *vs.* no-flicker trial

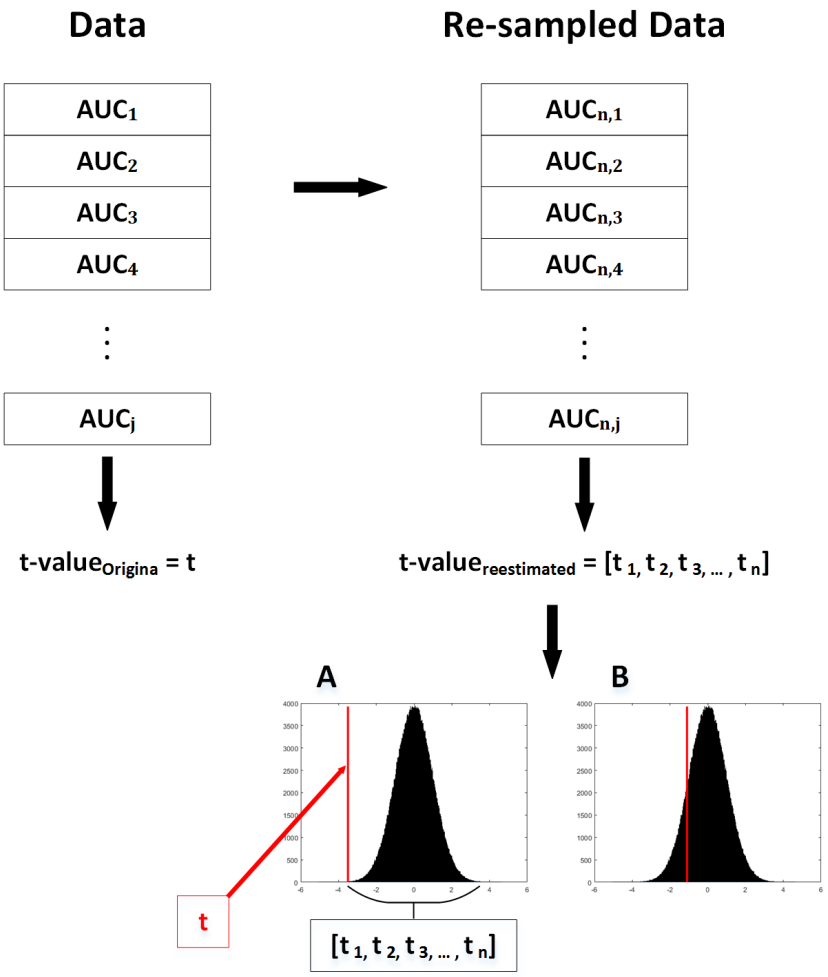

Figure 6.13: Bootstrap method for statistical parameter (t-value): Bootstrap method was performed on the outliers-removed-AUCs on j neurons. Before bootstrapping, the unpaired t-test was run between two groups to be compared and the t-value was obtained for the original data ($t - value_{Original}$). Then the original AUCs in both groups were re-sampled with replacement to generate n number of datasets from which n number of t-values were calculated. After this, it was tested whether or not the $t - value_{Original}$ falls within the histogram of n $t - value_{reestimated}$. For instance, the histogram A indicated a $t - value_{Original}$ which is out of the entire reestimated population; whereas, it is within the population in the histogram B. AUC: area-under-the-curve; j: number of neurons; n: number of iteration

In each comparison, firstly, two original datasets were statistically compared using unpaired t-test. After that, the same datasets were re-sampled n times (figure 6.13) and after each re-sampling, the same type of statistic was performed between the shuffled groups and t-values were calculated

$$t = \frac{\bar{A}_{g1} - \bar{A}_{g2}}{\sqrt{S^2 \left(\frac{1}{j_{g1}} + \frac{1}{j_{g2}}\right)}}, \tag{6.8}$$

where t is the t-value of unpaired t-test; $\bar{A}_{g1}$ and $\bar{A}_{g2}$ are the mean values for AUCs in group 1 and 2, respectively; S^2 is the common variance of two groups (6.9); j_{g1} and j_{g2} are the number of AUCs (also represents the number of neurons as there is one AUC per neuron) in group 1 and 2, respectively.

$$S^2 = \frac{\sum_{k=1}^{j}(A_k - \bar{A}_{g1})^2 + \sum_{k=1}^{j}(A_k - \bar{A}_{g2})^2}{j_{g1} + j_{g2} - 2}, \tag{6.9}$$

where A_k is the area-under-the-curve in each neuron.

If the original t-value fell into 95% of the total re-sampled t-values, we could dedicate that the original t-value is a representative of the total population and comparison between the two original groups is most probably correct. Therefore, neurons showing a significant difference between two comparison groups were considered as responsive neurons and the percentage of responsive neurons were calculated with regards to the total number of neurons (indicated as *%Total* in tables 6.2 through 6.6). However, some of these responsive neurons showed a decreased mean-value in flicker compared to no-flicker trials. Therefore, another percentage of responsive neurons are defined (indicated as (*%Local*) in tables 6.2 - 6.6) which shows what percentage of neurons among the responsive neurons have increased the mean-values in flicker compared to the no-flicker trials.

6.7 Results

6.7.1 Firing rate alteration

Results of paired statistical comparisons between the baseline and experiment epochs showed (figure 6.14) that a number of neurons responded to SSVEP frequencies. This response was either positive – i.e. the firing rate increased in experiment epochs compared to baseline – or negative (firing rate was reduced in experiment epoch compared to baseline). As these alterations occurred in SSVEP trials, both positively- and negatively-responded neurons were chosen as "responsive neurons" to SSVEPs. However, it was needed to test whether these changes were significantly different from the responses of *the same neurons* in "no-flickering" trials. A bin-to-bin comparison (e.g. each bin consisted of 91 sensory neurons or 129 motor neurons) was performed using the paired t-test between a responsive neuron in flicker trials and the same neuron in no-flicker trials. Results showed that both sensory and motor neurons were modulated by the SSVEP frequencies. However, only the positive-responded neurons in both sensory and motor neurons showed a significantly higher ($p<0.05$) firing rates when monkeys were exposed to flickering stimulus compared to the no-flickering stimulus (figure 6.14 A-D 3,4). The negatively-responded neurons also showed significant difference between the flicker and no-flicker trials; however, this difference was observed in the first few millisecond of the baseline epochs (figure 6.14 blue stars).

The density of bins with significantly higher firing rates in response to flickers was more in experiment epochs than in baseline epochs. This shows that flicker frequency which existed in experiment but not in the baseline epoch may have played a role in raising the firing rates. The SSVEP modulation of neurons was larger when monkey attended to low frequency (8.18Hz) than high frequency (12Hz).

Table 6.1: Percentage of neuronal pairs with synchronized firing rates)

Group (flicker *vs.* no-flicker)	%Baseline	%Experiment	$Ratio_{(Experiment/Baseline)}$
Sensory neuron (8.18Hz)	15	23	1.53
Sensory neuron (12Hz)	3	16	5.33
Sensory neuron (no-flicker)	6	13	2.17
Motor neuron (8.18Hz)	11	20	1.82
Motor neuron (12Hz)	3	14	4.67
Motor neuron (no-flicker)	5	11	2.20

6.7.2 Firing rate synchronization

To test how much the firing rates among different neurons are synchronized as a result of flickering objects, cross-correlation method was used between pairs of neurons. For this aim, the firing rates were estimated in bins of 10ms across neurons. The Pearson correlation coefficients were calculated between the firing rates of neurons in one independent epoch. The correlation coefficients between each neuronal firing rates with p-value$<$0.001 were considered as pairs of neurons with substantial correlations in their activities (figure 6.15 & 6.16). The percentage of synchronized neurons as well as the ratio of *experiment/baseline* in their percentage of significantly synchronized neurons are demonstrated in Table 6.1.

Results showed that the percentage of synchronized neurons increased in the experiment compared to the baseline epochs in all conditions. This included the no-flicker trials (figure 6.17) which was an unexpected result. However, the increase in flicker frequency of 12Hz in both sensory and motor neurons was higher compared to other conditions. This was prominent by observing the ratios. The synchronization increased 5.33$\times$ and 4.67$\times$ of the experiment epoch in sensory and motor neurons, respectively (Table 6.1). This is substantially larger ratio than other conditions.

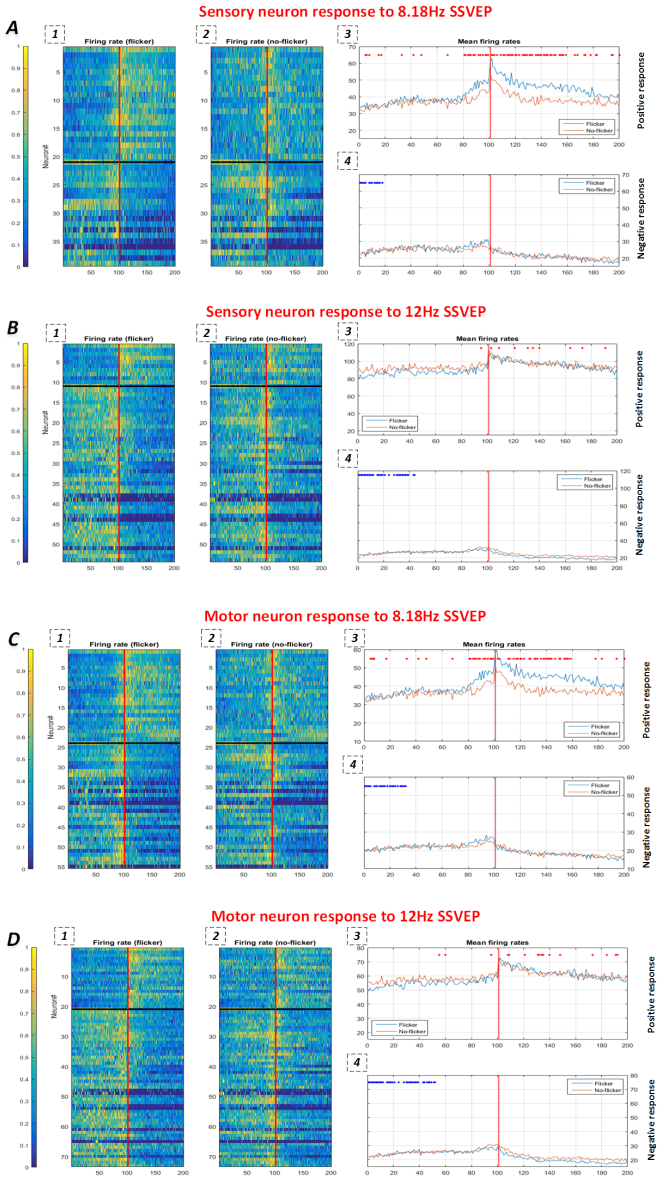

Figure 6.14: Firing-rate analysis on sensory/motor neurons: Neuronal responses to SSVEP frequencies. Results are shown in four blocks as A, B, C and D representing the responses of sensory neurons to SSVEP frequencies of 8.18Hz and 12Hz as well as the response of motor neurons to the similar frequencies. Each block consists of representation of firing rates to flicker (*A-D*, *1*) and no-flicker (*A-D*, *2*) trials. Red line separates the baseline and experimental epochs (each epoch consists of 100 bins of 10ms duration each). Black line separates the neurons with positive and negative responses. The average of firing rates are shown for flicker and no-flicker trials in both positive-response (*A-D*, *3*) and negative-response neurons (*A-D*, *4*). Red vertical lines in the latter four plots shown the onset when the stimulus appeared on the screen. Red (*) and blue (*) asterisks represent bins with significant difference ($p<0.05$) between flicker and no-flicker in increasing and decreasing responses, respectively.

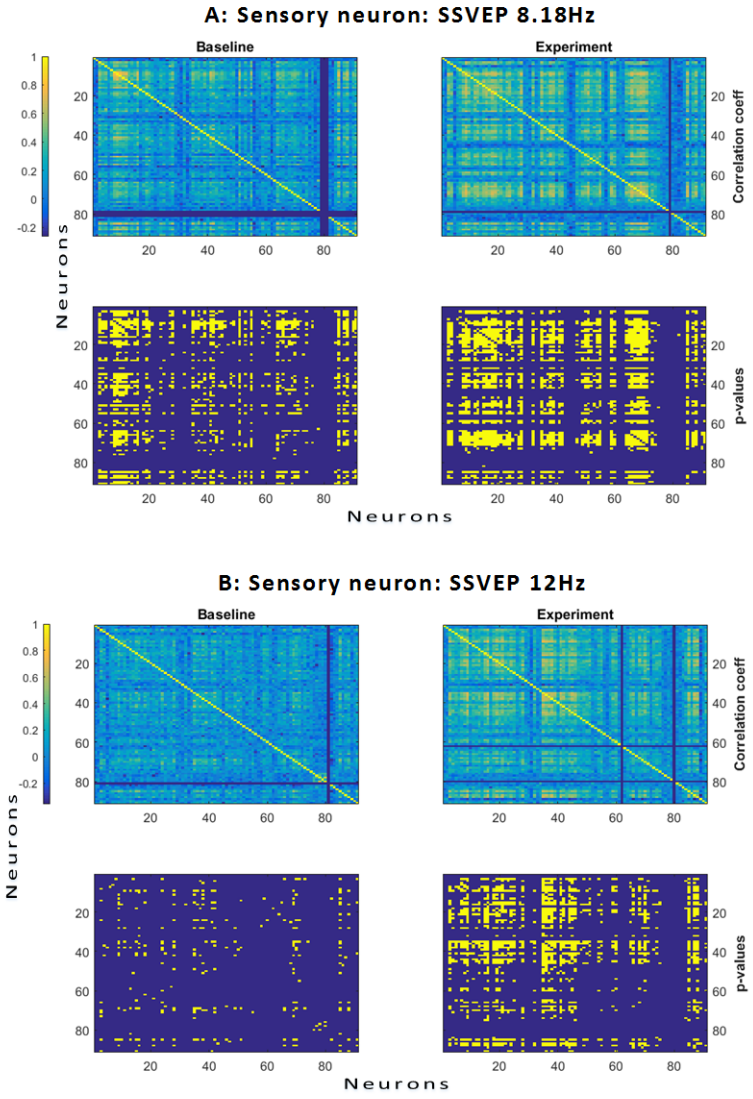

Figure 6.15: Pearson correlation coefficient of sensory neurons in flicker trials: pairs of different sensory neurons was correlated independently in baseline and experiment epochs in flicker trials. The set of two upper rows *(A)* correspond to the flicker frequency of 8.18Hz; whereas, the second set of two lower rows *(B)* are for 12Hz. Each set (A and B) consists of a correlation coefficient matrix. Larger coefficients are indicated lighter in the color-code. Furthermore, the matrices of p-values are also demonstrated where the light pixels indicate the significant ($p<0.001$) correlation of firing rates between pairs of neurons.

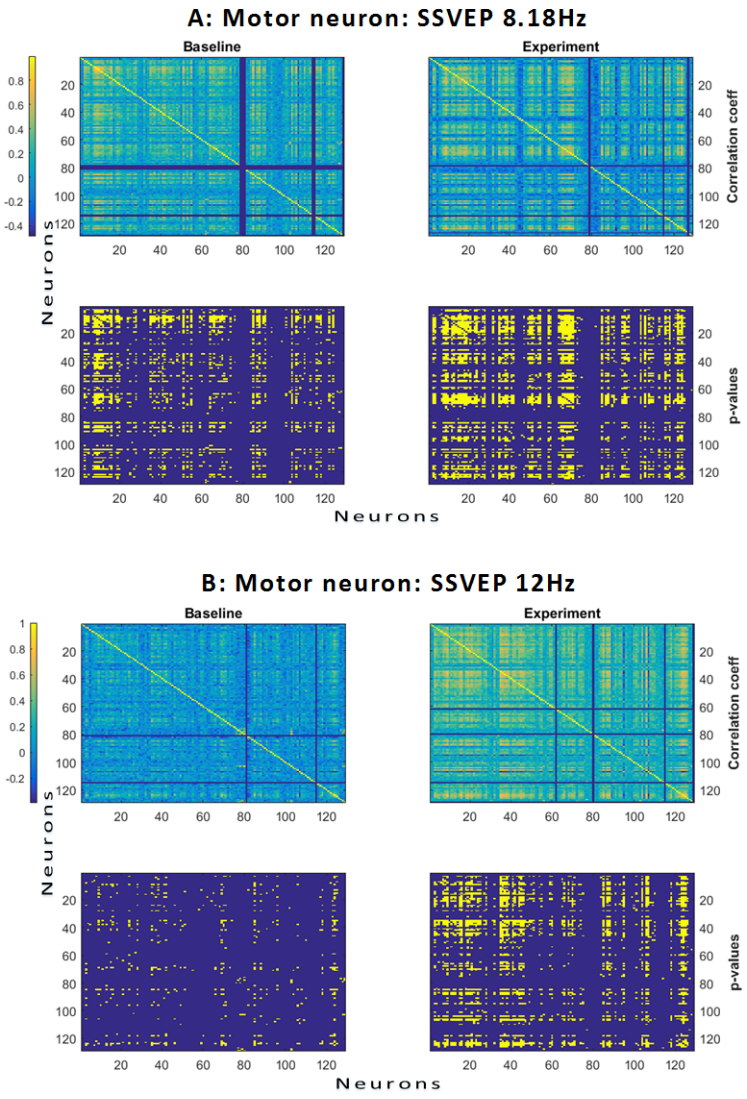

Figure 6.16: Pearson correlation coefficient of motor neurons in flicker trials: pairs of different motor neurons was correlated independently in baseline and experiment epochs in flicker trials. The set of two upper rows *(A)* correspond to the flicker frequency of 8.18Hz; whereas, the second set of two lower rows *(B)* are for 12Hz. Each set (*A* and *B*) consists of a correlation coefficient matrix. Larger coefficients are indicated lighter in the color-code. Furthermore, the matrices of p-values are also demonstrated where the light pixels indicate the significant ($p<0.001$) correlation of firing rates between pairs of neurons.

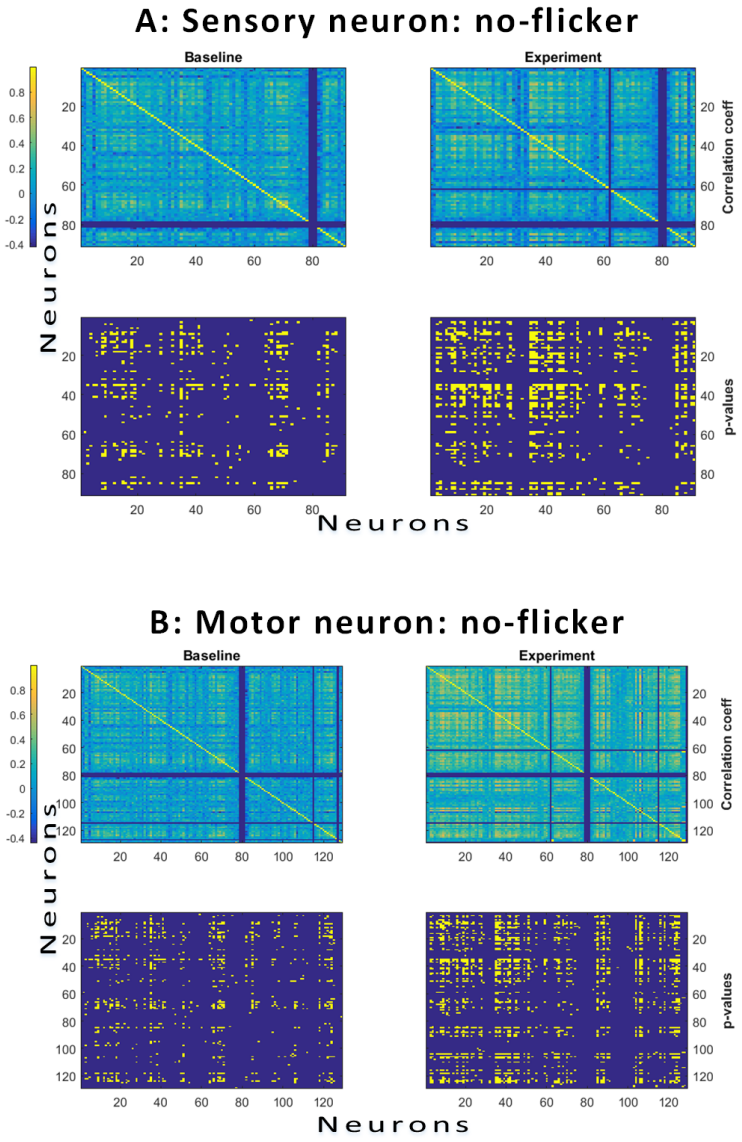

Figure 6.17: Pearson correlation coefficient of sensory and motor neurons in no-flicker trials: pairs of different sensory *(A)* and motor *(B)* neurons was correlated independently in baseline and experiment epochs in no-flicker trials. Each set (A and B) consists of a correlation coefficient matrix. Larger coefficients are indicated lighter in the color-code. Furthermore, the matrices of p-values are also demonstrated where the light pixels indicate the significant ($p<0.001$) correlation of firing rates between pairs of neurons.

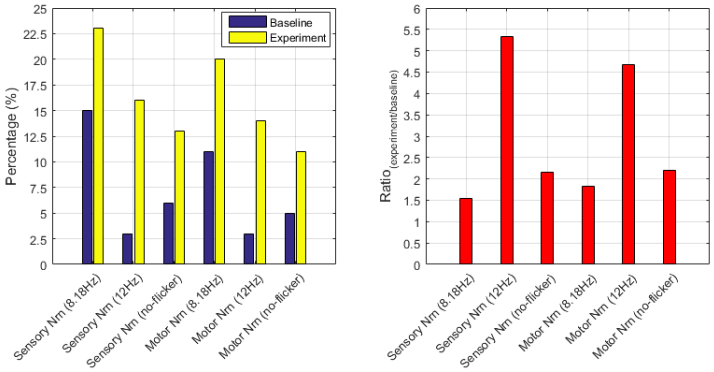

Figure 6.18: Percentage and ratios of correlated neurons: *(left)* the percentage of significantly correlated neurons has been shown in different conditions in flicker and no-flicker trials. The blue bars correspond to baseline epochs; whereas, the yellow bars are for experiment epochs. *(right)* The ratios of experiment/baseline epochs.

6.7.3 Frequency-band analysis

Finding the sample size (number of iteration in bootstrap): In order to find the number of replicates for the re-sampling purpose (bootstrapping), the number of samples (representing the number of iterations), was computed using the OC-curve (see equation 6.7). The number of samples obtained correspond to the statistical power of 80%. Figure 6.19 shows the number of iterations when flicker *vs.* no-flicker trials were compared in their baseline epochs; whereas, figure 6.20 demonstrates the number of iterations when flicker *vs.* no-flicker trials were compared in their experiment epochs. To keep the sample size consistent within a condition (e.g. in-target left), the maximum value of sample sizes (n obtained from the equation 6.7) was taken in one condition and iterated the AUCs in all neurons with the same sample size.

$$s_{ij} = max(\mathbf{n}_{ij}), \tag{6.10}$$

where s is the sample size for one condition, i is the neuron type ({Motor, Sensory}), j is the condition type ({left object (flicker), right object (flicker), left object (no-flicker), right object (no-flicker)}) and $\mathbf{n}$ is the column vector containing the sample sizes for each neuron in a certain condition type.

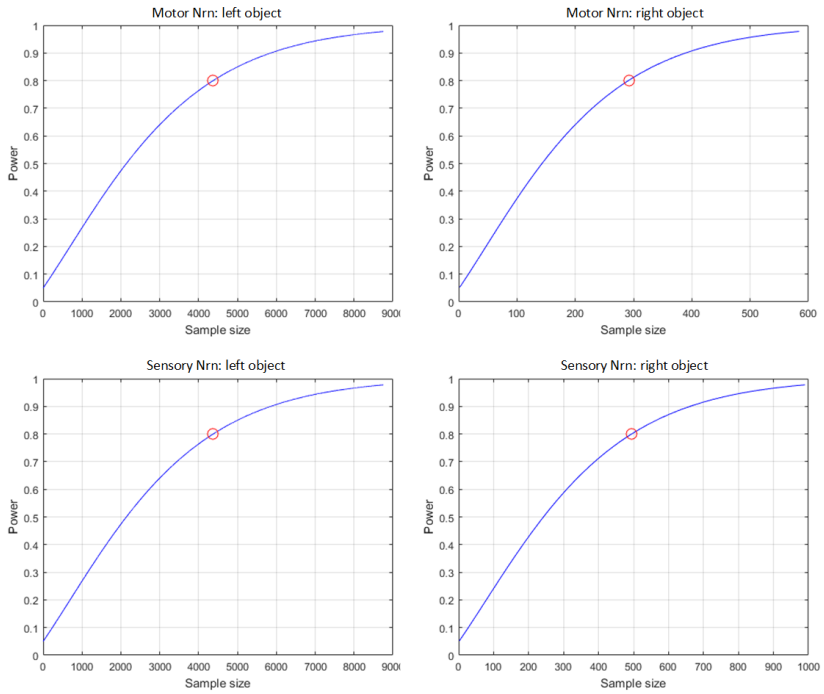

Figure 6.19: Sample size in baseline epochs: The number of samples (iterations for bootstrap re-sampling) were obtained when comparing the baseline epochs in flicker and no-flicker trials. Sample size for Motor neuron (left object) = 4375; Motor neuron (right object) = 292; Sensory neuron (left object) = 4377; Sensory neuron (right object) = 495. The flicker frequency for the left and right objects were 8.18Hz and 12Hz, respectively

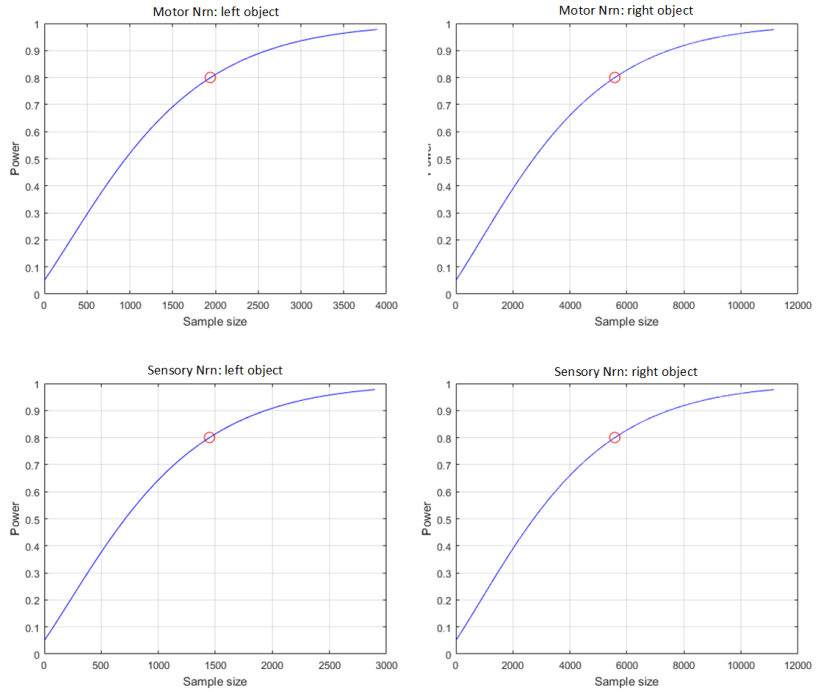

Figure 6.20: Sample size in experiment epochs: The number of samples (iterations for bootstrap re-sampling) were obtained when comparing the experiment epochs in flicker and no-flicker trials. Sample size for Motor neuron (left object) = 1944; Motor neuron (right object) = 5574; Sensory neuron (left object) = 1449; Sensory neuron (right object) = 5574. The flicker frequency for the left and right objects were 8.18Hz and 12Hz, respectively

Responsive neurons to flickering objects: Results from the unpaired t-tests between flicker and no-flicker trials showed that some neurons responded to the flicker stimulus. This was obvious because the percentage of neurons which had larger power in the flicker frequencies was significantly ($p<0.01$) higher compared to no-flicker trials. The comparison was done by paired t-test. To confirm that the t-value for the significant difference is the representative of entire population of trials (i.e. had we had more trials, the results would have still been similar) the re-sampled data were plotted on the histogram and tested if the original t-value is within 95% of t-values obtained from re-sampling procedure (see figure 6.21 and 6.22).

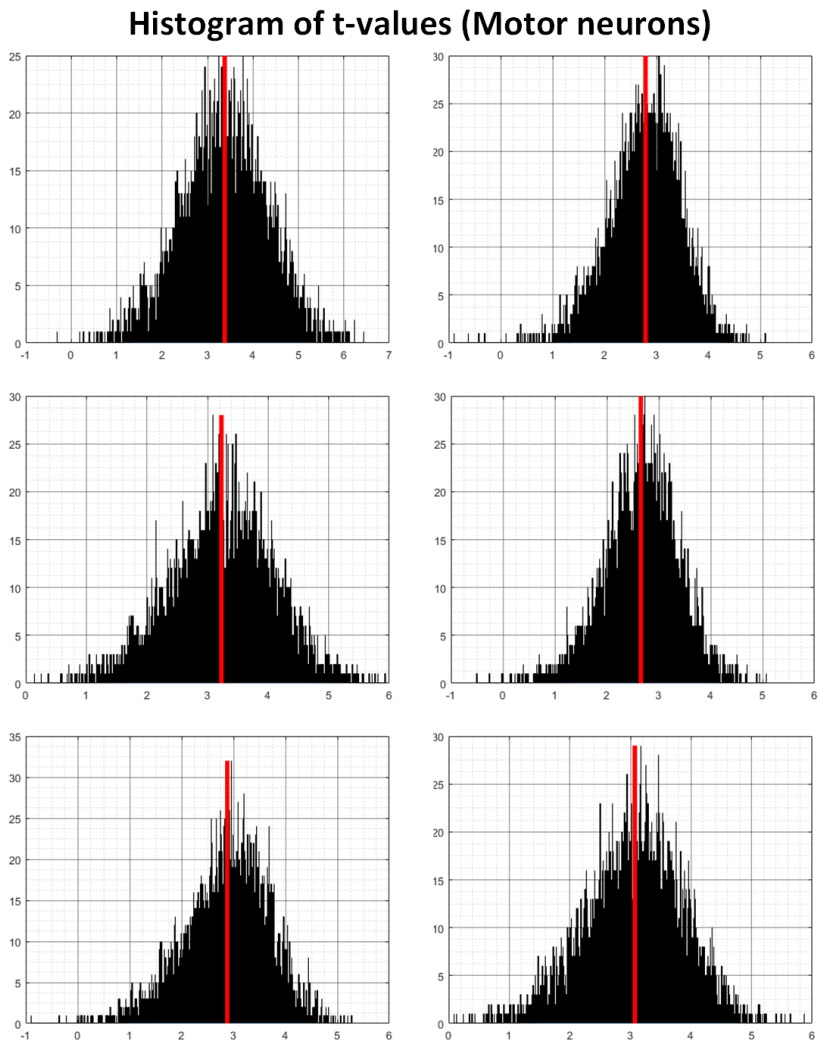

Figure 6.21: Histogram of re-sampled t-values: The histogram is for six motor neurons which showed significant increase in their AUC in flicker over no-flicker trials. The red line indicates the original t-value between the baseline epoch preceding 12Hz flicker *vs.* the baseline prior to no-flicker stimulus both in motor neurons. The histogram (bin width = 0.08) is plotted from the re-estimated t-values following 292 iterations.

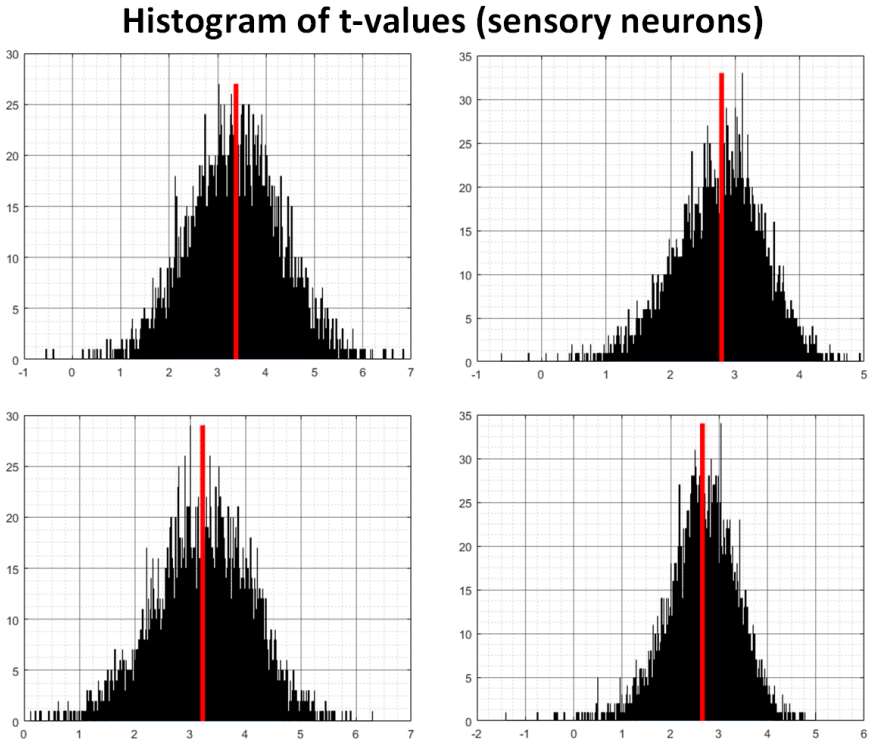

Figure 6.22: Histogram of re-sampled t-values: The histogram is for four sensory neurons which showed significant increase in their AUC in flicker over no-flicker trials. The red line indicates the original t-value between the baseline epoch preceding 12Hz flicker *vs.* the baseline prior to no-flicker stimulus both in sensory neurons. The histogram (bin width = 0.08) is plotted from the re-estimated t-values following 495 iterations.

Following re-sampling, it was observed that the original t-values are among t-values of the re-sampled AUCs. Therefore, the t-value could be a representative of larger population.

Results of the positively-responding neurons to the flicker stimulus shows that there is, at least partly, consistent increase in the amplitude of frequencies in the same range of flicker frequencies. Tables 6.2 through 6.6 show the percentage of neurons in which AUCs of the flicker frequency range was significantly ($p<0.01$) larger in flicker trials than in no-flicker trials.

Table 6.2: Percentage of responsive Motor & Sensory Neurons (Monkey M: **session# 1**)

	%Total(%Local)	
Group (flicker *vs.* no-flicker)	Motor Neurons	Sensory Neurons
Baseline: 8.18Hz flicker	00.00(00.00)	00.00(00.00)
Baseline: 12Hz flicker	04.65(100.00)	04.40(100.00)
Experiment: 8.18Hz flicker	17.83(71.88)	18.68(70.83)
Experiment: 12Hz flicker	05.43(24.14)	06.59(31.58)

Table 6.3: Percentage of responsive Motor & Sensory Neurons (Monkey M: **session# 2**)

	%Total(%Local)	
Group (flicker *vs.* no-flicker)	Motor Neurons	Sensory Neurons
Baseline: 8.18Hz flicker	01.50(21.04)	03.37(33.12)
Baseline: 12Hz flicker	06.77(77.79)	11.24(81.43)
Experiment: 8.18Hz flicker	15.79(78.93)	21.35(68.42)
Experiment: 12Hz flicker	05.26(47.14)	08.99(37.50)

Table 6.4: Percentage of responsive Motor & Sensory Neurons (Monkey M: **session# 3**)

	%Total(%Local)	
Group (flicker *vs.* no-flicker)	Motor Neurons	Sensory Neurons
Baseline: 8.18Hz flicker	00.83(16.67)	01.08(27.27)
Baseline: 12Hz flicker	04.96(85.71)	05.38(71.43)
Experiment: 8.18Hz flicker	14.88(78.26)	18.28(69.57)
Experiment: 12Hz flicker	04.96(28.57)	06.45(23.08)

Table 6.5: Percentage of responsive Motor & Sensory Neurons (Monkey M: **session# 4**)

	%Total(%Local)	
Group (flicker *vs.* no-flicker)	Motor Neurons	Sensory Neurons
Baseline: 8.18Hz flicker	00.00(00.00)	01.03(33.33)
Baseline: 12Hz flicker	03.50(71.83)	04.12(66.67)
Experiment: 8.18Hz flicker	11.19(76.19)	13.40(76.47)
Experiment: 12Hz flicker	04.90(46.67)	05.15(41.67)

Table 6.6: Percentage of responsive Motor & Sensory Neurons (Monkey M: **session# 5**)

	%Total(%Local)	
Group (flicker *vs.* no-flicker)	Motor Neurons	Sensory Neurons
Baseline: 8.18Hz flicker	01.44(28.57)	01.15(09.09)
Baseline: 12Hz flicker	02.88(57.14)	05.75(62.50)
Experiment: 8.18Hz flicker	12.23(77.27)	14.94(68.42)
Experiment: 12Hz flicker	03.60(55.56)	04.60(36.36)

6.8 Discussion

The current study was designed to understand the SSVEP representation in the somatosensory and motor cortices. Steady-state evoked potentials are stable oscillations that can be elicited by rapid repetitive visual, auditory and somatosensory stimuli. A typical way of inducing such kind of steady-state frequencies in the somatosensory cortex is SSSEPs (Stead-state somatosensory evoked potentials). In this method the tactile stimulations are delivered to the sensory organs and the recording is performed from the sensory and motor areas. Besides the conventional way of stimulation, evidence has shown that S1 and M1 areas respond to light-flash stimuli[177,188]. Results from this study is categorized into three different but interconnected sections in order to test the hypothesis introduced earlier in this chapter.

Results in the first section was to answer the first hypothesis to test whether SSVEPs alter the neuronal activity represented by firing rates. These results showed that both sensory and motor neurons are affected by the flicker frequencies. The effect was observed in two ways. One group of neurons responded by increasing (positively-responded) the firing rate and the other group by decreasing (negatively-responded). Negatively-responded neurons decreased their firing rates only in the first few millisecond of the baseline epochs in the flicker trials. As the effect of negatively-responded neurons was not observed in any other points, this part of the results was considered as inconclusive and no discussion will be dedicated for it.

Interestingly only the neuronal group with increased firing rates in response to the flickers showed significant difference in their experiment epochs compared to the experiment epochs of no-flicker trials. All comparisons between flicker trials and no-flicker trials were performed within the same neurons, and this enabled the use of paired t-test. As the number of significant points (bins) containing firing rates in the time-unit is much larger in the experiment rather than the baseline epochs of flicker compared to no-flicker trials, this indicates that such increase in firing rate is due to the SSVEPs. In the first glance this seems a very unconventional findings as the S1 and M1 neurons are specialized to be activated in sensory- and motor-related activities. However, these findings are in line with the literature showing that the particular neurons in M1 and S1 also respond to visual stimulus[177–179]. There have been several reports showing the existence of possible pathways from retina to pre-motor areas[192,193]. These findings were supported by recent monkey studies conducted by Shokur et al.[188]. The experiment was performed first by concurrent physical and virtual (P+V) stimuli and then by virtual only (V-only) stimulus. The physical stimulus was the brushing on the forearm; whereas, in the virtual stimulation monkey was observing an avatar hand being touched by a virtual ball on an LCD screen. They found that although the number of neurons which responded to the concurrent V+P was higher – obviously because of mechanical stimulation – yet some neurons were highly active in V-only stimulus. They argued that although such cortical activations are often interpreted as mirror responses to observation of an actions[182], validation of such argument is highly unlikely because simply viewing virtual touches without synchronous physical stimulation was insufficient for virtually evoked responses to develop. Modulation of S1 by visual information that differs from mirror responses has previously been reported in monkeys being trained for visuohaptic task that required short-term retention of tactile information[194]. Shokur et al.[188] also argued that M1 activity during V-only trials could not be present because of movements as there was no accompanying EMG** modulations. Similarly in our results, although the monkeys' arm was moving to locate the cursor in the target, the increase in firing rate is highly unlikely to be due to the movement effects. This is because the same condition applied to flicker and no-flicker trials equally, where in both the arm movement was included. This motor-related activities still can be observed in a time-period of a few millisecond before and after the onset of targets (see the peaks in average firing rates in figure 6.14 A-D, subplots 3-6). This was however, inevitable in our experiments due to the nature of the task which relied on moving the cursor. In future studies explicit arm movement can be eliminated by training monkeys to follow the target stimulus by eyes.

As shown in figure 6.14, increase in firing rate was much more continuous in 8.18Hz than 12Hz SSVEP frequency in both sensory and motor neurons. This could not be due to the lateralization effect (presentation of left stimulus in the right side of the brain and *vice versa*), as monkeys directly stared at the target flicker in each trial. Therefore, it is expected that the flickers are represented in both hemispheres. Neither could that be due to being right- or left-handed of monkeys as this factor was kept equal and monkey operated the joystick with the same hand overall the flicker and no-flicker trials. Thus, it is postulated that the effect is highly due to the visually-registered flicker frequencies. Therefore, results indicate that neurons are more sensitive to lower frequency (8.18Hz) than higher frequency (12Hz). The role of different SSVEP frequencies on brain networks has already been studied. Müller et al.[195] used magneto-encephalographic (MEG) recording to investigate whether discrete regions can be identified under different SSVEP frequencies. Three frequencies were used in their study as 6.0, 11.9 and 15.2Hz. They observed that the location of response alters based on the frequency shown to subjects. These results were supported by others[60] who

**Electromyogram

identified different origin of SSVEP generation in the range of 1-100Hz. Similar evidence was also presented in chapter 5 of this thesis where different scalp maps are demonstrated based on different frequencies. In line with Wu and Yao[67], one possibility that could explain the significant increase of firing rates in 8.18Hz than 12Hz would be that the origin of these two frequencies varied and the location recorded in the current study is most representative of the lower frequencies. To reveal more frequency-sensitive spatial resolution, one needs to record from a vast cortical area to localize different temporal frequencies. This was not in the scope of the current study as the objective was to see whether or not there is *any* response in these regions and the current finding was just enough to validate my hypothesis. In addition, such a localization was not possible because the electrodes were already implanted and fixed in monkeys' brain. Another reason that may explain the frequency-dependent response variation is the nature of the frequency characteristics. For example, studies[67] reported that the SSVEP amplitude and latency in lower frequency (8.3Hz in the study by Wu and Yao[67]) is more clear and stable than in the higher band (12Hz). This may be due to the increased signal-to-noise-ratio as the amplitude of signal diminishes as the SSVEP frequency raises. Results from the current study add on the previous findings by exploring the changes in the neuronal activity by analyzing in the single neuron level.

The second part of this chapter was to test the original hypothesis in which whether or not SSVEP-induced neuronal modulations are manifested as event-related neuronal synchrony (ERNS). SSVEP frequency enhanced the neuronal synchrony in sensory and motor neurons. Induction of synchronized firing rate by SSVEP frequency, in particular in the sensory and motor neurons was, to the best of our knowledge, the first study in the field. Previous studies have suggested that voluntary visual attention modulates neuronal spiking activities[196]. These studies have been exploring similar effects on the visual cortex. They showed that when visual stimuli are presented in the visual field, attention modulates neuronal spike rates for intrinsic oscillations[196] as well as the stimulus-induced frequencies such as SSVEP[197]. These SSVEP results with human observers support the idea that attention can substantially influence visual processing. Somatosensory activation has been reported in human fMRI[182,198,199] and EEG[200] studies while subjects were observing images of body parts being touched. As majority of previous results are explained by mirroring the action, results from current thesis show that at least in certain tasks, the *mirror* hypothesis could be just an alternative rather than a rule. Furthermore, findings from the present thesis demonstrated that neuronal firing rate synchronization in the sensory and motor areas happens in response to the visual flickering stimuli. Clearly the number of synchronized neurons in these areas may be much less than those in the visual cortex (this comparison has not been empirically shown in this thesis), but this is obviously because sensory and motor areas are not the primary and specialized regions for visual stimulation. A somewhat surprising finding from this study was the involvement of M1 in SSVEP-induced activation. As mentioned above, the firing rate synchronization in M1 could not be due to the motor movement as the conditions (e.g. magnitude of arm movement) were kept equal for flicker and no-flicker trials and the only factor which differed was indeed the flickers. Shokur et al.[188] suggested that the presence of somatosensory and visual responses in M1 indicates that the cortical mediation of visual stimulus is widely distributed throughout the frontal-parietal circuit. The strong interconnections between the S1 and M1 as well as their connection with the surrounding areas in the frontal and parietal areas provide a neuro-anatomical base for such a representation[180]. Furthermore, the absence of strict separation between the physiological function of somatosensory and motor cortices has been suggested to contribute in this phenomenon[201]. This notion has been supported by previous studies on rodents and primates[201,202]. Fitzsimmons[203] suggested that individual M1 and S1 cortical neurons may contribute to multiple computations simultaneously. Furthermore, other multi-electrode

recordings[204] have shown that there is a highly distributed and dynamic representation of multiple information streams in the cortex which may give rise to a responsive M1 to visual stimuli.

Observations of the correlated firing rates also showed that the neuronal synchronization was prominent in 12Hz flickering frequency rather than 8.18Hz. This may look to be in contrast to the findings from the previous results on the firing-rate alteration where firing rates increased more in response to lower flicker frequency. This suggests that even though firing rates varies in response to some events, these variations may not be necessarily synchronized between neurons. The current study raises such an interesting concept even though it remain unclear whether it is specific for M1 and S1 neurons or it is a general pattern in other brain regions such as neurons in the visual cortex. Further investigation is required for clarification of this pattern.

The last part of single neuron study on monkey was focused on the frequency analysis of the single neuron's activity. The amplitude of frequencies corresponding to SSVEPs were calculated in both experiment and baseline epochs. Ideally, I would expect that the SSVEP amplitudes in some neurons are larger in the experiment than in baseline epochs. This was partially obtained in our results showing that only in the higher SSVEP frequency range (12Hz) higher number of neurons had larger amplitude in the experiment epoch compared to the baseline. However, similar result was not observed in the low frequency range (8.18Hz). The fact that SSVEP oscillations only in high frequency caused neuronal response is inconsistent with findings from the first part of single-neuron study where the firing rates' response was more prominent in low SSVEP range. Whereas, it is consistent with the neuronal synchronization ability of high-frequency SSVEP. One trivial conclusion would be that the oscillations are indeed the outcome of neuronal synchronizations. But an interesting finding is that increased neuronal activity (firing rates) and generation of oscillations appears to be two independent phenomenon. This indicates that activity might be existing even though there is no oscillations detected from a specific region highlighting the necessity for combining different recording modalities for better signal detection of visual attention.

Chapter 7

Conclusions and future directions

7.1 Conclusion

The overall findings from this doctoral thesis can be categorized into two major parts. First is the macro-features obtained by EEG in human, and second, the micro-features acquired by the single neuron recordings in monkey.

This study was conducted to characterize the EEG signatures of visual attention in both overt and covert types of attentional orientation. While overlapping networks are identified in both types, I was interested in distinct pathways by which *ideally* two types of orientation can be identified by analyzing the EEG signals. Extracted features can be implemented as templates to drive external assistive devices such as BCIs with high precision on visual attention.

The visual task designed for this aim was based on steady-state visual evoked potentials (SSVEP) to measure a continuous performance of attention over several seconds. Results of the EEG study on humans revealed two major findings. *(1)* In the frequency-domain, the amplitude of the fundamental frequency was substantially higher in overt attention compared to covert attention. This was not an unexpected finding as subjects's gaze of attention was directly at the flicker stimulus, and therefore, the corresponding temporal frequency was registered almost intact. *(2)* When the stimulus was attended covertly, an interesting pattern emerged and it was increasing the second harmonic compared to the fundamental frequency. This pattern was not dominant in overt attention. These results already show that depending on the type of attention, we should expect different EEG signatures.

These findings on the frequency domain gave rise to the second hypothesis in the current research by trying to understand whether the outcome frequencies are originated from different neural sources. I found that when the SSVEP is attended overtly, the corresponding frequencies are extracted mostly from the primary visual cortex in the occipital area. The sources of activities shifts, however, to more anterior part in parietal and frontal lobes when attention is allocated covertly. This was an interesting finding clearly showing that the same type of input signals are handled in separate networks based on subjects orientation of attention.

The involvement of non-visual regions in response to the visual flickers was a motivation for the next step to explore structures in the parietal and frontal cortices more specifically. This aim was pursued by exploring the primary sensory (S1) and primary motor (M1) cortices in the rhesus monkey. A similar visual attention (SSVEP-based) task was presented to

the monkey while the data was collected using multi-unit electrodes. Each electrode recorded the spike activity of a single neuron. The data analysis was focused on two main aspects of neuronal activities: firing rates and frequency bands. Results from the firing rates indicated that presentation of flickering frequencies substantially increased the firing rates of neurons in both S1 and M1 areas. This enhancement was more continuous in lower flicker frequency. Furthermore, presentation of SSVEP to the monkey increased the neuronal synchronization. However, unlike the previous effect, the synchronization occurred more when the higher frequency flicker was presented. The latter finding was approved when the data was analyzed in the frequency domain in which the spectral analysis of the signals revealed larger amplitude in the higher SSVEP frequency. Consistent results in high-frequency SSVEP in both neuronal synchrony and spectral analysis showed that single neurons synchronization indeed results in the emerging the corresponding oscillation. However, since firing rates increased only in low- but not in high-frequency flickers, this suggests that neuronal activity is independent of occurrence of neural synchrony and eventually emergence of certain oscillations. In other words, despite the existence of the neuronal activities, the neural oscillations may not be detectable.

Combining findings from the monkeys with those of human studies, it could be concluded that the reason why certain oscillations are unexpectedly less dominant in certain regions (e.g. less activity in visual cortex in covert attention) is because the activation is there, but for some reason, covert attention was unable to synchronize the neuronal activities.
Another interesting application of current results would be to combine both recording modalities in implementation of assistive devices such as BCIs. Therefore, the BCI system benefits from the features of each individual modality by alternating between the features. This would give rise to a robust BCI system with more selective response to a certain brain function.

7.2 Study limitations

Human EEG study

- Performing the real-time experiments: the project was aiming to initiate a series of real-time experiment to apply the findings from the feature extraction of EEG data. This was not possible in the current circumstances due to time limitation.
- Number of human subjects: 18 subjects were selected out of 102 applications applied in June 2014. Most of the applicants were rejected due to not meeting the inclusion criteria. In addition, some applicants could not make a final appointment.

Monkey single-unit study

- Exploitation of covert attention in monkeys: in order to train monkeys to be involved in covert attention, we needed to have head fixation. This was not possible at the monkey lab of the Department of Neuroengineering as it was not defined in ethical protocol.
- Location of the electrodes in the brain: ideally, we would have to have the implants of the electrodes in specific locations well according to our EEG results in humans. However, the implantation of electrodes in the brain of an intact healthy monkey is an extremely long procedure (the ethical approval, operation, recovery, etc.). This was not possible during the 6 months of stay at Duke.
- Number of monkeys: two monkeys were recorded for the same experiment (monkey M and monkey C). However, monkey C was not cooperative during the experiments and did not perform the tasks properly.

7.3 Future directions

Future researches could inspire from the current thesis in the following directions:

- How a flickering stimulus is manipulated by different type of attention in the level of population response (EEG) as well as the neuronal response (single-unit)?
- Simultaneous recordings by EEG and single-unit approaches would reveal how two different responses correlate. This way makes it possible for extracting more distinct features related to attention.
- Findings from the current study can be implemented in real-time experiments to evaluate the level of visual attention

Bibliography

[1] M. I. Posner. Attention: the mechanisms of consciousness. *Proceedings of the National Academy of Sciences*, 91(16):7398–7403, aug 1994. DOI: 10.1073/pnas.91.16.7398.

[2] M. I. Posner. Attentional Networks and Consciousness. *Frontiers in Psychology*, 3, 2012. DOI: 10.3389/fpsyg.2012.00064.

[3] T. C. Sprague, S. Saproo, and J. T. Serences. Visual attention mitigates information loss in small- and large-scale neural codes. *Trends in Cognitive Sciences*, 19(4):215–226, apr 2015. DOI: 10.1016/j.tics.2015.02.005.

[4] J. Biederman. Age-Dependent Decline of Symptoms of Attention Deficit Hyperactivity Disorder: Impact of Remission Definition and Symptom Type. *American Journal of Psychiatry*, 157(5):816–818, may 2000. DOI: 10.1176/appi.ajp.157.5.816.

[5] S. V. FARAONE, J. BIEDERMAN, and E. MICK. The age-dependent decline of attention deficit hyperactivity disorder: a meta-analysis of follow-up studies. *Psychological Medicine*, 36(02):159, may 2005. DOI: 10.1017/S003329170500471X.

[6] A. P. Fleming and R. J. McMahon. Developmental Context and Treatment Principles for ADHD Among College Students. *Clinical Child and Family Psychology Review*, 15 (4):303–329, dec 2012. DOI: 10.1007/s10567-012-0121-z.

[7] J. G. Millichap. Etiologic Classification of Attention-Deficit/Hyperactivity Disorder. *PEDIATRICS*, 121(2):e358–e365, jan 2008. DOI: 10.1542/peds.2007-1332.

[8] G. Polanczyk and L. A. Rohde. Epidemiology of attention-deficit/hyperactivity disorder across the lifespan. *Current Opinion in Psychiatry*, 20(4):386–392, jul 2007. DOI: 10.1097/YCO.0b013e3281568d7a.

[9] M. Skounti, A. Philalithis, and E. Galanakis. Variations in prevalence of attention deficit hyperactivity disorder worldwide. *European Journal of Pediatrics*, 166(2):117–123, dec 2006. DOI: 10.1007/s00431-006-0299-5.

[10] C. K. Conners, J. N. Epstein, J. S. March, a. Angold, K. C. Wells, J. Klaric, J. M. Swanson, L. E. Arnold, H. B. Abikoff, G. R. Elliott, L. L. Greenhill, L. Hechtman, S. P. Hinshaw, B. Hoza, P. S. Jensen, H. C. Kraemer, J. H. Newcorn, W. E. Pelham, J. B. Severe, B. Vitiello, and T. Wigal. Multimodal treatment of ADHD in the MTA: an alternative outcome analysis. *Journal of the American Academy of Child and Adolescent Psychiatry*, 40(2):159–67, feb 2001. DOI: 10.1097/00004583-200102000-00010.

[11] L. L. Greenhill, J. M. Swanson, B. Vitiello, M. Davies, W. Clevenger, M. Wu, L. E. Arnold, H. B. Abikoff, O. G. Bukstein, C. K. Conners, G. R. Elliott, L. Hechtman,

S. P. Hinshaw, B. Hoza, P. S. Jensen, H. C. Kraemer, J. S. March, J. H. Newcorn, J. B. Severe, K. Wells, and T. Wigal. Impairment and deportment responses to different methylphenidate doses in children with ADHD: the MTA titration trial. *Journal of the American Academy of Child and Adolescent Psychiatry*, 40(2):180–7, feb 2001. DOI: 10.1097/00004583-200102000-00012.

[12] A. L. Vance, E. S. Luk, J. Costin, B. J. Tonge, and C. Pantelis. Attention deficit hyperactivity disorder: anxiety phenomena in children treated with psychostimulant medication for 6 months or more. *Australian and New Zealand Journal of Psychiatry*, 33(3):399–406, jan 1999. DOI: 10.1046/j.1440-1614.1999.00575.x.

[13] D. A. ZARIN, A. P. SUAREZ, H. A. PINCUS, E. KUPERSANIN, and J. M. ZITO. Clinical and Treatment Characteristics of Children With Attention-Deficit/Hyperactivity Disorder in Psychiatric Practice. *Journal of the American Academy of Child & Adolescent Psychiatry*, 37(12):1262–1270, dec 1998. DOI: 10.1097/00004583-199812000-00009.

[14] M. Arns, S. de Ridder, U. Strehl, M. Breteler, and A. Coenen. Efficacy of Neurofeedback Treatment in ADHD: The Effects on Inattention, Impulsivity and Hyperactivity: A Meta-Analysis. *Clinical EEG and Neuroscience*, 40(3):180–9, jul 2009. DOI: 10.1177/155005940904000311.

[15] C. G. Lim, T.-S. Lee, C. Guan, D. S. Sheng Fung, Y. B. Cheung, S. S. W. Teng, H. Zhang, and K. R. Krishnan. Effectiveness of a brain-computer interface based programme for the treatment of ADHD: a pilot study. *Psychopharmacology bulletin*, 43(1):73–82, jan 2010.

[16] C. G. Lim, T. S. Lee, C. Guan, D. S. S. Fung, Y. Zhao, S. S. W. Teng, H. Zhang, and K. R. R. Krishnan. A brain-computer interface based attention training program for treating attention deficit hyperactivity disorder. *PloS one*, 7(10):e46692, jan 2012. DOI: 10.1371/journal.pone.0046692.

[17] C.-Y. Chen, C.-L. Chen, C.-Y. Wu, H.-C. Chen, F.-T. Tang, and M.-K. Wong. Visual spatial attention in children with attention deficit hyperactivity disorder. *Chang Gung medical journal*, 25(8):514–521, 2002.

[18] J. M. Swanson, M. I. Posner, S. Potkin, S. Bonforte, D. Youpa, and C. Fiore. Activating tasks for the study of visual-spatial attention in ADHD children: A cognitive anatomic approach. *J Child Neurol*, 6:119–127, 1991.

[19] S. McDonald, K. Bennett, H. Chambers, and U. Castiello. Covert orienting and focusing of attention in children with attention deficit hyperactivity disorder. *Neuropsychologia*, 37(3):345–356, mar 1999. DOI: 10.1016/S0028-3932(98)00078-5.

[20] M. Carrasco and B. McElree. Covert attention accelerates the rate of visual information processing. *Proceedings of the National Academy of Sciences of the United States of America*, 98(9):5363–5367, 2001. DOI: 10.1073/pnas.081074098.

[21] L. Itti. <title>Real-time high-performance attention focusing in outdoors color video streams</title>. pages 235–243, jun 2002. DOI: 10.1117/12.469519.

[22] V. H. Hermann. *Trieatise on physiological optics*. Dover, New York, 1962.

[23] R. H. Wurtz and M. E. Goldberg. Activity of superior colliculus in behaving monkey. II. Effect of attention on neuronal responses. *J Neurophysiol*, 35(4):560–574, 1972.

[24] V. B. Mountcastle, J. C. Lynch, A. Georgopoulos, H. Sakata, and C. Acuna. Posterior parietal association cortex of the monkey: command functions for operations within extrapersonal space. *J Neurophysiol*, 38:871–908, 1975.

[25] B. Fischer and R. Boch. Enhanced activation of neurons in prelunate cortex before visually guided saccades of trained rhesus monkeys. *Experimental Brain Research*, 44 (2), oct 1981. DOI: 10.1007/BF00237333.

[26] L. Chelazzi, E. Miller, J. Duncan, and R. Desimone. A neural basis for visual search in inferior temporal cortex. *Nature*, 363:345–7, 1993. DOI: 10.1038/363345a0.

[27] T. Moore and M. H. Chang. Presaccadic discrimination of receptive field stimuli by area V4 neurons. *Vision Research*, 49(10):1227–1232, jun 2009. DOI: 10.1016/j.visres.2008.03.018.

[28] D. Felleman and D. Van Essen. Distributed hierarchical processing in the primate cerebral cortex. *Cerebral Cortex*, 1:1–47, 1991.

[29] R. Desimone and L. G. Ungerleider. *Neural mechanisms of visual processing in monkeys*. See Boller & Grafman, 1989.

[30] M. Goodale and A. Milner. Separate visual pathways for perception and action. *Trends in Neurosciences*, 15:20–25, 1992.

[31] R. a. Andersen. Multimodal representation of space in the posterior parietal cortex and its use in planning movements. *Annual review of neuroscience*, 20:303–330, 1997.

[32] M. J. Webster, J. Bachevalier, and L. G. Ungerleider. Connections of Inferior Temporal Areas TEO and TE with Parietal and Frontal Cortex in Macaque Monkeys. *Cerebral Cortex*, 4(5):470–483, 1994. DOI: 10.1093/cercor/4.5.470.

[33] M. S. Beauchamp. An fMRI Version of the Farnsworth-Munsell 100-Hue Test Reveals Multiple Color-selective Areas in Human Ventral Occipitotemporal Cortex. *Cerebral Cortex*, 9(3):257–263, apr 1999. DOI: 10.1093/cercor/9.3.257.

[34] S. Kastner and L. G. Ungerleider. MECHANISMS OF VISUAL ATTENTION IN THE HUMAN CORTEX. pages 315–341, 2000.

[35] E. Bisiach and G. Vallar. Hemineglect in humans. In F. Boller and J. Grafman, editors, *Handbook of Neuropsychology*, pages 195–222. Elsevier, Amsterdam, 1988.

[36] G. Vallar and D. Perani. The anatomy of unilateral neglect after right-hemisphere stroke lesions. A clinical/CT-scan correlation study in man. *Neuropsychologia*, 24(5): 609–622, jan 1986. DOI: 10.1016/0028-3932(86)90001-1.

[37] A. R. Damasio, H. Damasio, and H. C. Chui. Neglect following damage to frontal lobe or basal ganglia. *Neuropsychologia*, 18(2):123–132, jan 1980. DOI: 10.1016/0028-3932(80)90058-5.

[38] S. Kastner, W. De, R. Desimone, and L. G. Ungerleider. Mechanisms of directed attention in the human extrastriate cortex as revealed by functional MRI. *Science*, 282:108–111, 1998.

[39] M. Corbetta. Frontoparietal cortical networks for directing attention and the eye to visual locations: identical, independent, or overlapping neural systems? *Proceedings of the National Academy of Sciences of the United States of America*, 95(3):831–8, feb 1998.

[40] J. C. Culham, S. a. Brandt, P. Cavanagh, N. G. Kanwisher, a. M. Dale, and R. B. Tootell. Cortical fMRI activation produced by attentive tracking of moving targets. *Journal of neurophysiology*, 80(5):2657–2670, 1998. DOI: 9819271.

[41] G. G. Gregoriou, S. Paneri, and P. Sapountzis. Oscillatory synchrony as a mechanism of attentional processing. *Brain Research*, 1626:1–18, 2015. DOI: 10.1016/j.brainres.2015.02.004.

[42] C. a. Bosman, J.-M. Schoffelen, N. Brunet, R. Oostenveld, A. M. Bastos, T. Womelsdorf, B. Rubehn, T. Stieglitz, P. De Weerd, and P. Fries. Attentional stimulus selection through selective synchronization between monkey visual areas. *Neuron*, 75 (5):875–88, sep 2012. DOI: 10.1016/j.neuron.2012.06.037.

[43] R. Klein and M. Lawrence. Cognitive neuroscience of attention. In M. I. Posner, editor, *Cognitive Neuroscience of Attention*, chapter Ch.2, page 514. Guilford Publication Inc., New York, 2nd edition, 2012.

[44] M. I. Posner. Orienting of attention. *The Quarterly journal of experimental psychology*, 32(1):3–25, feb 1980.

[45] J. W. Bisley. The neural basis of visual attention. *The Journal of Physiology*, 589(1): 49–57, jan 2011. DOI: 10.1113/jphysiol.2010.192666.

[46] M. I. Posner and S. E. Petersen. The attention system of the human brain. *Annual review of neuroscience*, 13:25–42, jan 1990. DOI: 10.1146/annurev.ne.13.030190.000325.

[47] M. Ordikhani-Seyedlar, A. Khani, and M. A. Lebedev. Paradigm shifts in theories of attention. *Frontiers in Human Neuroscience*, Submitted, 2016.

[48] G. Rizzolatti, L. Riggio, I. Dascola, and C. Umiltá. Reorienting attention across the horizontal and vertical meridians: evidence in favor of a premotor theory of attention. *Neuropsychologia*, 25(1A):31–40, jan 1987.

[49] M. I. Posner, Y. Cohen, and R. D. Rafal. Neural Systems Control of Spatial Orienting. *Philosophical Transactions of the Royal Society B: Biological Sciences*, 298(1089):187–198, jun 1982. DOI: 10.1098/rstb.1982.0081.

[50] B. Hans. Uber das Elektrenkephalogramm des Menschen. *Arch. Psychiatr. Nervenkr*, 87:527–580, 1929.

[51] S. Sanei and J. Chambers. *EEG signal processing*. John Wiley & Sons, Ltd, 2007.

[52] Boundless. *Boundless Biology*. 2016. ISBN 11995-v408955.
URL `https://www.boundless.com/biology/`.

[53] P. Olejniczak. Neurophysiologic Basis of EEG. *Journal of Clinical Neurophysiology*, 23(3):186–189, jun 2006. DOI: 10.1097/01.wnp.0000220079.61973.6c.

[54] J. Martin. The collective electrical behavior of cortical neurons: the electroencephalogram and the mechanisms of epilepsy. In E. Kandel, J. Schwartz, and T. Jessel, editors, *Principles of neural science*, pages 777–791. Norwalk: Appleton and Lange, 1991.

[55] S. T. Morgan, J. C. Hansen, and S. a. Hillyard. Selective attention to stimulus location modulates the steady-state visual evoked potential. *Proceedings of the National Academy of Sciences of the United States of America*, 93(10):4770–4, may 1996.

[56] V. P. Clark and S. A. Hillyard. Spatial Selective Attention Affects Early Extrastriate But Not Striate Components of the Visual Evoked Potential. *Journal of Cognitive Neuroscience*, 8(5):387–402, sep 1996. DOI: 10.1162/jocn.1996.8.5.387.

[57] S. Yantis and J. Jonides. Abrupt visual onsets and selective attention: Voluntary versus automatic allocation. *Journal of Experimental Psychology: Human Perception and Performance*, 16(1):121–134, 1990. DOI: 10.1037/0096-1523.16.1.121.

[58] E. D. Adrian and B. H. C. Matthews. THE BERGER RHYTHM: POTENTIAL CHANGES FROM THE OCCIPITAL LOBES IN MAN. *Brain*, 57(4):355–385, 1934. DOI: 10.1093/brain/57.4.355.

[59] D. Regan. *Human brain electrophysiology: Evoked poetntials and evoked magnetic fields in science and medicine*. 1988.

[60] C. S. Herrmann. Human EEG responses to 1-100 Hz flicker: resonance phenomena in visual cortex and their potential correlation to cognitive phenomena. *Experimental Brain Research*, 137(3-4):346–353, apr 2001. DOI: 10.1007/s002210100682.

[61] C. S. Herrmann. Human EEG responses to 1-100 Hz flicker: Resonance phenomena in visual cortex and their potential correlation to cognitive phenomena. *Experimental Brain Research*, 137(3-4):346–353, 2001. DOI: 10.1007/s002210100682.

[62] Y. Zhang, P. Xu, T. Liu, J. Hu, R. Zhang, and D. Yao. Multiple Frequencies Sequential Coding for SSVEP-Based Brain-Computer Interface. *PLoS ONE*, 7(3):e29519, mar 2012. DOI: 10.1371/journal.pone.0029519.

[63] G. Rager and W. Singer. The response of cat visual cortex to flicker stimuli of variable frequency. *European Journal of Neuroscience*, 10(5):1856–1877, may 1998. DOI: 10.1046/j.1460-9568.1998.00197.x.

[64] J. Ding, G. Sperling, and R. Srinivasan. Attentional modulation of SSVEP power depends on the network tagged by the flicker frequency. *Cerebral cortex (New York, N.Y. : 1991)*, 16(7):1016–29, jul 2006. DOI: 10.1093/cercor/bhj044.

[65] P. Zhang, K. Jamison, S. Engel, B. He, and S. He. Binocular Rivalry Requires Visual Attention. *Neuron*, 71(2):362–369, jul 2011. DOI: 10.1016/j.neuron.2011.05.035.

[66] Z. Wu, D. Yao, Y. Tang, Y. Huang, and S. Su. Amplitude modulation of steady-state visual evoked potentials by event-related potentials in a working memory task. *Journal of Biological Physics*, 36(3):261–271, jun 2010. DOI: 10.1007/s10867-009-9181-9.

[67] Z. Wu and D. Yao. The Influence of Cognitive Tasks on Different Frequencies Steady-state Visual Evoked Potentials. *Brain Topography*, 20(2):97–104, oct 2007. DOI: 10.1007/s10548-007-0035-0.

[68] D. Sutoyo and R. Srinivasan. Nonlinear SSVEP responses are sensitive to the perceptual binding of visual hemifields during conventional eye rivalry and interocular percept rivalry. *Brain Research*, 1251:245–255, jan 2009. DOI: 10.1016/j.brainres.2008.09.086.

[69] F. Di Russo and D. Spinelli. Effects of sustained, voluntary attention on amplitude and latency of steady-state visual evoked potential: a costs and benefits analysis. *Clinical neurophysiology : official journal of the International Federation of Clinical Neurophysiology*, 113(11):1771–7, nov 2002.

[70] R. Srinivasan, F. A. Bibi, and P. L. Nunez. Steady-State Visual Evoked Potentials: Distributed Local Sources and Wave-Like Dynamics Are Sensitive to Flicker Frequency. *Brain Topography*, 18(3):167–187, mar 2006. DOI: 10.1007/s10548-006-0267-4.

[71] R. Srinivasan, E. Fornari, M. G. Knyazeva, R. Meuli, and P. Maeder. fMRI responses in medial frontal cortex that depend on the temporal frequency of visual input. *Experimental Brain Research*, 180(4):677–691, jun 2007. DOI: 10.1007/s00221-007-0886-3.

[72] M. a. Pastor, J. Artieda, J. Arbizu, M. Valencia, and J. C. Masdeu. Human cerebral activation during steady-state visual-evoked responses. *The Journal of neuroscience : the official journal of the Society for Neuroscience*, 23(37):11621–11627, 2003. DOI: 23/37/11621 [pii].

[73] M. Pastor, M. Valencia, J. Artieda, M. Alegre, and J. Masdeu. Topography of Cortical Activation Differs for Fundamental and Harmonic Frequencies of the Steady-State Visual-Evoked Responses. An EEG and PET H215O Study. *Cerebral Cortex*, 17(8): 1899–1905, aug 2007. DOI: 10.1093/cercor/bhl098.

[74] F. Li, Y. Tian, Y. Zhang, K. Qiu, C. Tian, W. Jing, and T. Liu. The enhanced information flow from visual cortex to frontal area facilitates SSVEP response : evidence from model-driven and data-driven causality analysis. *Nature Publishing Group*, (October):1–11, 2015. DOI: 10.1038/srep14765.

[75] J. Mast and J. D. Victor. Fluctuations of steady-state VEPs: interaction of driven evoked potentials and the EEG. *Electroencephalography and Clinical Neurophysiology*, 78(5):389–401, may 1991. DOI: 10.1016/0013-4694(91)90100-I.

[76] M. M. Müller, W. Teder-sälejärvi, and S. A. Hillyard. The time course of cortical facilitation during cued shifts of spatial attention. *Nature neuroscience*, 1:631–634, 1998.

[77] A. M. Norcia, L. G. Appelbaum, J. M. Ales, B. R. Cottereau, and B. Rossion. The steady-state visual evoked potential in vision research : A review. *Journal of vision*, 15(6):1–46, 2015. DOI: 10.1167/15.6.4.doi.

[78] R. B. Silberstein, M. A. Schier, A. Pipingas, J. Ciorciari, S. R. Wood, and D. G. Simpson. Steady-State Visually Evoked Potential topography associated with a visual vigilance task. *Brain Topography*, 3(2):337–347, 1990. DOI: 10.1007/BF01135443.

[79] B. Corp. EEG setup.
URL `http://www.biosemi.com/`.

[80] J. Ding, G. Sperling, and R. Srinivasan. Attentional modulation of SSVEP power depends on the network tagged by the flicker frequency. *Cerebral Cortex*, 16(7):1016–1029, 2006. DOI: 10.1093/cercor/bhj044.

[81] A. Delorme and S. Makeig. EEGLAB: an open source toolbox for analysis of single-trial EEG dynamics including independent component analysis. *Journal of neuroscience methods*, 134(1):9–21, mar 2004. DOI: 10.1016/j.jneumeth.2003.10.009.

[82] P. L. Nunez. *Electric fields of the brain*. Oxford University Press, 1981.

[83] M. S. Treder and B. Blankertz. (C)overt attention and visual speller design in an ERP-based brain-computer interface. *Behavioral and brain functions : BBF*, 6(February): 28, 2010. DOI: 10.1186/1744-9081-6-28.

[84] S. Walter, C. Quigley, S. K. Andersen, and M. M. Mueller. Effects of overt and covert attention on the steady-state visual evoked potential. *Neuroscience letters*, 519(1): 37–41, jun 2012. DOI: 10.1016/j.neulet.2012.05.011.

[85] P. Xu, C. Tian, Y. Zhang, W. Jing, Z. Wang, T. Liu, J. Hu, Y. Tian, Y. Xia, and D. Yao. Cortical network properties revealed by SSVEP in anesthetized rats. *Scientific reports*, 3:2496, jan 2013. DOI: 10.1038/srep02496.

[86] S. P. Kelly, J. J. Foxe, G. Newman, and J. a. Edelman. Prepare for conflict: EEG correlates of the anticipation of target competition during overt and covert shifts of visual attention. *The European journal of neuroscience*, 31(9):1690–700, may 2010. DOI: 10.1111/j.1460-9568.2010.07219.x.

[87] S. P. Kelly, E. Lalor, C. Finucane, and R. B. Reilly. A comparison of covert and overt attention as a control option in a steady-state visual evoked potential-based brain computer interface. *Conference proceedings : ... Annual International Conference of the IEEE Engineering in Medicine and Biology Society. IEEE Engineering in Medicine and Biology Society. Conference*, 7:4725–8, jan 2004. DOI: 10.1109/IEMBS.2004.1404308.

[88] M. Middendorf, G. McMillan, G. Calhoun, and K. Jones. Brain-computer interfaces based on the steady-state visual-evoked response. *IEEE Transactions on Rehabilitation Engineering*, 8(2):211–214, jun 2000. DOI: 10.1109/86.847819.

[89] P. Cavanagh. Visual cognition. *Vision Research*, 51(13):1538–1551, jul 2011. DOI: 10.1016/j.visres.2011.01.015.

[90] C. Harnois, I. Bodis-Wollner, and M. Onofrj. The effect of contrast and spatial frequency on the visual evoked potential of the hooded rat. *Experimental Brain Research*, 57:1–8, 1984.

[91] Z. Liang, J. King, and N. Zhang. Intrinsic Organization of the Anesthetized Brain. *Journal of Neuroscience*, 32(30):10183–10191, 2012. DOI: 10.1523/JNEUROSCI.1020-12.2012.

[92] M. Regan and D. Regan. A frequency domain technique for characterizing nonlinearities in biological systems. *Journal of Theoretical Biology*, 133(3):293–317, aug 1988. DOI: 10.1016/S0022-5193(88)80323-0.

[93] K. W. Jamison, A. V. Roy, S. He, S. A. Engel, and B. He. SSVEP signatures of binocular rivalry during simultaneous EEG and fMRI. *Journal of Neuroscience Methods*, pages 1–10, 2015. DOI: 10.1016/j.jneumeth.2015.01.024.

[94] Z. Lin, C. Zhang, W. Wu, and X. Gao. Frequency recognition based on canonical correlation analysis for SSVEP-based BCIs. *IEEE transactions on bio-medical engineering*, 54(6 Pt 2):1172–6, jun 2007. DOI: 10.1109/TBME.2006.886577.

[95] L. F. Nicolas-Alonso and J. Gomez-Gil. Brain computer interfaces, a review. *Sensors (Basel, Switzerland)*, 12(2):1211–79, jan 2012. DOI: 10.3390/s120201211.

[96] P. Horki, C. Neuper, G. Pfurtscheller, and G. Müller-Putz. Asynchronous steady-state visual evoked potential based BCI control of a 2-DoF artificial upper limb. *Biomedizinische Technik. Biomedical engineering*, 55(6):367–74, dec 2010. DOI: 10.1515/BMT.2010.044.

[97] Z. Wu, Y. Lai, Y. Xia, D. Wu, and D. Yao. Stimulator selection in SSVEP-based BCI. *Medical engineering & physics*, 30(8):1079–88, oct 2008. DOI: 10.1016/j.medengphy.2008.01.004.

[98] J. Xie, G. Xu, J. Wang, S. Zhang, F. Zhang, Y. Li, C. Han, and L. Li. Addition of visual noise boosts evoked potential-based brain-computer interface. *Scientific reports*, 4:4953, 2014. DOI: 10.1038/srep04953.

[99] W. Klonowski. Everything you wanted to ask about EEG but were afraid to get the right answer. *Nonlinear biomedical physics*, 3:2, 2009. DOI: 10.1186/1753-4631-3-2.

[100] W. Klonowski. From conformons to human brains: an informal overview of nonlinear dynamics and its applications in biomedicine. *Nonlinear biomedical physics*, 1(1):5, 2007. DOI: 10.1186/1753-4631-1-5.

[101] D. Tranchina, J. Gordon, R. Shapley, and J. Toyoda. Linear information processing in the retina: a study of horizontal cell responses. *Proceedings of the National Academy of Sciences of the United States of America*, 78(10):6540–2, 1981. DOI: 10.1073/pnas.78.10.6540.

[102] D. J. Wielaard, M. Shelley, D. McLaughlin, and R. Shapley. How simple cells are made in a nonlinear network model of the visual cortex. *The Journal of neuroscience : the official journal of the Society for Neuroscience*, 21(14):5203–5211, 2001.

[103] D. H. Hubel and T. N. Wiesel. Receptive fields, binocular interaction and functional architecture in the cat's visual cortex. *The Journal of Physiology*, 160(1):106–154, jan 1962. DOI: 10.1113/jphysiol.1962.sp006837.

[104] D. H. Hubel and T. N. Wiesel. Receptive fields and functional architecture of monkey striate cortex. *The Journal of Physiology*, 195(1):215–243, mar 1968. DOI: 10.1113/jphysiol.1968.sp008455.

[105] R. L. De Valois, D. G. Albrecht, and L. G. Thorell. Spatial frequency selectivity of cells in macaque visual cortex. *Vision Research*, 22(5):545–559, jan 1982. DOI: 10.1016/0042-6989(82)90113-4.

[106] L. P. O'Keefe, J. B. Levitt, D. C. Kiper, R. M. Shapley, and J. a. Movshon. Functional organization of owl monkey lateral geniculate nucleus and visual cortex. *Journal of neurophysiology*, 80(2):594–609, 1998.

[107] S. V. Girman, Y. Sauvé, and R. D. Lund. Receptive Field Properties of Single Neurons in Rat Primary Visual Cortex. pages 301–311, 2010.

[108] D. L. Glanzman. Spatial properties of cells in the rabbit's striate cortex. *The Journal of Physiology*, 340(1):535–553, jul 1983. DOI: 10.1113/jphysiol.1983.sp014779.

[109] B. Wandell. *Foundations of Vision*. Sinauer Associates, Inc., Sunderland, MA, apr 1995. DOI: 10.1002/col.5080210213.

[110] M. Ito and C. D. Gilbert. Attention Modulates Contextual Influences in the Primary Visual Cortex of Alert Monkeys. *Neuron*, 22(3):593–604, mar 1999. DOI: 10.1016/S0896-6273(00)80713-8.

[111] C. J. McAdams and R. C. Reid. Attention Modulates the Responses of Simple Cells in Monkey Primary Visual Cortex. *The Journal of neuroscience: the official journal of the Society for Neuroscience*, 25(47):11023–11033, 2005. DOI: 10.1523/JNEUROSCI.2904-05.2005.

[112] M. M. Moore. Real-world applications for brain-computer interface technology. *IEEE transactions on neural systems and rehabilitation engineering : a publication of the IEEE Engineering in Medicine and Biology Society*, 11(2):162–5, jun 2003. DOI: 10.1109/TNSRE.2003.814433.

[113] B. D. Haan, P. S. Morgan, and C. Rorden. Covert orienting of attention and overt eye movemens activate identical brain regions. *Brain research*, 1204:102–111, 2008.

[114] T. R. Sato and J. D. Schall. Effects of stimulus-response compatibility on neural selection in frontal eye field. *Neuron*, 38(4):637–648, 2003. DOI: 10.1016/S0896-6273(03)00237-X.

[115] K. G. Thompson, K. L. Biscoe, and T. R. Sato. Neuronal basis of covert spatial attention in the frontal eye field. *The Journal of neuroscience : the official journal of the Society for Neuroscience*, 25(41):9479–9487, 2005. DOI: 10.1523/JNEUROSCI.0741-05.2005.

[116] M. S. Beauchamp, L. Petit, T. M. Ellmore, J. Ingeholm, and J. V. Haxby. A parametric fMRI study of overt and covert shifts of visuospatial attention. *NeuroImage*, 14:310–321, 2001. DOI: 10.1006/nimg.2001.0788.

[117] H. Golla, P. Thier, and T. Haarmeier. Disturbed overt but normal covert shifts of attention in adult cerebellar patients. *Brain : a journal of neurology*, 128(Pt 7):1525–35, jul 2005. DOI: 10.1093/brain/awh523.

[118] A. Ignashchenkova, P. W. Dicke, T. Haarmeier, and P. Thier. Neuron-specific contribution of the superior colliculus to overt and covert shifts of attention. *Nature neuroscience*, 7(1):56–64, jan 2004. DOI: 10.1038/nn1169.

[119] R. B. Silberstein, J. Ciorciari, and A. Pipingas. Steady-state visually evoked potential topography during the Wisconsin card sorting test. *Electroencephalography and clinical neurophysiology*, 96(1):24–35, jan 1995.

[120] S. Panzeri, R. S. Petersen, S. R. Schultz, M. Lebedev, and M. E. Diamond. The role of spike timing in the coding of stimulus location in rat somatosensory cortex. *Neuron*, 29(3):769–77, mar 2001.

[121] M. M. Müller, T. W. Picton, P. Valdes-Sosa, J. Riera, W. A. Teder-Sälejärvi, and S. A. Hillyard. Effects of spatial selective attention on the steady-state visual evoked potential in the 20-28 Hz range. *Cognitive Brain Research*, 6(4):249–261, apr 1998. DOI: 10.1016/S0926-6410(97)00036-0.

[122] M. M. Muller, S. Andersen, N. J. Trujillo, P. Valdes-Sosa, P. Malinowski, and S. A. Hillyard. Feature-selective attention enhances color signals in early visual areas of the human brain. *Proceedings of the National Academy of Sciences*, 103(38):14250–14254, sep 2006. DOI: 10.1073/pnas.0606668103.

[123] S. K. Andersen, S. Fuchs, and M. M. Müller. Effects of Feature-selective and Spatial Attention at Different Stages of Visual Processing. *Journal of Cognitive Neuroscience*, 23(1):238–246, jan 2011. DOI: 10.1162/jocn.2009.21328.

[124] M. M. Müller, T. W. Picton, P. Valdes-Sosa, J. Riera, W. a. Teder-Sälejärvi, and S. a. Hillyard. Effects of spatial selective attention on the steady-state visual evoked potential in the 20-28 Hz range. *Brain research. Cognitive brain research*, 6(4):249–61, apr 1998.

[125] S. a. Hillyard, H. Hinrichs, C. Tempelmann, S. T. Morgan, J. C. Hansen, H. Scheich, and H. J. Heinze. Combining steady-state visual evoked potentials and f MRI to localize brain activity during selective attention. *Human brain mapping*, 5:287–292, 1997. DOI: 10.1002/(SICI)1097-0193(1997)5:4<287::AID-HBM14>3.0.CO;2-B.

[126] S. Makeig. EEGLAB Wikitorial. *NatGenet*, 14(1061-4036 LA - eng PT - Comment PT - Letter SB - IM):132–133, 1996.

[127] S. Makeig. Auditory event-related dynamics of the EEG spectrum and effects of exposure to tones. *Electroencephalography and Clinical Neurophysiology*, 86(4):283–293, apr 1993. DOI: 10.1016/0013-4694(93)90110-H.

[128] A. Delorme and S. Makeig. EEGLAB: an open source toolbox for analysis of single-trial EEG dynamics including independent component analysis. *Journal of Neuroscience Methods*, 134(1):9–21, mar 2004. DOI: 10.1016/j.jneumeth.2003.10.009.

[129] S. Makeig, A. Delorme, M. Westerfield, T.-P. Jung, J. Townsend, E. Courchesne, and T. J. Sejnowski. Electroencephalographic brain dynamics following manually responded visual targets. *PLoS biology*, 2(6):e176, jun 2004. DOI: 10.1371/journal.pbio.0020176.

[130] R. Oostenveld and T. F. Oostendorp. Validating the boundary element method for forward and inverse EEG computations in the presence of a hole in the skull. *Human Brain Mapping*, 17(3):179–192, nov 2002. DOI: 10.1002/hbm.10061.

[131] K. Gramann, J. Onton, D. Riccobon, H. J. Mueller, S. Bardins, and S. Makeig. Human brain dynamics accompanying use of egocentric and allocentric reference frames during navigation. *Journal of cognitive neuroscience*, 22:2836–2849, 2010. DOI: 10.1162/jocn.2009.21369.

[132] T.-P. Jung, S. Makeig, M. Westerfield, J. Townsend, E. Courchesne, and T. J. Sejnowski. Analysis and visualization of single-trial event-related potentials. *Human Brain Mapping*, 14(3):166–185, nov 2001. DOI: 10.1002/hbm.1050.

[133] K. Nakayama. Sustained and Transient Components. 29(Ii):1631–1647, 1989.

[134] J. M. Ales, J. L. Yates, and A. M. Norcia. V1 is not uniquely identified by polarity reversals of responses to upper and lower visual field stimuli. *NeuroImage*, 52(4): 1401–1409, 2010. DOI: 10.1016/j.neuroimage.2010.05.016.

[135] S. J. Luck. *An introduction to the event-related potential technique*. MIT press, 2nd edition, 2014. ISBN 9780262324045.

[136] S. K. Andersen, S. A. Hillyard, and M. M. Müller. Attention Facilitates Multiple Stimulus Features in Parallel in Human Visual Cortex. *Current Biology*, 18(13):1006–1009, 2008. DOI: 10.1016/j.cub.2008.06.030.

[137] S. E. Watamura, K. A. Devine, and S. S. Robertson. The Dynamics of Attention during Free Looking. *PLoS ONE*, 8(2):2–9, 2013. DOI: 10.1371/journal.pone.0056428.

[138] M. Belmonte. Shifts of visual spatial attention modulate a steady-state visual evoked potential. *Brain research. Cognitive brain research*, 6(4):295–307, apr 1998.

[139] J. Bosch-Bayard, P. Valdes-Sosa, T. Virues-Alba, E. Aubert-Vazquez, E. R. John, T. Harmony, J. Riera-Diaz, N. Trujillo-Barreto, P. Valdés-Sosa, T. Virues-Alba, E. Aubert-Vázquez, E. R. John, T. Harmony, J. Riera-Díaz, and N. Trujillo-Barreto. 3D statistical parametric mapping of EEG source spectra by means of variable resolution electromagnetic tomography (VARETA). *Clinical EEG and Neuroscience*, 32 (2):47–61, 2001. DOI: 10.1177/155005940103200203.

[140] L. Prichep, E. John, L. Gugino, W. Kox, and R. Chabot. Quantitative EEG assessment of changes in the level of sedation/hypnosis during surgery under general anaesthesia. In C. Jordan, D. Vaughan, and D. Newton, editors, *Memory and awareness in anaesthesia IV*, chapter 8, page 380. Proceedings of the Fourth International Symposium, 2000. ISBN 978-1-78326-174-1.

[141] D. Pizzagalli. Electroencephalography and high-density electrophysiological source localization. In J. Cacioppo, L. Tassinary, and G. Berntson, editors, *Handbook of Psychophysiology*, chapter 8. Cambridge University Press, 3rd edition, 2007. ISBN 9780521844710.

[142] J. Ebersole, H. Stefan, and C. Baumgartner. Encephalographic and magnetoencephalographic source modeling. In J. Engel, T. Pedley, and J. Aicardi, editors, *Epilepsy: A Comprehensive Textbook, Volume 3*, page 3056. Lippincott Williams & Wilkins, 2007. ISBN 978-0781757775.

[143] M. Iwasaki and R. Burgess. Magnetoencephalography in the evaluation of the irritative zone. In H. Luders, editor, *Textbook of epilepsy surgery*, chapter 59, page 1648. 2008. ISBN 978-1841845760.

[144] X. Bai and B. He. On the Estimation of the Number of Dipole Sources in EEG Source Localization. *Clinical Neurophysiology*, 72(2):181–204, 2011. DOI: 10.1038/nature13314.A.

[145] R. J. Schafer and T. Moore. Attention Governs Action in the Primate Frontal Eye Field. *Neuron*, 56(3):541–551, nov 2007. DOI: 10.1016/j.neuron.2007.09.029.

[146] K. M. Armstrong, M. H. Chang, and T. Moore. Selection and Maintenance of Spatial Information by Frontal Eye Field Neurons. *Journal of Neuroscience*, 29(50):15621–15629, dec 2009. DOI: 10.1523/JNEUROSCI.4465-09.2009.

[147] S. E. Petersen, M. I. Posner, and A. Manuscript. The attention system of the human brain: 20 years after. *Annual review of neuroscience*, 35(35):73–89, 2012. DOI: 10.1146/annurev-neuro-062111-150525.The.

[148] T. Egner, J. M. P. Monti, E. H. Trittschuh, C. A. Wieneke, J. Hirsch, and M.-M. Mesulam. Neural Integration of Top-Down Spatial and Feature-Based Information in Visual Search. *Journal of Neuroscience*, 28(24):6141–6151, jun 2008. DOI: 10.1523/JNEUROSCI.1262-08.2008.

[149] H. A. Slagter, A. Kok, N. Mol, and J. L. Kenemans. Spatio-temporal dynamics of top-down control: directing attention to location and/or color as revealed by ERPs and source modeling. *Cognitive Brain Research*, 22(3):333–348, mar 2005. DOI: 10.1016/j.cogbrainres.2004.09.005.

[150] H.-T. Hsu, I.-H. Lee, H.-T. Tsai, H.-C. Chang, K.-K. Shyu, C.-C. Hsu, H.-H. Chang, T.-K. Yeh, C.-Y. Chang, and P.-L. Lee. Evaluate the Feasibility of Using Frontal SSVEP to Implement an SSVEP-Based BCI in Young, Elderly and ALS Groups. *IEEE Transactions on Neural Systems and Rehabilitation Engineering*, 4320(c):1–1, 2015. DOI: 10.1109/TNSRE.2015.2496184.

[151] K. A. Schneider. Retinotopic Organization and Functional Subdivisions of the Human Lateral Geniculate Nucleus: A High-Resolution Functional Magnetic Resonance Imaging Study. *Journal of Neuroscience*, 24(41):8975–8985, oct 2004. DOI: 10.1523/JNEUROSCI.2413-04.2004.

[152] K. A. Schneider. Visual Responses of the Human Superior Colliculus: A High-Resolution Functional Magnetic Resonance Imaging Study. *Journal of Neurophysiology*, 94(4):2491–2503, apr 2005. DOI: 10.1152/jn.00288.2005.

[153] K. A. Schneider and S. Kastner. Effects of Sustained Spatial Attention in the Human Lateral Geniculate Nucleus and Superior Colliculus. *Journal of Neuroscience*, 29(6): 1784–1795, feb 2009. DOI: 10.1523/JNEUROSCI.4452-08.2009.

[154] L. A. Benevento and G. P. Standage. The organization of projections of the retinorecipient and nonretinorecipient nuclei of the pretectal complex and layers of the superior colliculus to the lateral pulvinar and medial pulvinar in the macaque monkey. *The Journal of Comparative Neurology*, 217(3):307–336, jul 1983. DOI: 10.1002/cne.902170307.

[155] B. J. Casey, M. C. Davidson, Y. Hara, K. M. Thomas, A. Martinez, A. Galvan, J. M. Halperin, C. E. Rodríguez-Aranda, and N. Tottenham. Early development of subcortical regions involved in non-cued attention switching. *Developmental Science*, 7(5):534–542, 2004. DOI: 10.1111/j.1467-7687.2004.00377.x.

[156] J. Cavanaugh. Subcortical Modulation of Attention Counters Change Blindness. *Journal of Neuroscience*, 24(50):11236–11243, 2004. DOI: 10.1523/JNEUROSCI.3724-04.2004.

[157] D. Zhang, A. Maye, X. Gao, B. Hong, A. K. Engel, and S. Gao. An independent brain-computer interface using covert non-spatial visual selective attention. *Journal of neural engineering*, 7(1):16010, feb 2010. DOI: 10.1088/1741-2560/7/1/016010.

[158] C. Babiloni, F. Carducci, F. Cincotti, P. M. Rossini, C. Neuper, G. Pfurtscheller, and F. Babiloni. Human Movement-Related Potentials vs Desynchronization of EEG Alpha Rhythm: A High-Resolution EEG Study. *NeuroImage*, 10(6):658–665, dec 1999. DOI: 10.1006/nimg.1999.0504.

[159] J. J. Foxe, G. V. Simpson, and S. P. Ahlfors. Parieto-occipital approximately 10 Hz activity reflects anticipatory state of visual attention mechanisms. *Neuroreport*, 9(17): 3929–3933, 1998. DOI: 10.1097/00001756-199812010-00030.

[160] V. Romei, J. Gross, and G. Thut. On the Role of Prestimulus Alpha Rhythms over Occipito-Parietal Areas in Visual Input Regulation: Correlation or Causation? *Journal of Neuroscience*, 30(25):8692–8697, jun 2010. DOI: 10.1523/JNEUROSCI.0160-10.2010.

[161] S. Hanslmayr, A. Aslan, T. Staudigl, W. Klimesch, C. S. Herrmann, and K.-H. Bäuml. Prestimulus oscillations predict visual perception performance between and within subjects. *NeuroImage*, 37(4):1465–1473, oct 2007. DOI: 10.1016/j.neuroimage.2007.07.011.

[162] K. Linkenkaer-Hansen. Prestimulus Oscillations Enhance Psychophysical Performance in Humans. *Journal of Neuroscience*, 24(45):10186–10190, nov 2004. DOI: 10.1523/JNEUROSCI.2584-04.2004.

[163] P. Jasiukaitis and G. Hakerem. The Effect of Prestimulus Alpha Activity on the P300. *Psychophysiology*, 25(2):157–165, mar 1988. DOI: 10.1111/j.1469-8986.1988.tb00979.x.

[164] W. Klimesch. EEG alpha and theta oscillations reflect cognitive and memory performance: a review and analysis. *Brain Research Reviews*, 29(2-3):169–195, apr 1999. DOI: 10.1016/S0165-0173(98)00056-3.

[165] O. Jensen. Oscillations in the Alpha Band (9-12 Hz) Increase with Memory Load during Retention in a Short-term Memory Task. *Cerebral Cortex*, 12(8):877–882, aug 2002. DOI: 10.1093/cercor/12.8.877.

[166] T. a. Rihs, C. M. Michel, and G. Thut. Mechanisms of selective inhibition in visual spatial attention are indexed by alpha-band EEG synchronization. *The European journal of neuroscience*, 25(2):603–10, jan 2007. DOI: 10.1111/j.1460-9568.2007.05278.x.

[167] B. F. Händel, T. Haarmeier, and O. Jensen. Alpha Oscillations Correlate with the Successful Inhibition of Unattended Stimuli. *Journal of Cognitive Neuroscience*, 23 (9):2494–2502, sep 2011. DOI: 10.1162/jocn.2010.21557.

[168] M. S. Worden, J. J. Foxe, N. Wang, and G. V. Simpson. Anticipatory biasing of visuospatial attention indexed by retinotopically specific alpha-band electroencephalography increases over occipital cortex. *The Journal of neuroscience*, 20(6):RC63, 2000. DOI: Rc63.

[169] M. Benedek, R. J. Schickel, E. Jauk, A. Fink, and A. C. Neubauer. Alpha power increases in right parietal cortex reflects focused internal attention. *Neuropsychologia*, 56C:393–400, feb 2014. DOI: 10.1016/j.neuropsychologia.2014.02.010.

[170] N. R. Cooper, R. J. Croft, S. J. Dominey, A. P. Burgess, and J. H. Gruzelier. Paradox lost? Exploring the role of alpha oscillations during externally vs. internally directed attention and the implications for idling and inhibition hypotheses. *International Journal of Psychophysiology*, 47(1):65–74, jan 2003. DOI: 10.1016/S0167-8760(02)00107-1.

[171] M. Benedek, S. Bergner, T. Könen, A. Fink, and A. C. Neubauer. EEG alpha synchronization is related to top-down processing in convergent and divergent thinking. *Neuropsychologia*, 49(12):3505–3511, oct 2011. DOI: 10.1016/j.neuropsychologia.2011.09.004.

[172] S. Palva and J. M. Palva. Functional roles of alpha-band phase synchronization in local and large-scale cortical networks. *Frontiers in Psychology*, 2(SEP):1–15, 2011. DOI: 10.3389/fpsyg.2011.00204.

[173] H. Head and G. Holmes. Sensory disturbances from cerebral lesions. *Brain*, 34(2-3): 102–254, 1911. DOI: 10.1093/brain/34.2-3.102.

[174] H. Gastaut and J. Hunter. An experimental study of the mechanism of photic activation in idiopathic epilepsy. *Electroencephalography and Clinical Neurophysiology*, 2 (1-4):263–287, jan 1950. DOI: 10.1016/0013-4694(50)90058-7.

[175] P. Buser and M. Imbert. Sensory projections to the motor cortex in cats: a microelectrode study. In W. Rosenblith, editor, *Sensory communication*, pages 607–626. MIT, Cambridge, 1961.

[176] P. D. Wall, A. G. Rémond, and R. L. Dobson. Studies on the mechanism of the action of visual afferents on motor cortex excitability. *Electroencephalography and Clinical Neurophysiology*, 5(3):385–393, aug 1953. DOI: 10.1016/0013-4694(53)90080-7.

[177] B. Dubrovsky and E. Garcia-Rill. Convergence of tectal and visual cortex input to pericruciate neurons. *Experimental Neurology*, 33(3):475–484, dec 1971. DOI: 10.1016/0014-4886(71)90119-1.

[178] E. Garcia-Rill and B. Dubrovsky. Responses of motor cortex cells to visual stimuli. *Brain Research*, 82(2):185–194, dec 1974. DOI: 10.1016/0006-8993(74)90597-6.

[179] K. Bignall. Comparison of optic afferents to primary visual and polysensory areas of cat neocortex. *Experimental Neurology*, 17(3):327–343, mar 1967. DOI: 10.1016/0014-4886(67)90110-0.

[180] D. Pandya and H. Kuypers. CORTICO-CORTICAL CONNECTIONS IN THE RHESUS MONKEY. *Brain research*, 21(October):13–36, 1968.

[181] C. N. WOOLSEY. Some observations on brain fissuration in relation to cortical localization of function. In C. Tower and J. Schade, editors, *Structure and Function of the Cerebral Cortex*, pages 66–68. Elsevier, Amsterdam, 1960.

[182] M. Schaefer, B. Xu, H. Flor, and L. G. Cohen. Effects of different viewing perspectives on somatosensory activations during observation of touch. *Human Brain Mapping*, 30 (9):2722–2730, sep 2009. DOI: 10.1002/hbm.20701.

[183] A. Maravita and A. Iriki. Tools for the body (schema). *Trends in Cognitive Sciences*, 8(2):79–86, feb 2004. DOI: 10.1016/j.tics.2003.12.008.

[184] M. Pazzaglia, G. Galli, G. Scivoletto, and M. Molinari. A Functionally Relevant Tool for the Body following Spinal Cord Injury. *PLoS ONE*, 8(3):e58312, mar 2013. DOI: 10.1371/journal.pone.0058312.

[185] M. Botvinick and J. Cohen. Rubber hands feel touch that eyes see. *Nature*, 391(6669): 756–756, feb 1998. DOI: 10.1038/35784.

[186] H. H. Ehrsson. Touching a Rubber Hand: Feeling of Body Ownership Is Associated with Activity in Multisensory Brain Areas. *Journal of Neuroscience*, 25(45):10564–10573, nov 2005. DOI: 10.1523/JNEUROSCI.0800-05.2005.

[187] M. Tsakiris and P. Haggard. The Rubber Hand Illusion Revisited: Visuotactile Integration and Self-Attribution. *Journal of Experimental Psychology: Human Perception and Performance*, 31(1):80–91, 2005. DOI: 10.1037/0096-1523.31.1.80.

[188] S. Shokur, J. E. O'Doherty, J. a. Winans, H. Bleuler, M. a. Lebedev, and M. a. L. Nicolelis. Expanding the primate body schema in sensorimotor cortex by virtual touches of an avatar. *Proceedings of the National Academy of Sciences of the United States of America*, 110(37):15121–6, sep 2013. DOI: 10.1073/pnas.1308459110.

[189] P. J. Ifft. *Brain-Machine Interface for Reaching: Accounting for Target Size, Multiple Motor Plans, and Bimanual Coordination*. PhD thesis, Duke University, 2014.

[190] D. L. Kimmel, D. Mammo, and W. T. Newsome. Tracking the eye non-invasively: simultaneous comparison of the scleral search coil and optical tracking techniques in the macaque monkey. *Frontiers in Behavioral Neuroscience*, 6, 2012. DOI: 10.3389/fnbeh.2012.00049.

[191] D. Montgomery. Analysis of variance. In *Design and Analysis of Experiments*, chapter Determinin, page 105. 2013. ISBN 978-1-118-09793-9.

[192] M. Meulders. Integration contrale des afferences visuelles. *journal of Physiology (Paris)*, 62:61–109, 1970.

[193] P. Buser and K. Bignall. Nonprimary Sensory Projections on the Cat Neocortex. pages 111–165. 1967. DOI: 10.1016/S0074-7742(08)60152-X.

[194] Y.-D. Zhou and J. M. Fuster. Visuo-tactile cross-modal associations in cortical somatosensory cells. *Proceedings of the National Academy of Sciences*, 97(17):9777–9782, aug 2000. DOI: 10.1073/pnas.97.17.9777.

[195] M. M. Müller, W. Teder, and S. a. Hillyard. Magnetoencephalographic recording of steady-state visual evoked cortical activity. *Brain topography*, 9(3):163–8, 1997. DOI: 10.1007/BF01190385.

[196] A. Suzuki, M. Grabowecky, and K. Paller. Neuronal and Neural-Population Mechanisms of Voluntary Visual-Spatial Attention. In G. Mangun, editor, *Cognitive Electrophysiology of Attention: Signals of the Mind*, chapter 3, pages 35–38. Elsevier, 2014. ISBN 978-0-12-398451-7.

[197] Y. Joon Kim, M. Grabowecky, K. A. Paller, K. Muthu, and S. Suzuki. Attention induces synchronization-based response gain in steady-state visual evoked potentials. *Nature Neuroscience*, 10(1):117–125, jan 2007. DOI: 10.1038/nn1821.

[198] S.-J. Blakemore. Somatosensory activations during the observation of touch and a case of vision-touch synaesthesia. *Brain*, 128(7):1571–1583, apr 2005. DOI: 10.1093/brain/awh500.

[199] C. Keysers, B. Wicker, V. Gazzola, J.-L. Anton, L. Fogassi, and V. Gallese. A Touching Sight. *Neuron*, 42(2):335–346, apr 2004. DOI: 10.1016/S0896-6273(04)00156-4.

[200] I. Bufalari, T. Aprile, A. Avenanti, F. Di Russo, and S. M. Aglioti. Empathy for Pain and Touch in the Human Somatosensory Cortex. *Cerebral Cortex*, 17(11):2553–2561, nov 2007. DOI: 10.1093/cercor/bhl161.

[201] J. M. Carmena, M. A. Lebedev, R. E. Crist, J. E. O'Doherty, D. M. Santucci, D. F. Dimitrov, P. G. Patil, C. S. Henriquez, and M. A. L. Nicolelis. Learning to Control a Brain-Machine Interface for Reaching and Grasping by Primates. *PLoS Biology*, 1(2): e42, oct 2003. DOI: 10.1371/journal.pbio.0000042.

[202] F. Matyas, V. Sreenivasan, F. Marbach, C. Wacongne, B. Barsy, C. Mateo, R. Aronoff, and C. C. H. Petersen. Motor Control by Sensory Cortex. *Science*, 330(6008):1240–1243, nov 2010. DOI: 10.1126/science.1195797.

[203] N. A. Fitzsimmons. Extracting kinematic parameters for monkey bipedal walking from cortical neuronal ensemble activity. *Frontiers in Integrative Neuroscience*, 3, 2009. DOI: 10.3389/neuro.07.003.2009.

[204] M. Nicolelis, L. Baccala, R. Lin, and J. Chapin. Sensorimotor encoding by synchronous neural ensemble activity at multiple levels of the somatosensory system. *Science*, 268 (5215):1353–1358, jun 1995. DOI: 10.1126/science.7761855.

Appendix 1

The scientific contribution of this work is listed as belows:

Journal articles

- **Mehdi Ordikhani-Seyedlar*** , Mikhail A. Lebedev, Helge B.D. Sorensen, Sadasivan Puthusserypady. Neurofeedback Therapy for Enhancing Visual Attention: State-of-the-Art and Challenges. *Frontiers in Neuroscience*; 10, Aug. 2016 (1-15), doi:10.3389 /fnins.2016.00352.
- **Mehdi Ordikhani-Seyedlar*** , Abbas Khani and Mikhail Lebedev. Paradigm shifts in theories of attention. Submitted (Apr, 2016) to *Frontiers in Human Neuroscience*. Status: revision.

Conference contribution

- **Mehdi Ordikhani-Seyedlar**, Arjun Ramakrishnan, Mikhain A. Lebedev, Sadasivan Puthusserypady, Miguel A.L. Nicolelis. Steady-state visual evoked potentials in monkey somatosensory and motor cortical areas. SFN 45^{th} Annual Meeting; Oct 17-21, 2015; Chicago, Il, USA.
- **Mehdi Ordikhani-Seyedlar**, Helge B.D. Sorensen, Troels W. Kjaer, Sadasivan Puthusserypady. Sources of the brain activation in visual attention: a novel feature for electroencephalography-based brain-computer interface. SFN 44^{th} Annual Meeting; Nov 15-19, 2014; Washington, DC, USA.
- **Mehdi Ordikhani-Seyedlar**, Helge B.D. Sorensen, Troels W. Kjaer, Hartwig R. Siebner, Sadasivan Puthusserypady. SSVEP Modulation by Covert and Overt Attention: Novel Features for BCI in Attention Neuro-rehabilitation. Conf Proc IEEE Eng Med Biol Soc. 2014;2014:5462-5. doi: 10.1109/EMBC.2014.6944862.

Appendix 2

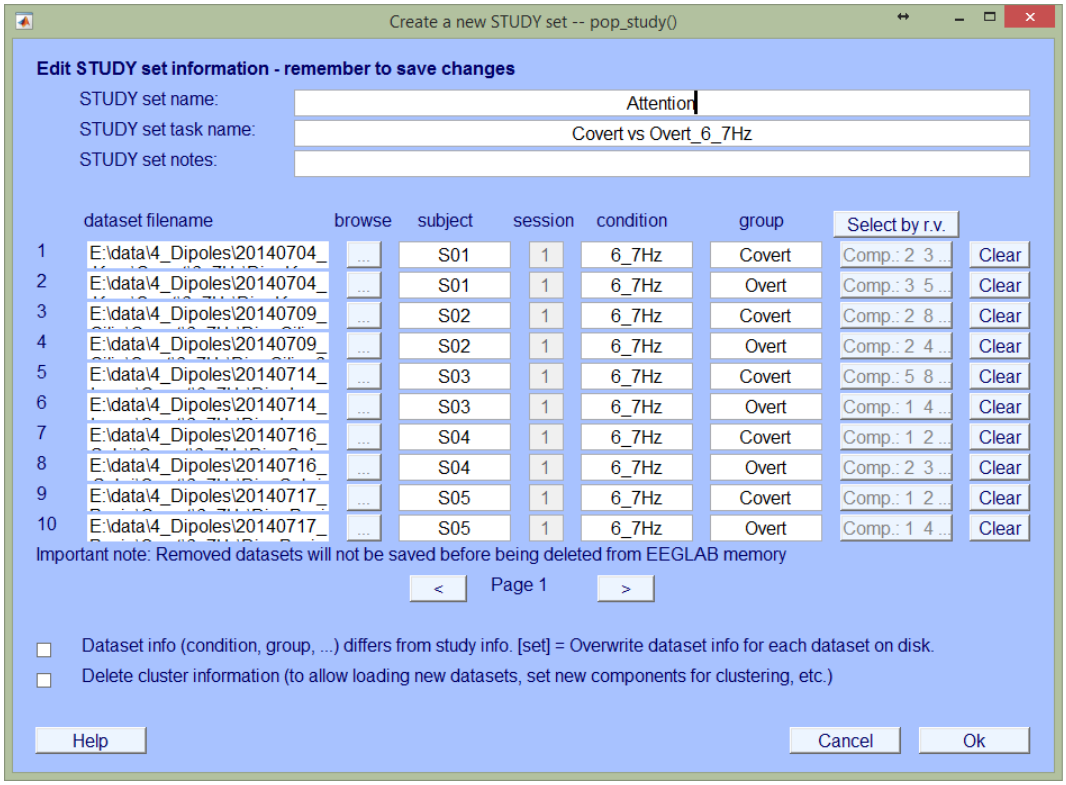

Figure 7.1: **Creating a new STUDY set 1:** Dipole files from all subjects were fed into EEGLAB for finding the common spatial pattern. Dipole files were the merged files from SSVEP frequencies which were presented simultaneouly at ethe same session (6&7Hz in this figure shown in column *condition*). Both overt and covert groups were uploaded for later comparisons (located in *group* column). The column names by *Select by r.v.* selects the components based on their residual variances which in our case is $\leqslant 15\%$.

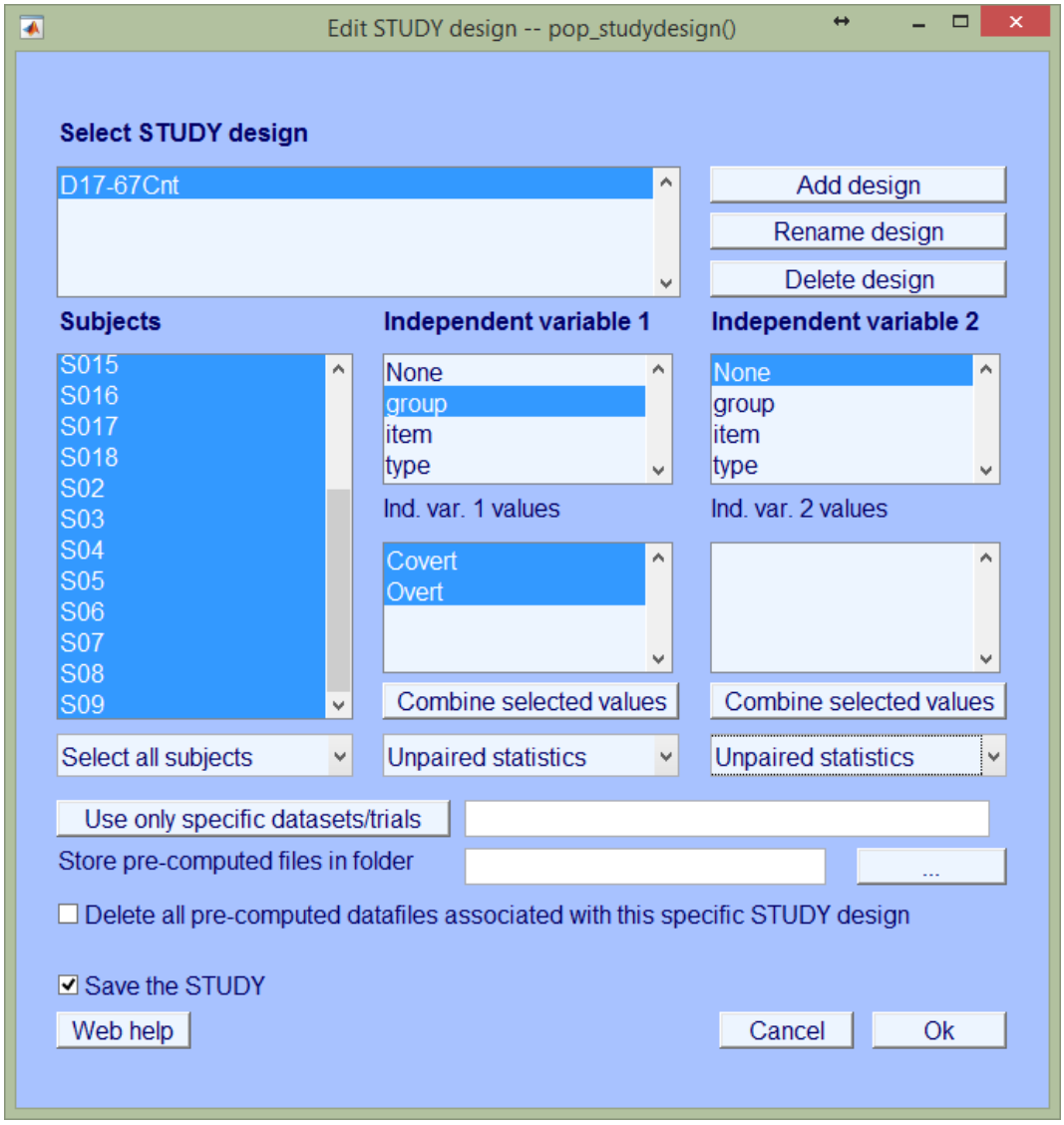

Figure 7.2: **STUDY design:** The data were designed to compared the two groups of overt and covert attention. In this figure the *Subjects* contains all subjects included in the analysis (N=18); *Independent variable 1 & 2* contains the variables we are interested to compare the data in those respects. In this study we were only interested in group comparisons (covert vs overt which are shown in *Ind. var 1 values*); therefore, disregarded the other variables. For statistical analysis we used unpaired method as the number of trials might vary among subjects.

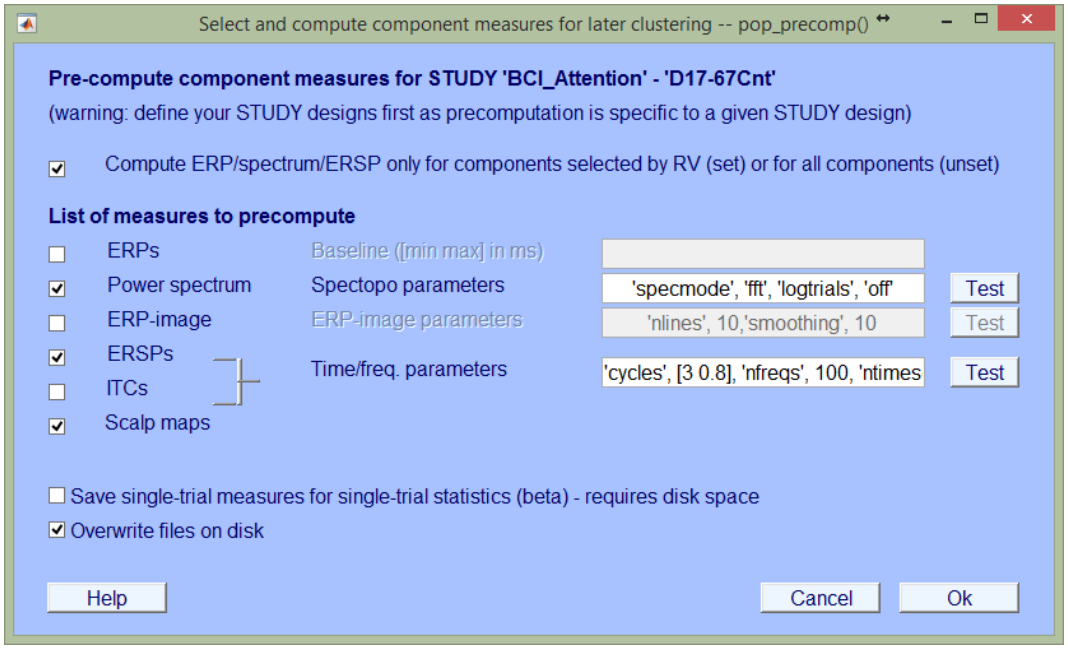

Figure 7.3: **Pre-computing:** The designed data were pre-computed for the parameters: Power spectrum, ERSPs and Scalp maps. In this step the selected parameters are computed for all subjects and all groups (covert & overt attention).

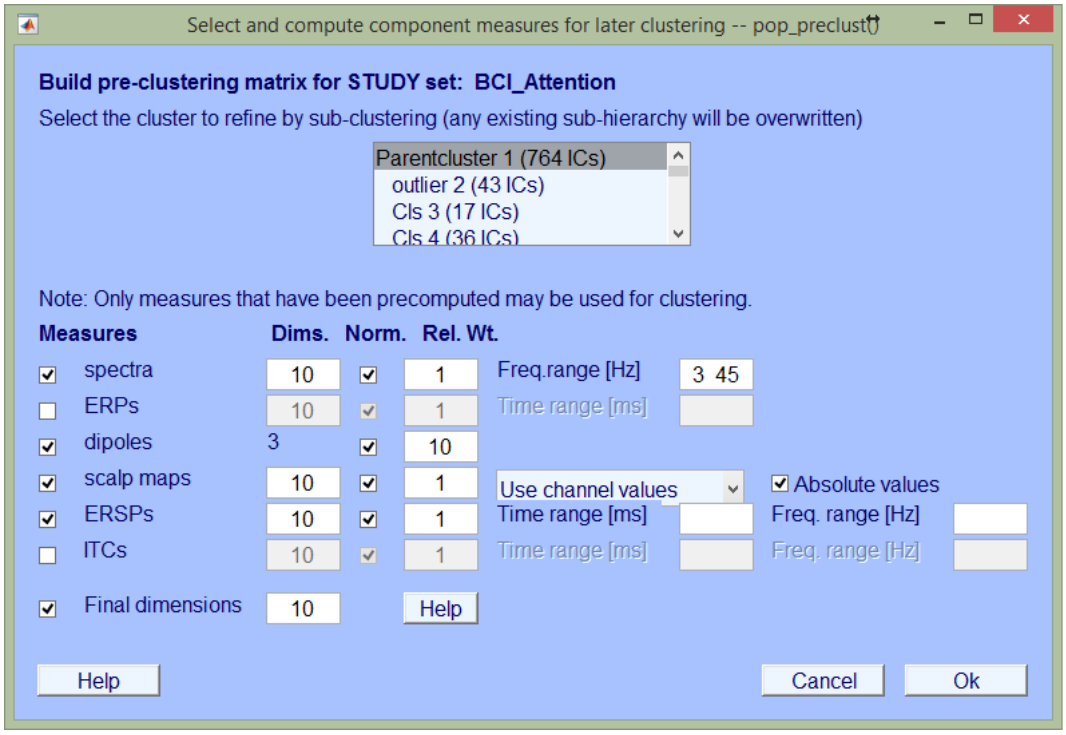

Figure 7.4: **Pre-clustering:** The check-boxes on the *Measures* section allow the selection of the component activity measures for clustering. The aim of the pre-clustering is to compute N-dimensional cluster position vector for each component. The cluster position vectors are required to measure the distance of components from each other in the N-dimensional cluster space. N is an arbitrary value; however, for numeric reasons we kept it in relatively low value (by default $N = 10$). Therefore, it reduces the cluster position vectors to an N-dimensional principal subspace by using PCA. In the *Norm* column, we checked the boxes to normalize the N-principal dimensions to obtain equivariant matrices in each measures. The column *Rel Wt.* allowed us to choose relative weights for each measure. Finally, we had the option to select a frequency-range to be analyzed in that specific limit (3-45Hz). The *final dimensions* is to further dimension reduction in the component distance measure for clustering. The clustering algorithm work best in lower dimensions. In our case the overall dimensionality is N=33. By checking this box this number wil be reduced to 10 using the PCA decomposition.

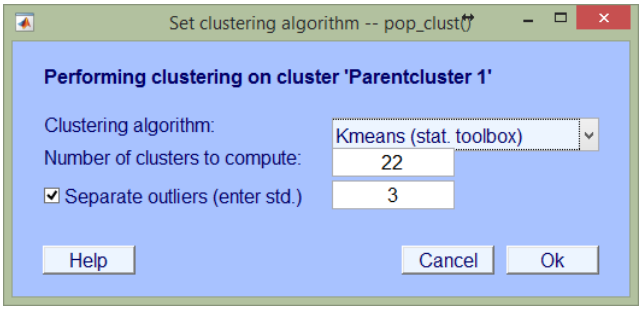

Figure 7.5: **Clustering:** The interface for clustering in EEGLAB. k-means algorithm was used in our study. Th number of clusters are calculated with equation5.4.

www.elektro.dtu.dk
Department of Electrical Engineering
Biomedical Engineering
Technical University of Denmark
Ørsteds Plads
Building 348
DK-2800 Kgs. Lyngby
Denmark
Tel: (+45) 45 25 38 00
Fax: (+45) 45 93 16 34
Email: info@elektro.dtu.dk